

Estimation of Evapotranspiration from Satellite
Remote Sensing and Meteorological Data over the
Fogera Flood Plain - Ethiopia

Temesgen Enku
February, 2009

Estimation of Evapotranspiration from Satellite Remote Sensing and Meteorological Data over the Fogera Flood Plain - Ethiopia

by

Temesgen Enku

This thesis submitted to the International Institute for Geo-information Science and Earth Observation in partial fulfilment of the requirements for the degree of Master of Science in Geo-information Science and Earth Observation, Specialisation: Integrated Watershed Modelling and Management.

Thesis Assessment Board

Chairman	Prof. Dr. Ing. W. Verhoef	WRS Department, ITC, Enschede
External Examiner	Drs. J. Grant	Vrije Universiteit, Amsterdam
First Supervisor	Dr. Ir. C. van der Tol	WRS Department, ITC, Enschede
Second Supervisor	Dr. A.S.M. Gieske	WRS Department, ITC, Enschede



**INTERNATIONAL INSTITUTE FOR GEO-INFORMATION SCIENCE AND EARTH OBSERVATION
ENSCHDE, THE NETHERLANDS**

Disclaimer

This document describes work undertaken as part of a programme of study at the International Institute for Geo-information Science and Earth Observation. All views and opinions expressed therein remain the sole responsibility of the author, and do not necessarily represent those of the institute.

Dedicated to
My dearest father Aba Enku Nigussie
and
My late mother Woyinitu Beyene
Symbol of strength and endurance

Abstract

Evapotranspiration (ET) is not only an important component in the land surface energy balance, but also major component in the water cycle and an important parameter in water resources management. Conventional methods for ET estimation which use meteorological data can only be used to estimate ET at certain location, but not at a larger scale. This limitation can be overcome by using a combination of ground based and remote sensing data in a surface energy balance model. In this study, the annual cycle of ET in for the Fogera flood plain, in northwest Ethiopia is estimated, using MODIS images, weather station data and the surface energy balance model SEBS. The results were compared to conventional ground based methods.

The Fogera flood plain is located east of Lake Tana, in northwest Ethiopia. The area is about 500 km² and elevation of 1800 m, flooding occurs frequently during the rainy season. Rice is the major crop.

A meteorological station was installed in the flood plain in June 2008, recording standard meteorological values at 5-min interval. In addition, eddy covariance instruments were installed for 3 days in September 2008. MODIS products were downloaded and processed with monthly intervals. Weather station data and the MODIS products were used as input for SEBS to calculate monthly images of ET of the whole floodplain. For months where no weather station data were available, daily data of the nearby weather station in Bahir Dar were used. Eddy covariance data of three days were used as validation.

The annual actual ET from SEBS in the year 2008 was 1519 mm, while P-M reference ET was 1498 mm. The annual ET over the area was larger by about 17 % from the mean annual rainfall of the floodplain. The excess ET was from the flooding caused mainly by the rivers. The spatial and temporal variation of ET over the flood plain was also evaluated. The actual ET from SEBS was larger than the P-M ETo during the wet seasons and lower in drier periods. Spatial variation of ET was well pronounced in drier periods than wet seasons. The instantaneous albedo from the remote sensing method was less by 15% from the daily albedo computed from the eddy flux tower observation.

The ground based conventional methods Penman-Monteith (P-M), Priestley-Taylor, Makkink, and Abtew simple equations were used for the estimation of reference ET. A comparison of these methods showed that simple radiation methods like Makkink and Abtew equations perform as well as P-M in the area. A sensitivity analysis of P-M for input variables showed that reference ET is most (and equally) sensitive to incoming solar radiation and air temperature, and least sensitive to wind speed. This explains why simple ET methods based on either radiation or temperature perform well.

The temperature method that only uses maximum temperature was used in this area. This method was found to perform comparable with other conventional methods. With this method, it was possible to estimate ETo with less than 10 % error from P-M reference ET when daily estimations are compared and with in 2 % error when yearly estimations compared.

Key words: Evapotranspiration, MODIS, SEBS, Penman-Monteith

Acknowledgements

First and foremost my deepest thanks go to Almighty God, your grace is always with me.

I would like to express my gratitude to the ITC fellowship program for giving me this opportunity to pursue my MSc. degree here in the Netherlands; without it this was impossible.

My deep gratitude goes to my first supervisor Dr. Ir. Christiaan van der Tol for his unlimited and tireless guidance during my thesis work starting from data collection to final thesis writing work. My special thanks go to my second supervisor Dr. Ambro Gieske for his tireless guidance, support and for his constructive comments during the whole thesis work.

My gratitude also goes to the course director of WREM Ir. Arno van Lieshout for his valuable advice during my stay in ITC.

I also would like to appreciate Dr. Ben Maathuis for his valuable advice and support during my stay here ITC, Netherlands.

I would like to express my gratitude to Mr. Esayas Kaba academic vice dean of Engineering Faculty of Bahir Dar University for his cooperation to use laboratory equipment during the field campaign and for his valuable input during importing field equipment.

In addition, I like to thank Mr. Ruduwan Mehadi for his cooperation to get meteorological data easily at Bahir Dar and sending me latest data.

Last but not least I would like to thank the Ethiopian community here in ITC whom friendship comforted me a lot during my stay.

Table of contents

1. Introduction	1
1.1. General	1
1.2. Research problem	1
1.3. Research objectives	2
1.4. Research questions	2
1.5. Hypothesis	2
1.6. Background and literature review	2
1.7. Outline of the thesis	5
2. Study area	7
2.1. General	7
2.2. Flooding patterns	7
2.3. Climate	8
2.4. Soils	10
2.5. Crop type and cropping pattern	10
3. Materials and data	12
3.1. Materials	12
3.1.1. Woreta weather station (WWS)	12
3.1.2. Eddy flux tower	12
3.1.3. Sonic anemometer (CSAT3)	13
3.1.4. Net radiometer (CNR1)	15
3.1.5. Datalogger (CR5000)	15
3.2. Data	16
3.2.1. Meteorological data	16
3.2.2. Woreta weather station data	16
3.2.3. Eddy flux data	17
3.2.4. GPS data	17
3.2.5. Remote sensing data	17
4. Methodology	19
4.1. General	19
4.2. Ground based evapotranspiration estimation methods	20
4.2.1. Penman-Monteith method	20
4.2.2. Priestley-Taylor method	21
4.2.3. Modified Makkink method	21
4.2.4. Simple Abteu equation	21
4.2.5. Penman-Monteith sensitivity analysis	22
4.3. Micrometeorology	22
4.3.1. Sensible heat flux and friction velocity	22
4.3.2. Evaporative fraction	24
4.3.3. Radiation and temperature	24
4.3.4. Surface albedo	26

4.4.	Remote sensing	26
4.4.1.	Introduction	26
4.4.2.	MODIS products.....	27
4.4.3.	Surface reflectance 8-day L3 global 500 m (MOD09A1).....	28
4.4.4.	Land surface temperature (MOD11A1 daily LST)	30
4.4.5.	Leaf area index (LAI).....	30
4.4.6.	Images used in the analysis.....	30
4.4.7.	Land cover classification.....	32
4.4.8.	Instantaneous Image processing in SEBS.....	32
4.4.9.	Image downloading, re projection and sub setting.....	33
4.4.10.	Atmospheric correction (SMAC).....	33
4.4.11.	Land surface emissivity computation.....	33
4.4.12.	Land surface temperature.....	34
4.4.13.	Aerodynamic roughness height (z_{om})	34
4.4.14.	Zero-plane displacement height (d)	36
4.5.	Surface Energy Balance Systems (SEBS)	37
4.5.1.	General.....	37
4.5.2.	Energy balance equation.....	37
4.5.3.	Land surface albedo.....	38
4.5.4.	Radiation.....	38
4.5.5.	Soil heat flux estimation.....	38
4.5.6.	Fractional vegetation cover	38
4.5.7.	Normalized difference vegetation index (NDVI).....	39
4.5.8.	Sensible heat flux	39
4.5.9.	Evaporative fraction	40
4.5.10.	Ancillary weather data for SEBS algorithm	42
5.	Data analysis	43
5.1.	Introduction.....	43
5.2.	Woreta weather station and the eddy flux tower	43
5.2.1.	Temperature.....	43
5.2.2.	Relative humidity	44
5.2.3.	Radiation.....	45
5.3.	Woreta and Bahir Dar station data comparisons	47
6.	Results and discussion.....	50
6.1.	Conventional methods	50
6.1.1.	Priestley Taylor vs Penman-Monteith	50
6.1.2.	Modified Makkink and P-M ETo comparison.....	51
6.1.3.	Abteu simple equation vs P- M ETo.....	52
6.1.4.	Estimation of ETo from maximum temperature data only.....	53
6.1.5.	Sensitivity analysis	54
6.2.	Micrometeorology.....	56
6.2.1.	Sensible heat flux	57
6.2.2.	Latent heat flux.....	58
6.2.3.	Evaporative fraction	59
6.2.4.	Surface albedo	59

6.2.5.	Roughness height for momentum transfer.....	60
6.3.	Remote sensing Results	61
6.3.1.	Comparison of SEBS actual evapotranspiration to P - M reference ET	61
6.3.2.	Spatio-temporal distribution of SEBS ET over the entire flood plain	62
6.3.3.	Spatio-temporal variations of SEBS actual ET over rice fields	65
6.3.4.	Deriving single crop coefficient (Kc) for rice field	65
7.	Conclusions and recommendations	69
7.1.	Conclusions.....	69
7.2.	Recommendations.....	70
	Appendix - A FAO-56 method for net radiation computation.....	71
	Appendix - B MODIS spectral bands	75
	Appendix - C Sensitivity analysis result	78
	Appendix - D Daily evapotranspiration maps.....	80
	Appendix - F Some of the daily albedo maps	82
	Appendix - G Weighted average vegetation height computation around the eddy flux tower	83
	References.....	88

List of figures

Figure 2-1 Location map of the Fogera flood plain	8
Figure 2-2 Mean monthly rainfall distribution (2004 -2007).....	9
Figure 2-3 Mean monthly maximum, mean, and minimum temperature.....	9
Figure 2-4 Land use map of the Fogera flood plain	11
Figure 2-5 Rice field in the flood plain Photo taken (September 2008)	11
Figure 3-1 The Woreta weather station installed on 23 June 2008 at about 2 km from Woreta town.	12
Figure 3-2 Plot of location of the Woreta weather station and eddy flux tower.....	13
Figure 3-3 Eddy flux tower.....	14
Figure 3-4 Flux tower installed during the field campaign	14
Figure 3-5 CR5000 data logger	15
Figure 4-1 General methodology flow chart	19
Figure 4-2 Global tiles with the respective tile of study area.....	28
Figure 4-3 Day of the year product of (a) December 2007 and (b) July 2008	29
Figure 5-1 Temperature correlation between WWS and flux tower sensors.....	43
Figure 5-2 Sonic temperature and flux tower temperature sensor comparison	44
Figure 5-3 Relative humidity correlation between the flux tower and the WWS station measurements.....	44
Figure 5-4 Measured radiation (a) scatter plot radiation from WWS vs radiation from CNR1 (b) Solar radiation vs time during sunlight hours on 23 September 2008	45
Figure 5-5 Net radiation correlation	46
Figure 5-6 Correlation between instant solar radiation and daily solar radiation.....	47
Figure 5-7 (a) Maximum and minimum temperature graphs measured at Woreta weather station and Bahir Dar station (June 24 - Nov. 8, 2008) (b) maximum temperature correlations at WWS vs Bahir Dar stations.....	48
Figure 5-8 Correlation between instantaneous temperature at WWS vs daily maximum temperature at Bahir Dar station.....	49
Figure 6-1 Scatter plot of P-T vs P-M ETo with (a) Woreta and (b) Bahir Dar data.....	51
Figure 6-2 Scatter plot of Makkink vs P-M at two stations at (a) WWS and (b) Bahir Dar stations	52
Figure 6-3 Scatter plot Abtew vs P-M equation at Bahir Dar station for drier months.....	53
Figure 6-4 Scatter plot new method vs P-M ETo for the year 2007.....	54
Figure 6-5 Monthly weather variables at Bahir Dar station in the year	55
Figure 6-6 Sensitivity analysis results of ETo to input variables, (a) January - 08 (b) April - 08 (c) July - 08 and (d) October – 08.....	56
Figure 6-7 Sensible heat flux comparison between (a) eddy covariance, from friction velocity and from SEBS..	58
Figure 6-8 Daily variation of evaporative fraction in clear sky days	59
Figure 6-9 Daily surface albedo variation.....	60
Figure 6-10 Scatter plot of SEBS actual ET vs P- M reference ET on (a) wet season and (b) dry season	62
Figure 6-11 Daily actual ET, daily and monthly reference ET, and daily solar radiation and maximum temperature	62
Figure 6-12 Histogram of three different days in a year over the Fogera flood plain	63
Figure 6-13 Spatio-temporal distribution of ET over the Fogera flood plain with respective histogram.....	64

Figure 6-14 Spatio-temporal distribution map of ET over the rice field with respective histogram in the Fogera flood plain (a), (b) 7 July 2008 (c),(d) 6 September 2008 and (e),(f) 7 December 2007 66

Figure 6-15 Spatio-temporal distribution map of Kc over the rice field with respective histogram (a), (b) 7 July 2008 (c),(d) 6 September 2008 and (e),(f) 7 December 2007 68

List of tables

Table 3-1 Stations and type of data collected for (2004-2007).....	16
Table 3-2 Part of Woreta weather station data.....	16
Table 3-3 Part of the net radiometer (CNR1) data.....	17
Table 3-4 Part of GPS data collected.....	17
Table 3-5 Collected and downloaded MODIS products.....	18
Table 4-1 MODIS Technical specifications.....	26
Table 4-2 MODIS visible and some of thermal bands.....	27
Table 4-3 MODIS products acquired.....	27
Table 4-4 Sub setting and re-projection parameters	28
Table 4-5 Date and type of images used for analysis.....	31
Table 4-6 Land use classes with its associated z_{om} values.....	35
Table 5-1 Instantaneous and daily solar radiation relation	46
Table 5-2 Maximum, minimum, mean temperature and mean relative humidity comparison between the WWS and Bahir Dar data	47
Table 5-3 Measured and calibrated values of transmissibility and the coefficient “ a ”	49
Table 6-1 Comparison of P-T with P-M.....	50
Table 6-2 Comparison of Makkink with the P-M method	51
Table 6-3 Comparison of latent heat flux from eddy flux tower and Abtew actual ET	52
Table 6-4 Comparison of Abtew with the P-M method.....	52
Table 6-5 Comparison of new method with the P-M method on daily and yearly basis.....	54
Table 6-6 Monthly average weather variables at the Bahir Dar station (2008)	55
Table 6-7 Comparison of sensible heat flux from SEBS estimation and eddy covariance method.....	57
Table 6-8 Latent heat flux comparison with ET_o	58
Table 6-9 Comparison of instantaneous and daily evaporative fraction	59
Table 6-10 Instant and daily albedo computed from the CNR1 observations.....	60
Table 6-11 Daily and monthly ET in the year 2008.....	61

1. Introduction

1.1. General

The demand for fresh water is increasing due to the population increase which influences the increase in agricultural production. But the amount of fresh water in the globe is limited and unevenly distributed over space and time. Hence, well planned and organized water resources management is required at local and regional scales. Evapotranspiration (ET) is one of the major components in the study of hydrological processes both in the mass balance and energy balance approaches.

The higher solar radiation in tropical areas leads for strong evaporative conditions. The surface water and the shallow subsurface water storage in strong evaporative areas are more vulnerable for higher ET. It may be greater than the annual rainfall in arid and semi arid areas which leads water deficits in such areas.

Globally, evapotranspiration is maximum near the equator and minimum at the poles. This has similar pattern with the amount of solar radiation and temperature which are the main deriving forces for the phase change (liquid/solid to gas) in respective areas on annual basis (Dingman, 2002). About 62% (72,000 km³/year) of the precipitation falls on the land surface evapotranspired globally (Dingman, 2002). This fraction rose to 85 % for the African continent where arid and semi-arid area dominate. Out of the total ET from the continents, about 97% is lost through evapotranspiration from the land surface and the rest 3 % is lost from open water surfaces (Dingman, 2002).

Quantitative assessment and understanding of evapotranspiration is the basis for the assessment of water resources and vital for irrigation management practices and hydrological modelling.

1.2. Research problem

The Fogera flood plain is fertile land for agricultural production. The Ribb and Gumara rivers are the main rivers flowing through the flood plain. A multi-purpose dam is under construction on the Ribb river up stream of the flood plain. Dam construction is to continue in the Gumara river in the near future. These dams are designed for irrigation during the dry season and minimizing flooding risk in the flood plain during the rainy season. The flood plain was considered as the main command area for future irrigation purposes. Hence knowledge and quantification of surface energy fluxes in this area is important for many purposes to be practiced.

Several environmental disciplines, like hydrology, meteorology, agronomy, and irrigation management practices require knowledge of the land surface energy fluxes through the different components of the energy balance systems. Reliable maps of surface energy fluxes are important for assessing surface-atmosphere interactions in the area. The amount of water lost through evapotranspiration in the Fogera flood plain is not well known. The high potential for crop production of this area is not fully utilized. Wise use of limited water resources is important for maximizing

production through irrigation management practices; this will be addressed through the knowledge and understanding of the quantity and processes of evapotranspiration.

1.3. Research objectives

The main objective of this study is to estimate spatio-temporal distribution of evapotranspiration using remotely sensed data and estimation of ET by different conventional methods that require meteorological data. To achieve these main objectives the specific objectives to be accomplished are:

- Estimation of reference evapotranspiration from ground based meteorological data using Penman-Monteith method, Priestley-Taylor method, and estimation of ET from simple radiation equations,
- Prepare land use map of the study area,
- Application of Surface Energy Balance Systems (SEBS) for the estimation of ET from satellite data, and
- Comparison of different conventional methods in estimations of ET.

1.4. Research questions

The main research questions intended to be addressed in this study are:

- How can ground based measurements be used to improve remote sensing estimation of ET?
- To which weather variable/variables is the Penman-Monteith reference ET most sensitive to?
- Which ground based method gives better estimate of evapotranspiration compared to P-M reference ET?
- How does ET vary spatially and temporally over the Fogera flood plain?
- Can ET be estimated from solar radiation and/or temperature data only?

1.5. Hypothesis

Evapotranspiration in the area is as high as the mean annual rainfall and it is mainly determined by net radiation and temperature.

1.6. Background and literature review

Evapotranspiration is a general term that includes all the processes that water in the liquid state or solid state change in to gaseous state (water vapor). The term hence includes evaporation from open water surface, from bare soil, transpiration through plant leaves and sublimation from snow and ice surfaces (Dingman, 2002). This phase change is mainly derived by the availability of solar energy at the evaporating and transpiring surfaces. Both processes occur simultaneously and quantifying these processes separately is almost impossible.

Evapotranspiration is an important factor in the global, regional and local hydrological processes. It is the bridge which links mass balance and energy balance equations in the study of hydrology. Since quantification and direct measurement of evapotranspiration is very difficult task it is usually quantified as the residual value in both the mass balance and energy balance equations. This was the main reason why evaporation was poorly quantified in the history of hydrology.

These days the Penman Monteith (Allen, 1998) method is used as a standard and it is most widely used method globally for estimation of ET (Bois et al., 2008; Dingman, 2002; Gieske, 2003). But knowledge of spatial variation of evapotranspiration (ET) is still limited. Ground based methods estimate and measure ET at point locations. But the spatial variation of the turbulent fluxes due to land cover, and topographical changes limit the application of ground based methods for larger spatial areas. To overcome these bottlenecks, remote sensing techniques is an appropriate method. Nowadays there are different models developed for the estimation of ET from remote sensing data. SEBS (Su, 2002), SEBAL (Bastiaanssen, 1998), and TSEB (Norman et al., 1995) are some of them. The remote sensing methods allow estimation of energy fluxes even for inaccessible areas.

SEBS is one of the models developed based on the energy balance principles, and calculates the latent heat flux as a residual of net radiation from sensible and soil heat fluxes estimations. SEBS was tested in different places and found to give good estimates of surface energy fluxes. In central Arizona it was tested by Su (2002) and reported good results, McCabe and Wood (2006) in their study in central Iowa, USA showed that SEBS latent heat flux agree well with the tower flux measurements, and in Spain, the SEBS sensible heat flux estimate was found to be comparable with the measurements made by a scintillometer (Jia et al., 2003).

There was no sound study made on the estimation of ET over the Fogera flood plain. Kebede et al. (2006) and Abeyou (2008) have done the water balance of Lake Tana at different time and using different data set. They estimated ET of the lake basin. On the other hand, SMEC (2007) in its report, on the hydrological study of the Tana-Beles sub-basins has made a rough estimation of ET over the Fogera flood plain to be 140 mm, 117 mm, 116 mm, and 129 mm in the months of June, July, August and September respectively. The Waterwatch (2005), in its Remote Sensing Studies of Tana-Beles Sub Basins has reported that the Lake Tana open water evaporation was 1588 mm/year greater than the annual rainfall on the lake, 1541mm, and an average evapotranspiration of 672 mm/year over the lake basin. This estimation was made from the remote sensing data. Generally there was no sound study made on the estimation of evapotranspiration in the Fogera flood plain. Hence this study will be the first to estimate the reference and actual evapotranspiration of the Fogera flood plain using remote sensing technique and ground based conventional methods using meteorological data.

Evapotranspiration estimation methods

Direct measurement of evapotranspiration is still a difficult task. Much use is still depending on the empirical methods. The different approaches to estimate ET could be categorised in to main groups as:

- Water balance methods
- Micro-meteorological methods, and
- Energy balance (Remote sensing) techniques

1. Water balance methods

The main assumption in this method is that, it is possible to close the water balance in the well defined catchments. Hence, ET can be estimated as a residue provided that other components are known in a specified period of time in year or in a month. From the general water balance equation ET can be estimated as:

$$ET = P + Q_{in} + G_{in} - Q_{out} - G_{out} - \Delta S \quad (1.1)$$

where ET is the evapotranspiration, P is the precipitation, Q_{in} , G_{in} are the incoming surface water flow and ground water flow to the study area under consideration respectively, Q_{out} , G_{out} are the out going surface water flow and ground water flow out of the study area under consideration respectively, and ΔS is the change in the storage in the catchments. The dimension of these quantities could be expressed as [L] or [L³]. In this method exact quantification of the components still remains difficult especially on larger scale. Here, if the components are quantified accurately ET can be estimated accurately too.

a) Lysimeters

A Lysimeter is an artificially extracted undisturbed soil column. The principle of lysimeters is based on the weight changes of the soil volume. Evaporation is accurately estimated here, after accurately measuring of other water balance components in the soil volume. These days, this method is assumed as the exact method of estimating ET, and used as a validation for other estimates.

b) Evaporation pan

Evaporation pan is the most widely used instrument for estimating ET. The pan is circular cylinder usually with a diameter of 120.7 cm, 25 cm deep and made of galvanized iron. The pan is filled with water to 5 cm below the rim. Measurements are made in the 10 cm diameter stilling well. Pan coefficient is used to relate pan evaporation to the reference ET (Eddy Moors, 2008).

2. Micro-meteorological methods

Micro-meteorological methods measure ET in terms of water vapour flux. These methods help in estimation of ET independent of other mass balance components.

a) Eddy-correlation method

Eddy correlation method follows statistical approach than deterministic approach. It is this makes the eddy correlation method the most direct way to measure ET (Eddy Moors, 2008). The covariance of the fluctuations of the vertical wind speed and the specific humidity from the mean is a direct measure of the latent heat flux. It is expressed as (Brutsaert, 2005; Dingman, 2002; Eddy Moors, 2008):

$$\lambda E = \lambda \rho_a \overline{w'q'} \quad (1.2)$$

where λE (W/m²) is the latent heat flux, λ (J/kg) latent heat of vaporization, ρ_a (kg/m³) is the density of the air, $\overline{w'q'}$ is the covariance of the fluctuations of the vertical wind speed and specific humidity from their respective mean.

b) Bowen ratio method

Bowen ratio (B) is defined as the ratio of sensible heat flux to latent heat flux and hence it is directly related to the differences in temperature and humidity between the two heights. It is expressed as (Bowen, 1926):

$$B = \gamma \frac{\Delta T}{\Delta e} \quad (1.3)$$

where γ (hPa/K) is the psychrometric constant, ΔT , Δe are the change in temperature and humidity between two measuring heights respectively. Combining equation (1.3) with the energy balance equation one finds,

$$\lambda E = \frac{R_n - G}{1 + B} \quad (1.4)$$

To use this method two air temperature and atmospheric humidity sensors, net radiometer and an estimate of soil heat flux (G) are required.

3. Energy balance (Remote sensing) techniques

Traditional micrometeorological, climatological, and hydrological methods, usually developed and validated at local scales, are difficult to use in the estimation of regional turbulent heat fluxes over heterogeneous land surfaces. Remote sensing technology has brought the hope to overcome this difficulty due to the efficient temporal and large spatial coverage provided by satellite observations of land surfaces. Remote sensing techniques use satellite radiometric data for the estimation of ET over a larger spatial scale. Remote sensing techniques use the principle of energy balance where ET is estimated as residue after other energy components are determined. The general energy balance equation is expressed as:

$$R_n = \lambda E + H + G \quad (1.5)$$

where R_n is the net radiation (W/m^2), H is the sensible heat flux (W/m^2), and G is the soil heat flux (W/m^2).

1.7. Outline of the thesis

The outline of this thesis is explained briefly as follows:

In chapter one the general introduction, research problem, research objectives, research questions, hypotheses, and background and literature review is explained.

Chapter two contains the general description of the study area; the climate condition, flooding pattern, the cropping pattern and the soil condition are explained.

In chapter three the materials used for data collection and the type and the extent of data collected for this thesis were explained.

Chapter four is about the general methodology of the thesis. It contains four sub sections; the first section is about the different types of ground based conventional methods, the second is about the micro-meteorology, the third is about the general remote sensing methods, and the last section is about the SEBS algorithm.

In chapter five the collected data from different stations and sensors are analysed.

In chapter six results are presented. The results from different ground based are compared. The spatio-temporal variation of ET over the entire Fogera flood plain and over the rice field is presented.

Finally in chapter 7 conclusions and recommendations are presented.

2. Study area

2.1. General

Fogera flood plain is found north western part of Ethiopia, about 625 km far from the capital Addis Ababa, and about 60 km north of Bahir Dar town. Fogera is known by its flat terrain.

Fogera administrative district (locally called “woreda”) is one of the 105 woredas in the Amhara regional state in Ethiopia. It is under the Debub Gondar Zone, Fogera Woreda is bordered on the south by Dera, on the west by Lake Tana, on the north by Kemekem, and on the east by Farta woreda. The towns in this woreda are Woreta and Amed ber, Woreta is the capital of the woreda. The Rivers pass through this woreda include the Gumara and Ribb, with catchments area of 1283 km² and 1302 km² (Abeyou, 2008) respectively. Both drain into Lake Tana.

Based on figures published by the Central Statistical Agency of Ethiopia in 2005, this woreda has an estimated total population of 256,496, of whom 125,530 were males and 130,966 were females; with an estimated area of 1,095.00 square kilometers, Fogera has an estimated population density of 234.2 people per square kilometer.

The Fogera flood plain found at the west end of the woreda, bounded by Lake Tana in the west, the Gumara river in south, Ribb river in the north, and the Bahir Dar–Gondar road in the east. The location of the flood plain is bounded in 11°45’N to 12°03’N and 37°29’E to 37°49’E, it is approximately about 15 km east-west and 34 km north-south. It has an elevation of about 1800m amsl. SMEC (2007) reported the area of the flood plain to be about 490 km².

The Fogera flood plain is the largest flood plain around Lake Tana, Dembia and Berha Ambo flood plains are located north of the lake with maximum inundation area of, 290 km² and 63 km² respectively (SMEC, 2007).

2.2. Flooding patterns

The Fogera flood plain is frequently affected by flood due to 13 small catchments that contribute runoff to the flood plain with a total drainage area of about 658 km² (SMEC, 2007), overtopping of the Gumara and Ribb rivers over the banks, Tana water level increase and the direct rainfall on the area contributes also for flooding. Due to the flat terrain of the area, the flooding water rarely drains. Because of this reason, the soil is wet for longer period even after the rainy season is over.

There have been many destructive floods recorded in the years of 1996, 1998, 1999, 2000, 2001, 2003 and 2006. The 1996 flood set a new record for flooded area, while 2006 flood was recorded with its long duration and damage (Dagnachew and Woubet, 2008). In the year 2006, the heavy rain, caused rising of the Lake level, overtopping of Ribb and Gumara rivers and high volume of water flow in the smaller catchments, making thousands of people homeless. Thousands of heads of cattle death and

loss of whole silos of grain, and significant tracts of grazing and farmland were washed away. The flood plain is shown in Fig.2-1.

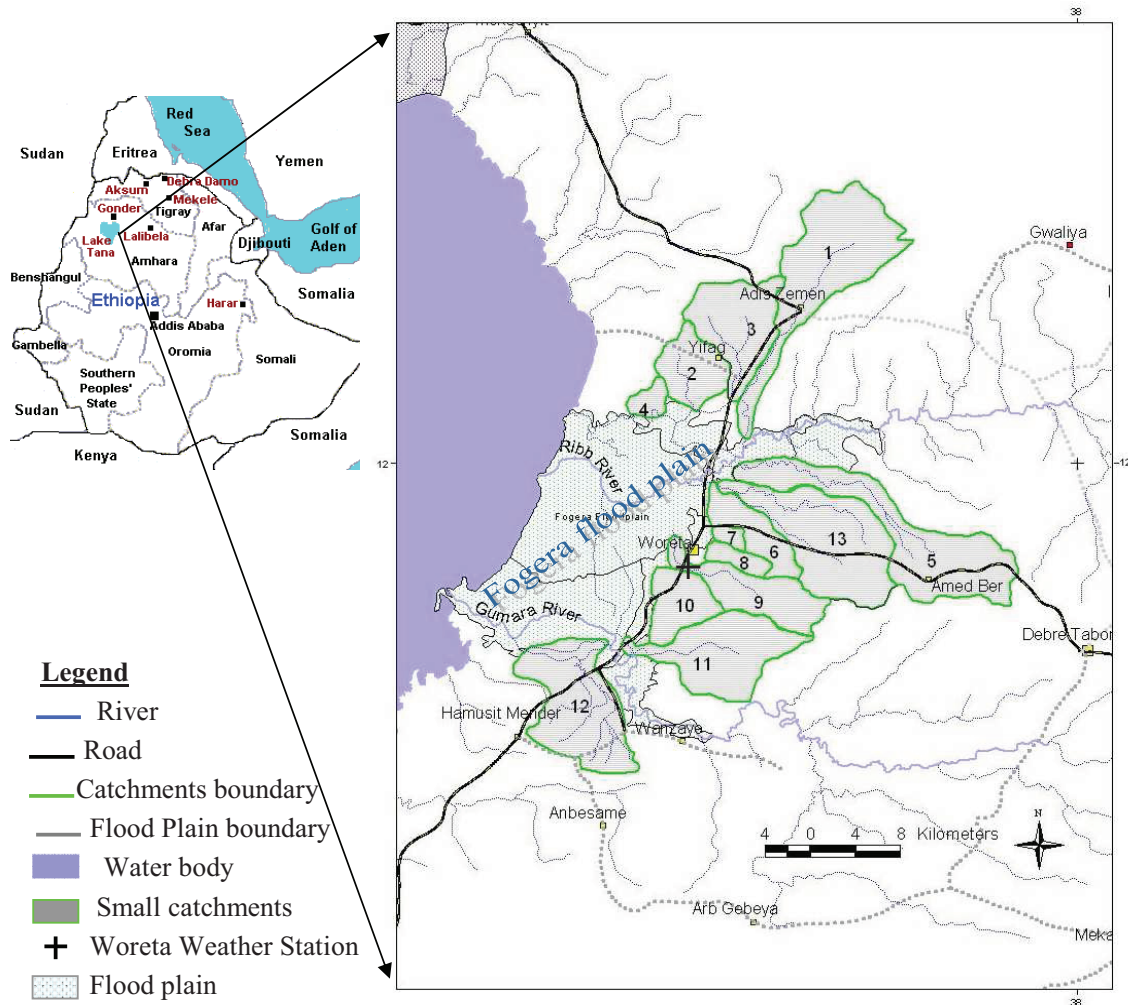


Figure 2-1 Location map of the Fogera flood plain
(Source: SMEC report, 2007)

2.3. Climate

The climate of the area is mainly controlled by the seasonal migration of Inter tropical convergence zone. Total annual rainfall in the flood plain ranges from about 1100 mm to 1530 mm/year. The mean monthly temperature of the area is about 19 °C, monthly mean maximum temperature of about 27.3 °C, and monthly mean minimum temperature is 11.5 °C (Dagnachew and Woubet, 2008). The rainy season in this area starts in June and ends in September. The mean monthly rainfall in the flood plain ranges from 0.4 mm in January to 414 mm in August, and with mean annual rainfall of 1296 mm. The monthly rainfall distribution in a year is shown in Fig.2-2, and the mean monthly maximum, mean, and minimum temperature is shown in the Fig. 2-3.

The Thiessen polygon rainfall distribution from the five weather stations around the flood plain was done for the years (2004-2007). Out of the total mean annual rainfall over the flood plain, 67.4% of the area was covered by the Woreta station record. The rest, 19.5%, 7%, 3.1% and 3% of the area were contributed by, Wanzaye, Yifag, Amedber and Addis Zemen station records respectively.

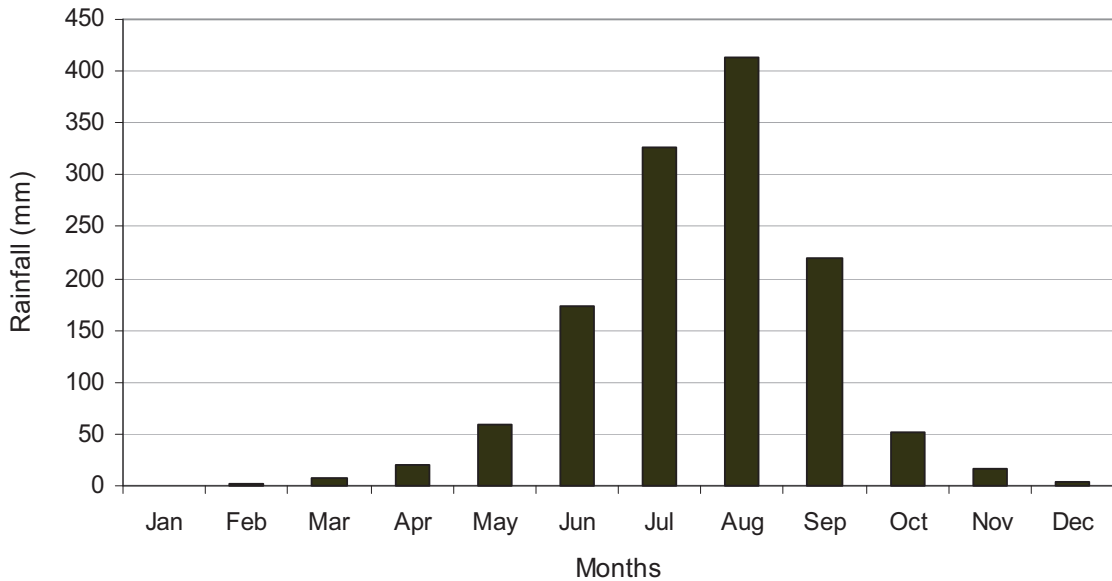


Figure 2-2 Mean monthly rainfall distribution (2004 -2007)

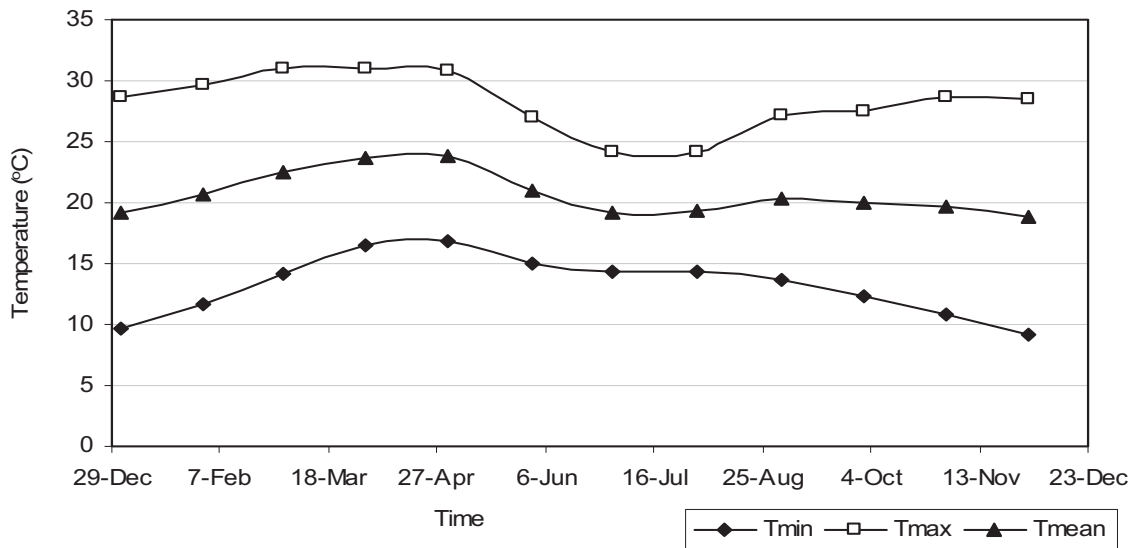


Figure 2-3 Mean monthly maximum, mean, and minimum temperature

The monthly runoff in the rivers varies from a minimum value of 1.9 m³/s and 16.8 m³/s in May, 2003 to a maximum value of 2602.8 m³/s and 6250 m³/s in August, 1996 and the mean monthly flow rate in the rivers was 460 m³/s and 1132 m³/s in Rib and Gumara rivers respectively.

2.4. Soils

The major soil types in the Fogera woreda exhibit a general relationship with altitude and slopes. Vertisols and Fluvisols are generally dominating soil types in the woreda and especially the lowland flat plains, valley bottoms and river terraces. Texturally these soils are sandy clay and sandy loam respectively (Dagnachew and Woubet, 2008).

Fluvisols are soil types where sedimentary structures are clearly recognizable in the soil profile. This type of soil is usually found on level topography, usually flooded by surface water and/or ground water rising; like river flood plains, deltas and coastal lowlands like Woreta flood plain.

2.5. Crop type and cropping pattern

The area is predominantly agricultural land with some grass land. The main growing period over the area is in the rainy season, from June to November. The majority of the agricultural land was covered by the rice crop during this period. Maize and teff are the other common crops in the area.

These days rice is the main and widely growing crop in the Fogera flood plain. The first rice produced in this area was in 1992, and wide production was started in 1997 (Personal communication with the local people). Rice is resistant to water logging and the area is water logged for longer period during the rainy season. This makes the Fogera flood plain best for rice production. Rice is usually sowed in June, although it depends on the rainfall distribution. The majority of the rice growing in this area is species known to be X-Jigna, named after the name of local place called Jigina. This species will be ready for harvesting after about 5 months (Personal communication with the local people).

The other main crops in the area are maize, teff and other cereals. Maize is sowed in May and harvested in October, where as teff is sowed in July and August and harvested in November and December. After harvesting of the rainy season crops, land will be prepared for the second cropping pattern like chickpea, onions or tomato. (Personal communication with the local people). The local people used to grow crops and vegetables following the rainy season using supplemental irrigation. The Gumara and the Rib Rivers are widely used for local irrigation scheme in the dry season.

The land use/cover classification made from Landsat decadal product of October, 2005, show that about 80% of the flood plain was used for agricultural purpose and the rest 13%, 5% and 2% was grass land, forest and water body respectively. The classified land use map is shown in the Fig. 2-4.

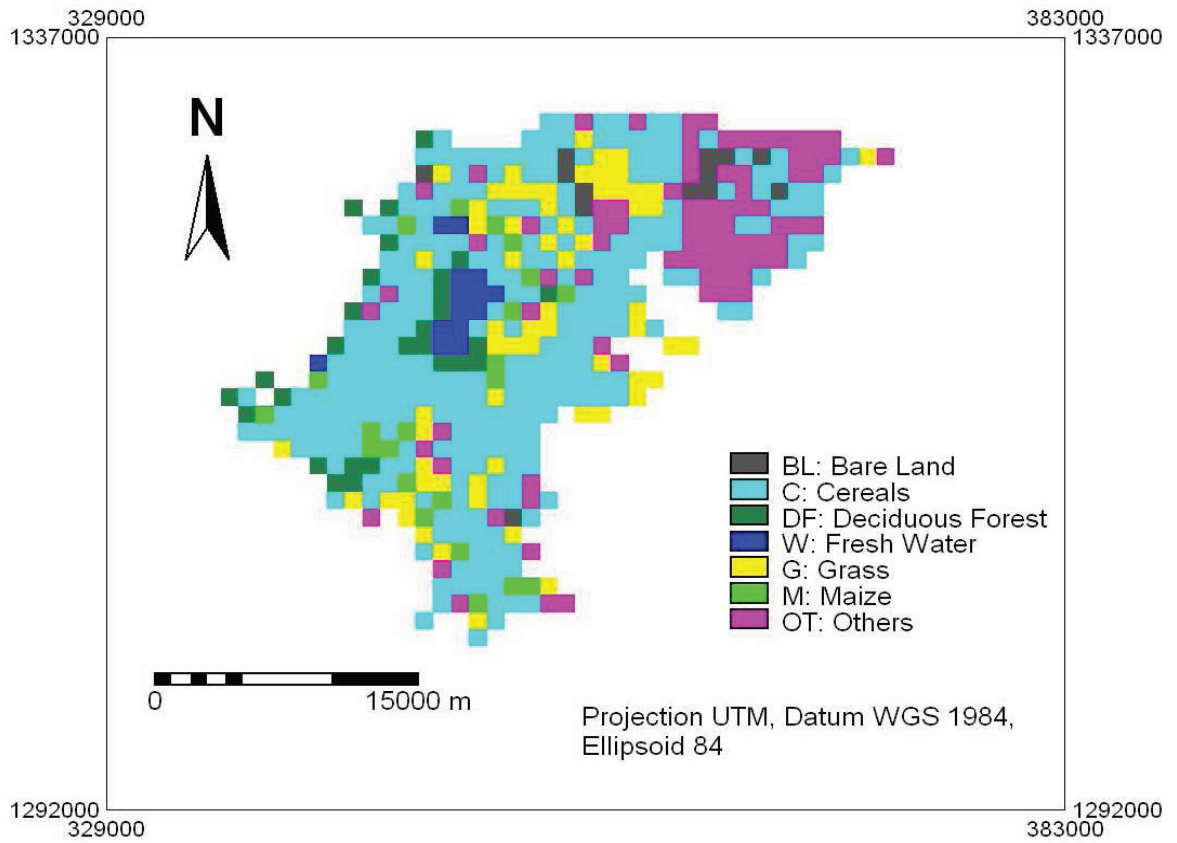


Figure 2-4 Land use map of the Fogera flood plain



Figure 2-5 Rice field in the flood plain Photo taken (September 2008)

3. Materials and data

3.1. Materials

3.1.1. Woreta weather station (WWS)

A new weather station was installed in the Fogera flood plain in June, 2008, near Woreta town. This weather station, hereafter called Woreta weather station (WWS) was located at $11^{\circ} 54' 22''$ N and $37^{\circ}41'26''$ E, at east end of the flood plain about 2 km south of the Woreta town. From the SRTM digital elevation model, the elevation of the weather station is 1811 m. The sensors mounted in this weather station are: pyranometer (measures the incoming solar radiation), relative humidity, temperature, wind speed, wind direction, soil moisture and soil temperature sensors. These sensors are connected with a HOBO datalogger which data is recorded at averages of 5-minute. The weather station pictures are shown Fig.3-1.

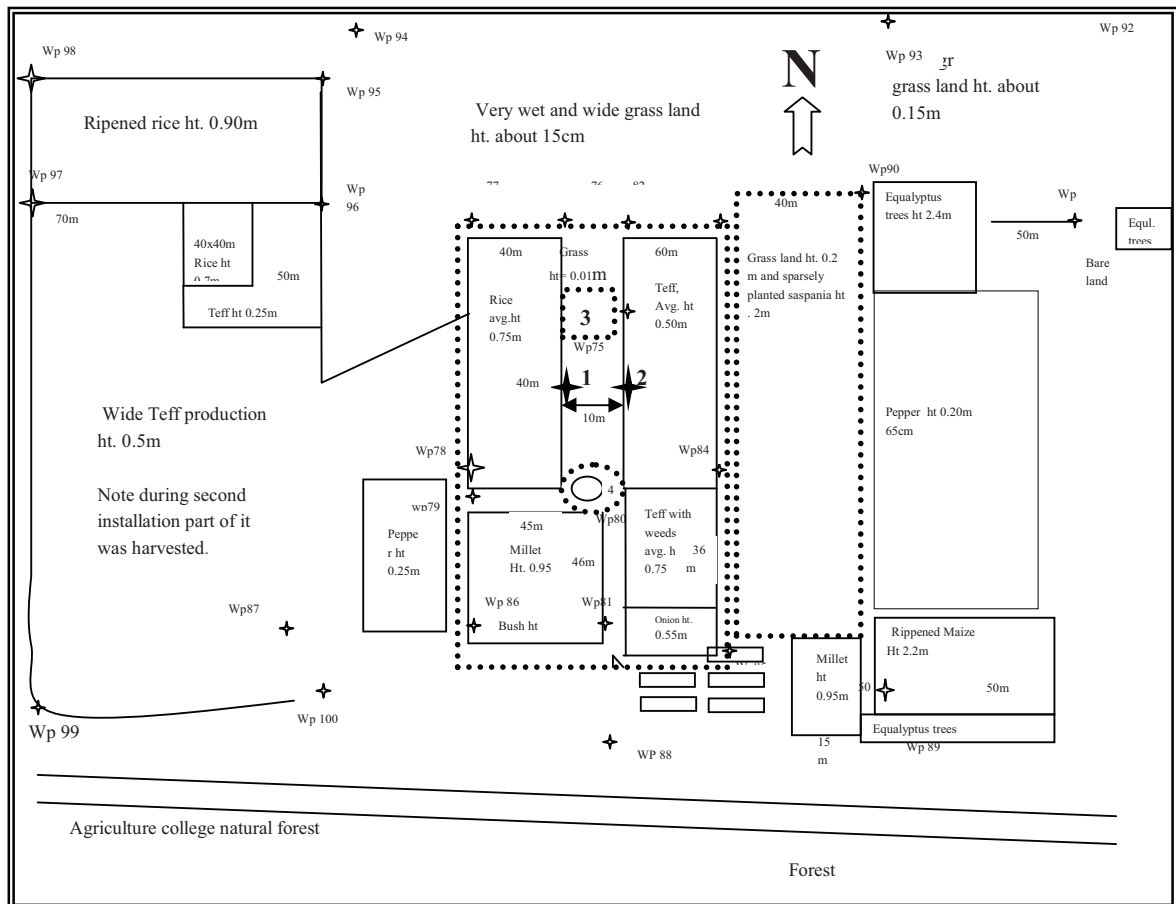


Figure 3-1 The Woreta weather station installed on 23 June 2008 at about 2 km from Woreta town.

3.1.2. Eddy flux tower

A Field campaign was arranged in September, 2008 in the study area. During this period different equipment were used to collect data. During this field campaign an eddy flux tower was installed east of the study area at a location of $11^{\circ} 54' 22''$ N and $37^{\circ}41'26''$ E with in 20 m distance from the new Woreta weather station, near the previous Woreta Agricultural College at about 2 km south of Woreta town. The eddy flux tower was made from wooden mast, mounted with the sonic anemometer (CSAT3, Campbell Scientific Inc. Logan, Utah, USA), net radiometer (CNR1, Kipp & Zonen, Deft, The Netherlands), and humidity and temperature sensors. These sensors were connected to the

Campbell Scientific data logger (CR5000). The location of the weather station and eddy flux tower installed is shown in Fig. 3-2 and the sketch of the eddy flux tower installed is shown in Fig.3-3.



NB: Not to scale

Legend

1, 2 - Locations of the eddy flux tower

3 - Location of weather station

.... Fences around the weather station

Figure 3-2 Plot of location of the Woreta weather station and eddy flux tower

3.1.3. Sonic anemometer (CSAT3)

The sonic anemometer (CSAT3, Campbell Scientific Inc. Logan, Utah, USA) measures the sonic temperature, T_s and wind speed in three directions u , v (horizontal), and w (vertical). This data was measured at a frequency of 20 Hz.

The CSAT3 used in eddy covariance principle to measure the turbulent fluctuations of horizontal and vertical wind. From the turbulent wind fluctuations, momentum flux and friction velocity will be calculated. (<http://www.campbellsci.com/csats3>). The sonic anemometer was installed at a height of 3.3 m above the ground level.

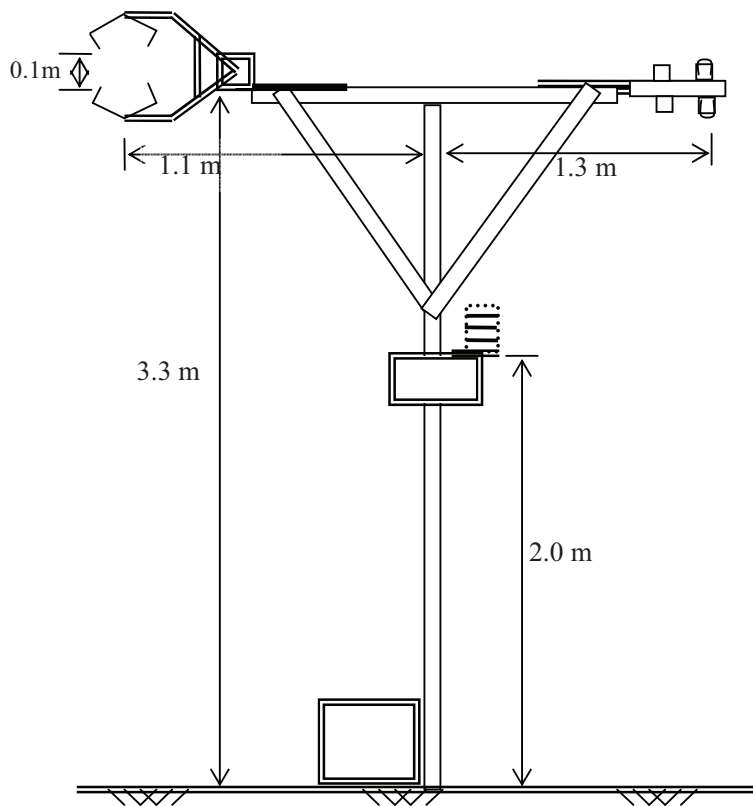


Figure 3-3 Eddy flux tower



Figure 3-4 Flux tower installed during the field campaign

3.1.4. Net radiometer (CNR1)

The four component net radiometer (CNR1, Kipp & Zonen, Deft, The Netherlands) measures the incoming short-wave and long-wave infra red (IR) radiation and surface-reflected short-wave and outgoing long-wave IR radiation. It consists of a pyranometer and pyrgeometer pair that faces upward and a complementary pair that faces downward. The pyranometers and pyrgeometers measure shortwave and far infrared radiation, respectively. All four sensors were calibrated to an identical sensitivity coefficient. The radiometer's internal temperature measured using a built in PT100 resistance. The sensor has a response time of 18 seconds and an expected accuracy for daily totals of $\pm 10\%$. (<http://www.campbellsci.com/cnr1>). The data was collected at a frequency of 1/3 Hz and recorded every 5 minutes in the data logger. It was mounted on the wooden eddy flux tower at the same level with sonic anemometers shown in the Figures 3-3 and 3-4.

3.1.5. Datalogger (CR5000)

CR5000 is a high performance, integrated datalogger/data acquisition system with a built-in keyboard, graphics display, with a card slot. It is used for high speed environmental applications. It works with the LoggerNet computer program. All the sensors on the flux tower were connected to the (CR5000, Campbell Scientific Inc. Logan, Utah, USA data logger). The logger records the data from the sensors at every 5 minutes average. (<http://www.campbellsci.com/cr5000>). The CR5000 data logger used is shown in Fig. 3-5.



Figure 3-5 CR5000 data logger

In addition Etrex Garmin Global Positioning system (GPS) was used for collecting land cover/land use data and global positions for geo-referencing satellite images.

3.2. Data

Prior to, during and after the field work period different data were collected. These are: meteorological data, eddy flux tower data, GPS data and remote sensing data.

3.2.1. Meteorological data

During the field campaign, meteorological data was collected from Bahir Dar meteorology branch office for the stations near flood plain for the period of 2004 to 2007. The station names and data collected are listed in the Table 3-1.

Table 3-1 Stations and type of data collected for (2004-2007)

Station name	Coordinate of station		Type of data collected in the stations					
	X	Y	RF	Tmax	Tmin	RH	SS	WS
Bahir Dar	324382	1280212	x	x	x	x	x	x
Woreta	357442	1318334	x	x	x			
Wanzaye	356145	1303734	x	x	x			
Amdber	368276	1312592	x	x	x			
Yifag	360220	1338024	x					
Addis Zemen	366661	1342283	x	x	x			

where RF - rainfall, T_{max} - maximum daily temperature, T_{min} - minimum daily temperature, RH - Relative humidity, SS - sunshine hours and WS - wind speed.

3.2.2. Woreta weather station data

The weather variables recorded in this new station are air temperature, relative humidity, air pressure, incoming solar radiation, wind direction, wind speed, soil temperature and soil moisture at depths of 10 cm, 25 cm and 50 cm; these variables are observed at frequency of 1Hz and the average was recorded at 5 minutes interval with the HOBO data logger. This weather station has four months of record. The five minutes interval weather variables data was collected during the field campaign. The data was recorded in the format shown in Table 3-2.

Table 3-2 Part of Woreta weather station data

No.	Time GMT+3:00	Air			Wind	Wind	Soil moisture		Solar Rad.	Soil Temp.	
		Temp. (°C)	RH (%)	Pressure (mbar)	Speed (m/s)	Dir. (°)	10 cm (m ³ /m ³)	25 cm (m ³ /m ³)	(W/m ²)	10 cm (°C)	25 cm (°C)
	6/23/2008										
1	16:40	25.4	54.9	819.05	4.1	299	0.262	0.223	503.1	25.31	24.58
	6/23/2008										
2	16:45	24.9	56.1	819.25	3.7	307.5	0.263	0.223	186.9	25.33	24.58
	6/23/2008										
3	16:50	24.5	56.7	819.35	3.9	294.8	0.263	0.223	144.4	25.33	24.60
	6/23/2008										
4	16:55	24.2	56.3	819.55	3.9	294.8	0.263	0.223	120.6	25.36	24.60
	6/23/2008										
5	17:00	24.1	57.5	819.65	3.5	286.4	0.263	0.223	101.9	25.38	24.60
	6/23/2008										
6	17:05	23.8	58.8	819.75	3.3	296.2	0.263	0.223	84.4	25.38	24.63

3.2.3. Eddy flux data

The eddy flux was installed on September 22, 2008 and data was collected until Sep. 25, 2008. The flux tower was removed for some time and reinstalled on Sep.28 morning and finally removed on September 29, 2008. During this period three full days' data and three partial days' data were collected from the eddy flux tower. The three full days' data are, Sep.23, 24 & 28, and the three partial days' data are Sep. 22, 25 and 29.

For the above mentioned durations wind speed in three directions and the sonic temperature measured at 20 Hz with the CSAT3, the short wave solar radiation incoming and outgoing and infrared long wave radiation incoming and out going measured at 1/3 Hz with CNR1, and the temperature and relative humidity data was collected from the CR5000 data logger. The net radiometer, relative humidity and the air temperature five minute's interval data was recorded in the format shown in the Table 3-3.

Table 3-3 Part of the net radiometer (CNR1) data

Time GMT+3:00	Rsi (W/m ²)	Rso (W/m ²)	Rli_Rsens (W/m ²)	Rli_Rsens (W/m ²)	Resistance (ohm)	Tsensor (°C)	Tair (°C)	RH (per thousand)
9/22/2008 13:55	134.815	19.883	-82.557	0.946	1.093	24.01	23.47	749.52
9/22/2008 14:00	128.675	19.341	-79.639	0.841	1.092	23.68	23.41	832.48
9/22/2008 14:05	119.660	18.232	-76.903	1.855	1.091	23.38	23.31	843.24
9/22/2008 14:10	114.465	17.460	-76.210	2.241	1.090	23.18	23.29	844.59

3.2.4. GPS data

Ground truth data was collected during the field work period using GPS. Part of the data is shown in the Table 3-4.

Table 3-4 Part of GPS data collected

Way Point	North (Decimal degree)	East (Decimal degree)	Description
11	11.95035	37.71012	In the east wide rice, west wide rice field
12	11.95035	37.71012	Road crossing to Debre Tabor
13	11.97182	37.7091	In the east grassland + rice, west wide rice field
14	11.98937	37.71063	East, wide rice field, west wide rice field
15	11.99348	37.71095	On culvert, east rice, west some eucalyptus tree, and rice
16	12.00095	37.71173	East, wide rice field, west wide rice field

3.2.5. Remote sensing data

Instantaneous and composite MODIS products were collected. The eight-day composite reflectance (MOD09A1), eight-day composite leaf area index (MOD15A2) and the daily land surface temperature (MOD11A1) products were collected from MODIS ftp site: (<ftp://e4ftl01u.ecs.nasa.gov/MOLT/>). Two Instantaneous images (MOD021KM) and its respective geo-location files (MOD03) were acquired from Level 1 and Atmosphere Archive and Distribution System (LAADS) ftp site:

(<ftp://ladsweb.nascom.nasa.gov/allData/5/>). With respect to this, MODIS atmospheric products of aerosol optical depth and water vapour content data were collected from LAADS site, (http://ladsweb.nascom.nasa.gov/browse_images/l2_browser.html?form=AADS&browsetype=Level+2) From the web site (http://jwocky.gsfc.nasa.gov/teacher/ozone_overhead_v8.html), the ozone content data was collected. The MODIS products, collected are shown in Table 3-5.

Table 3-5 Collected and downloaded MODIS products

Short name	Product Type and name	Raster type	Resolution (m)	Temporal granularity
MOD09A1	Surface Reflectance Bands 1-7	tile	500	8 day
MOD11A1	Land Surface Temperature and Emissivity	tile	1000	daily
MOD15A2	Leaf Area Index-FPAR	tile	1000	8 day
MOD021KM	Instantaneous Image Product	swath	250-1000	instant
MOD03	Geo-location file	swath	-	instant

In addition, Landsat decal product image was collected from website:

http://glovis.usgs.gov/ImgViewer/Java2ImgViewer.html?limitMissions=FALSE&mission=LANDSAT_ARCHIVE&sensor=SLCOFF&lat=11.5&lon=36.9, for land cover classification.

4. Methodology

4.1. General

This chapter deals with four subsections. The first is about ground based conventional evapotranspiration (ET) estimation methods. The second is about micrometeorology, the third is about detailed remote sensing methods and the last is about the SEBS algorithm. The general methodology followed in this thesis is explained in the Fig. 4-1.

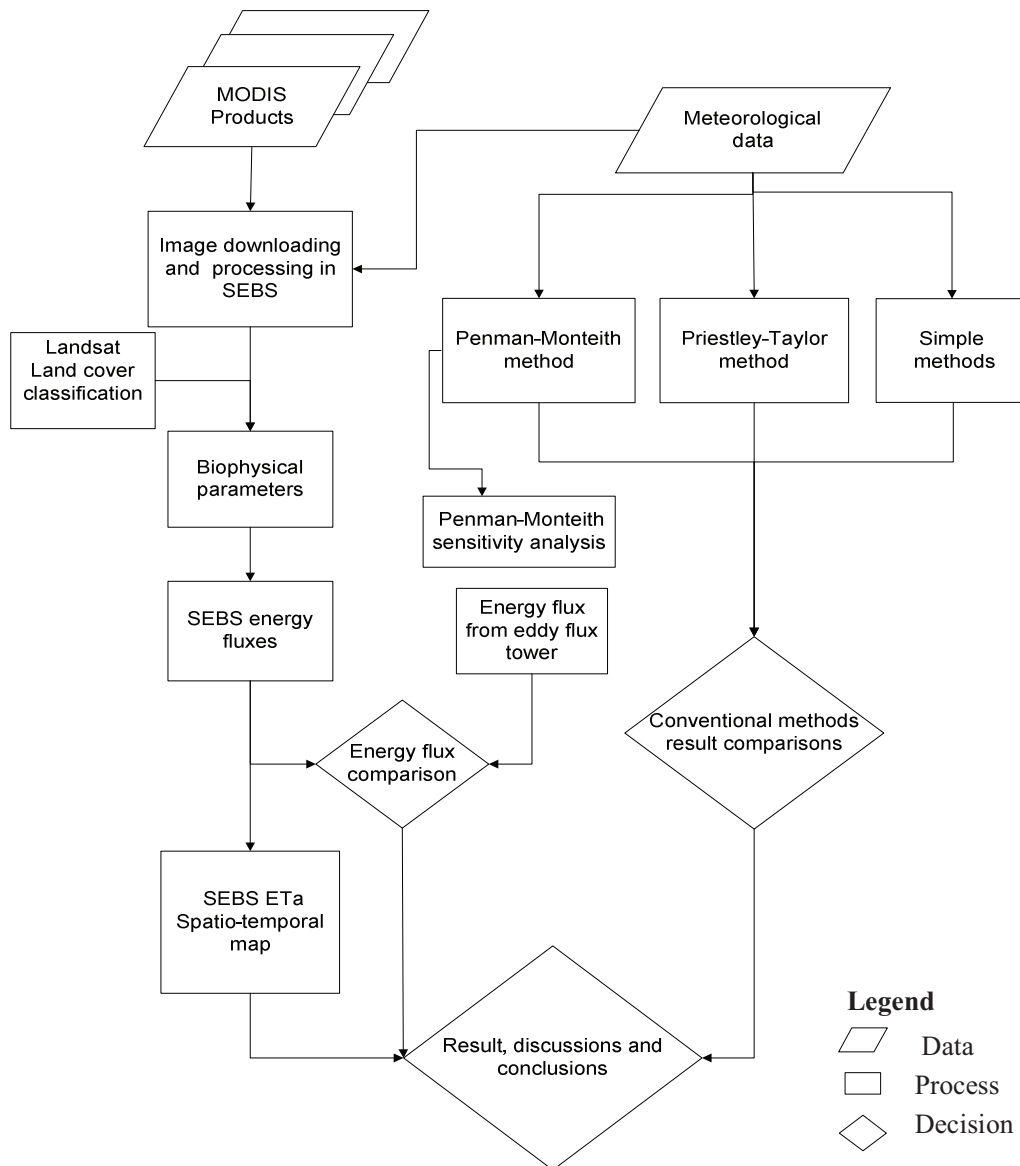


Figure 4-1 General methodology flow chart

4.2. Ground based evapotranspiration estimation methods

Information on evapotranspiration (here after called ET), or consumptive water use, is significant for water resources planning and irrigation scheduling. In this study the following methods will be used for the estimation of ET over the Fogera flood plain. Using the under mentioned methods the reference/actual evapotranspiration will be estimated in the year 2008, and the results of these methods will be compared with Penman-Monteith method, which is globally accepted as a standard method. Finally sensitivity analysis for P-M reference ET to the input variables will be done.

4.2.1. Penman-Monteith method

The Penman-Monteith equation (Monteith, 1965; Penman, 1948), is a physically based combination approach that incorporates energy and aerodynamic considerations has been commonly used for plant canopies. The Penman-Monteith (here after called P-M) equation produce direct estimates of actual ET (ET_a), but require knowledge of the P-M canopy resistance (Sumner and Jacobs, 2005). Generally P-M equation gives acceptable ET estimates for practical applications (Widmoser, In press). This method requires measurement of net radiation, soil heat flux, air temperature, relative humidity, and wind speed. The calculation of the net radiation and the assumption of soil heat flux were following the FAO-56 methodology. Reference evapotranspiration (ET_o) is the potential ET from a hypothetical green grass of uniform height, 0.12 m, well watered, and a constant albedo of 0.23 with fixed surface resistance of 70 s/m (Allen, 1998). The Penman-Monteith method, which is considered as a global standard method (Bois et al., 2008; Dingman, 2002; Gieske, 2003; Rana and Katerji, 2000) and it is widely used globally.

After the aerodynamic resistance, $r_a = 208/u_2$ and the surface resistance $r_s = 70$ s/m are estimated; for the reference crop, the general Penman-Monteith equation (A-1) of Appendix A can be rewritten as:

$$ET_o = \frac{0.408\Delta(R_n - G) + \gamma \frac{900}{T + 273} u_2 (e_s - e_a)}{\Delta + \gamma(1 + 0.34u_2)} \quad (4.1)$$

where ET_o is reference evapotranspiration (mm/day),

R_n is the net radiation at the crop surface (MJ /(m^2 day)),

G is the soil heat flux density (MJ /(m^2 day)), assumed to be zero, on daily bases.

T mean daily air temperature at 2 m height ($^{\circ}C$),

u_2 wind speed at 2 m height (m /s),

e_s saturation vapour pressure (kPa),

e_a actual vapour pressure (kPa),

$e_s - e_a$ saturation vapour pressure deficit (kPa),

Δ slope vapour pressure curve (kPa/ $^{\circ}C$),

γ psychrometric constant (kPa / $^{\circ}C$).

The detailed computations of each input for ET_o are shown in Appendix A.

4.2.2. Priestley-Taylor method

The Priestley-Taylor (1972) equation was developed for open water and wet land surfaces, so Priestly-Taylor (here after called P-T) equation gives better results (Brutsaert, 2005) when soil moisture is not a limiting factor for evapotranspiration. Fogera flood plain is wet for longer period in the year. That is why this method was selected as one of the methods in the determination of ETo in the Fogera flood plain. Here, the P-T ETo estimation will be evaluated with, the standard P-M method and locally applicable coefficient will be proposed for the study area. P-T equation requires measurement of net radiation, soil heat flux, and air temperature. The P-T equation is expressed as:

$$ET_o = \alpha \left(\frac{\Delta}{\Delta + \gamma} \right) \left(\frac{R_n - G}{\lambda} \right) \quad (4.2)$$

where α is usually taken as 1.26, ET_o is in mm/day, input parameters as mentioned in equation (4.1).

It was reported that the coefficient α varies in the range of 1.3 ± 0.03 for wet land surfaces (Priestley and Taylor, 1972), $\alpha=1.74$ for arid climates, and $\alpha=1.26$ in humid climates.

4.2.3. Modified Makkink method

The modified Makkink method is widely used method in west Europe (Hiwot, 2008). It is a modified P-T equation, which uses incoming solar radiation instead of net radiation (Brutsaert, 2005). Here it is applied to test the applicability of the model in the Fogera flood plain area. This method is one of the simplest radiation models: it requires only the average air temperature and the incoming solar radiation. In the same way this will be compared with P-M method and locally calibrated coefficient will be proposed. The modified Makkink method is defined as (De Bruin, 1981):

$$ET_o = 0.65 \frac{\Delta}{\lambda(\Delta + \gamma)} R_s \quad (4.3)$$

where R_s is the incoming solar radiation MJ/(m² day).

4.2.4. Simple Abtew equation

This method requires only single parameter, solar radiation for estimation of ET. The method was tested in wetlands and open waters in different places and found to give a comparable result with complex methods (Abtew, 1996; Assefa and Nangia, 2005; Assefa et al., 2008). This simple method gives actual ET when soil moisture is not a limiting factor for ET and in drier conditions it gives potential ET (Abtew, 1996).

$$ET = k \frac{R_s}{\lambda} \quad (4.4)$$

where ET (mm/day) is the daily evapotranspiration from wetland or shallow open water k is taken as 0.53, this coefficient could be adjusted according to the local situation (Abtew and Obeysekera, 1995). If this method performs well in the study area ET will be calculated easily on daily basis from the radiation data only. A locally calibrated coefficient will be proposed for the study area, after comparing the result with the Penman-Monthieith reference ET.

4.2.5. Penman-Monteith sensitivity analysis

A sensitivity analysis is an important technique to improve understanding of the dominant climatic variables in the estimation of reference ET (ET_o) in an area of interest. Reference ET is a measure of evaporative power of the atmosphere. ET_o is independent of the crop type, the age of the vegetation and management practices. This could be estimated from the meteorological data only. Sensitivity of ET_o to the input variables vary with space and time (Gong et al., 2006). “In humid climate, reference evapotranspiration provides an upper limit for actual ET and in an arid climate it indicates the total available energy for actual ET” (Gong et al., 2006).

For sensitivity analysis of P-M ET_o, incoming solar radiation MJ/(m² day), relative humidity (%), air temperature (°C), and wind speed (m/s) inputs were selected. Sensitivity was done on monthly basis. The average of weather variables mentioned above were taken over a month and sensitivity analysis was done increasing and decreasing by 10 %, 20 % and 30 % from the average value of these variables for each run. To avoid nonsense computations in the sensitivity analysis of minimum and maximum temperature and relative humidity, the average air temperature and relative humidity and their amplitudes were calculated (Bois et al., 2008). The minimum and the maximum values were taken under considerations while sensitivity for these variables was done. For the calculation of net radiation solar angles of 15th of each month were used. This was done for all months in a year 2008. In this analysis it was assumed that the maximum and minimum temperature and relative humidity increase and decrease simultaneously in the analysis of the respective variables. As there was no maximum and minimum relative humidity record at Bahir Dar station, the mean daily relative humidity was used for the sensitivity analysis. Sensitivity analysis for the months from July to October, 2008 the Woreta weather station data was used, while, for the rest of the year, the Bahir Dar station data was used as there was no record in the Woreta station during this period.

4.3. Micrometeorology

As explained in the previous chapters, field work was arranged in the study area. During the field work period, an eddy flux tower was installed in the study area near the weather station at a distance of about 20 m from the Woreta weather station. Measurements were made with the sensors mounted on the flux tower. Three full days’ data and three other partial days’ data were collected during the field campaign. The sonic anemometer (CSAT3) measures at a frequency of 20 Hz and the net radiometer at a frequency of 1/3 Hz. Sensible heat flux and the friction velocity were calculated at half-hourly intervals using ECPACK software from eddy covariance data. Net radiation was averaged and stored at five minutes interval in the data logger during the measurement period, which is averaged over half hour period.

4.3.1. Sensible heat flux and friction velocity

The eddy flux data was analyzed and sensible heat flux (H) and friction velocity (u_*), and the mean wind speed in the three orthogonal directions were calculated with ECPACK software. ECPACK is open source software with a complete data analysis package that computes fluxes from eddy-covariance data. This software can be obtained from the website of the Meteorology and Air Quality Group of Wageningen University (under Research Joint Eddy-covariance Project) at:

(<http://www.unidata.ucar.edu/packages/netcdf>). From the sonic anemometer's wind speed and sonic temperature measurement, sensible heat flux was calculated as:

$$H = \rho_a c_p \overline{w'T'} \quad (4.5)$$

where H (W/m^2) is the sensible heat flux, ρ_a (kg/m^3) is the density of the air, c_p (J/kg K) is specific heat capacity of the air, $\overline{w'T'}$ is the covariance between the fluctuations of vertical wind speed and the sonic temperature. Friction velocity is a measure of the intensity of turbulence in the planetary boundary layer. This is calculated as:

$$u_* = \left(-\overline{v'w'} \right)^{1/2} \quad (4.6)$$

where u_* (m/s), is the friction velocity v' (m/s) is the horizontal instantaneous velocity fluctuation from the average, w' (m/s) is the vertical instantaneous velocity fluctuation from the average.

In the ECPACK software, the system was rotated in the mean wind direction and rotated in such a way that the mean vertical wind speed was zero, and the covariance of the fluctuations of the lateral horizontal wind speed when perpendicular to the main wind speed (v) and vertical wind speed was zero.

The data was prepared in such a way that sensible heat flux, friction velocity and wind speed were to be computed at half hour intervals.

Sensible heat flux was also calculated from ground measurements of vegetation height and radiometric surface temperature as:

$$H = -\rho_a c_p \frac{(T_a - T_s)}{r_{ah}} \quad (4.7)$$

where H is the sensible heat flux (W/m^2), T_a is the air temperature (K), T_s is the radiometric surface temperature (K), and r_{ah} is the aerodynamic resistance for heat transfer (s/m). Aerodynamic resistance for heat transfer was calculated as:

$$r_{ah} = \frac{\ln\left(\frac{z-d}{z_{om}}\right) \ln\left(\frac{z-d}{z_{oh}}\right)}{k^2 u} \quad (4.8)$$

where z (m) reference measuring height, d (m) zero plane displacement height, z_{om} (m) roughness height for momentum, and z_{oh} (m) roughness height for heat transfer.

From the measured vegetation height, horizontal wind speed and the computed friction velocity, roughness height for momentum transfer (z_{om}), roughness height for heat transfer (z_{oh}), and zero plane displacement height (d), have been computed as follows:

$$z_{om} = (z - d) e^{-\left(\frac{u}{u_*}\right)^k} \quad (4.9)$$

$$z_{oh} = 0.1z_{om} \quad (4.10)$$

$$d = \frac{2}{3} z_{veg} \quad (4.11)$$

where u is the measured horizontal wind velocity (m/s), u_* is the friction velocity (m/s), z_{veg} is the measured vegetation height around the eddy flux tower was 0.65m (m). k is the von Karman's constant (0.41). The slope of u/u_* best fit line was used for the estimation of roughness height in equation (4.9).

The roughness height for momentum transfer computed from equation (4.9) and equation (4.18) were compared to each other and with the estimation from the remote sensing technique using SEBS (Su, 2002) algorithm equation (4.19). The sensible heat flux from the eddy flux tower was also compared with the remote sensing estimations.

4.3.2. Evaporative fraction

Evaporative fraction is defined as the ratio of latent heat flux to the available energy.

$$\Lambda = \frac{\lambda E}{R_n - G} \quad (4.12)$$

where Λ is evaporative fraction, $\lambda E = (R_n - G - H)$ is latent heat flux (W/m^2), R_n net radiation (W/m^2), G is soil heat flux (W/m^2) and, H is sensible heat flux (W/m^2) determined from equation (4.5). Soil heat flux from the measured soil temperature and radiometric surface temperature was estimated as:

$$G = -C_1 \left(\frac{T_1 - T_s}{z_1 - z_s} \right) \quad (4.13)$$

where $C_1 = 1.1$ ($\text{W/m}^\circ\text{C}$), is the thermal conductivity of soil for saturated silt and clay soils (Kersten, 1949), T_1 ($^\circ\text{C}$) is the soil temperature at depth of $z_1 = 0.1$ m, T_s ($^\circ\text{C}$) is the temperature at the surface z_s (m). Daily average evaporative fraction is defined as the ratio of the daily latent heat flux to the daily available energy. Where, the available energy is the difference of the net radiation and the soil heat flux. Soil heat flux is considered negligible on daily basis. Evaporative fraction is assumed to be constant over the daily basis (Hoedjes et al., 2008; Li et al., 2008; Su, 2002).

4.3.3. Radiation and temperature

The Woreta weather station has four months (July to October, 2008) records to be used for estimation of ET in the area. For the rest of the year the Bahir Dar weather station record were adapted for the estimation of ET by both remote sensing techniques and conventional methods. In addition during the field work period, the CNR1 was used to measure the net radiation from 22 -29 September, 2008. The robustness of data at the Woreta weather station and the eddy flux tower was checked by comparing the same variables from different sensors. The incoming solar radiation, air temperature and relative humidity were compared with one another.

CNR1 measures incoming and outgoing solar radiation, incoming and outgoing long wave radiation, and the sensor temperature. Here, the radiation due to temperature of the sensor was corrected during net radiation calculations. Net radiation is the sum of the net short wave radiation (R_{ns}) and the net long wave radiation (R_{nl}).

$$R_n = (1 - \alpha)R_s \downarrow + \varepsilon R_l \downarrow - \varepsilon \sigma (T_s)^4 \quad (4.14)$$

where α is the broad band surface albedo, σ Stefan-Boltzmann constant ($5.67 \times 10^{-8} \text{ W}/(\text{m}^2\text{K}^4)$), R_s is incoming short wave radiation (W/m^2), R_l is incoming long wave radiation (W/m^2), ε emissivity of the surface (for wet soil with vegetation 0.98 was assumed), T_s is radiometric surface temperature (K).

From the measured net long wave radiation radiometric surface temperature was calculated as:

$$T_s = \left(\frac{R_l \uparrow - (1 - \varepsilon)R_l \downarrow}{\sigma \varepsilon} \right)^{\frac{1}{4}} \quad (4.15)$$

Net radiation was also calculated both from measured solar radiation at WWS, and from measured sunshine hours at Bahir Dar station using FAO-56 method (Allen, 1998), explained in detail in Appendix A.

Daily net radiation was calculated from the daily broad band albedo and the daily transmissivity of the atmosphere as:

$$R_{n24} = (1 - \alpha_{24})\tau_{24}R_{a24} - a\tau_{24} \quad (4.16)$$

where R_{n24} is the daily net radiation $\text{MJ}/(\text{m}^2\text{day})$, α_{24} is the daily albedo, τ_{24} is the daily transmissivity, R_{a24} is the daily extraterrestrial solar radiation $\text{MJ}/(\text{m}^2\text{day})$ determined from equation (A.4) Appendix A, a is a coefficient determined from the CNR1 measurement of net radiation $\text{MJ}/(\text{m}^2\text{day})$. Teixeira (2008) recommends for the local calibration of daily atmospheric transmissivity (τ_{24}) and the coefficient “ a ” of equation (4.16). This was calibrated using the net radiation measurement at the site, during the field campaign. Atmospheric transmissivity was calculated from the ratio of the measured (and calculated) incoming solar radiation to extraterrestrial solar radiation for each day of the year. These calibrated values were used for the computation of daily net radiation in equation (4.16).

For months January to June, November and December 2008 there was no record of data in the new weather station. During this period the Bahir Dar weather station data was used for the estimation of ET both in remote sensing technique and ground based conventional methods. In addition, as the recent data of December was not yet available, the 2007 data was used. Bahir Dar area and the Fogera flood plain have similar climatic conditions. Both have almost similar elevations of about 1800 m. The correlation of the incoming solar radiation, relative humidity, daily maximum, daily minimum, and mean temperatures between the Bahir Dar and Woreta weather station records were checked for its suitability for estimation of ET in the Flood plain, see (chapter 5). The Bahir Dar data has only daily maximum and minimum temperature and daily mean relative humidity measurement.

4.3.4. Surface albedo

The measured incoming and outgoing solar radiation during the field campaign was used for the instantaneous albedo and the daily albedo computations. Daily albedo was computed as a ratio of the measured outgoing to the incoming solar radiation over the day from the CNR1 measurement. The instantaneous albedo computed from equation (4.21) during the satellite overpass was compared with the daily albedo observed from CNR1. This comparison was based on pixel level at the eddy flux tower. A correction coefficient was developed to be applied for the computations of daily net radiation, where there was no measurement of incoming and outgoing solar radiation.

4.4. Remote sensing

4.4.1. Introduction

In this study, MODIS (Moderate Resolution Imaging Spectroradiometer) on board of Terra, products were used for the estimation of ETa.

MODIS (Moderate Resolution Imaging Spectroradiometer) is an instrument aboard the Terra (EOS AM) launched in December 1999 and Aqua (EOS PM) launched in May 2002. Terra's orbit around the earth is timed so that it passes from north to south across the equator in the morning, while Aqua passes south to north over the equator in the afternoon. It has a viewing swath width of 2,330 km and views the entire surface of the earth every one to two days. Its detectors measure 36 spectral bands between 0.405 and 14.385 μm , with bands 1-19 and band 26 in the visible and near infrared range, and remainder bands are in the thermal range from 3 to 15 μm and it acquires data at three spatial resolutions of 250m, 500m, and 1,000m. MODIS wide spectral resolution and viewing swaths, makes measurements useful in a wide variety of earth system science disciplines.

(http://terra.nasa.gov/About/MODIS/modis_swath.html). MODIS technical specifications and some of the visible and thermal band widths are shown in Table 4.1 and 4.2 respectively.

Table 4-1 MODIS Technical specifications

Orbit:	705 km, 10:30 a.m. descending node (Terra) or 1:30 p.m. ascending node (Aqua), sun-synchronous, near-polar, circular
Scan Rate:	20.3 rpm, cross track
Swath Dimensions:	2330 km (cross track) by 10 km (along track at nadir)
Telescope:	17.78 cm diam. off-axis, a focal (collimated), with intermediate field stop
Size:	1.0 x 1.6 x 1.0 m
Weight:	228.7 kg
Power:	162.5 W (single orbit average)
Data Rate:	10.6 Mbps (peak daytime); 6.1 Mbps (orbital average)
Quantization:	12 bits
Spatial Resolution:	250 m (bands 1-2), 500 m (bands 3-7), 1000 m (bands 8-36)
Design Life:	6 years

Table 4-2 MODIS visible and some of thermal bands

Primary use	Band	Bandwidth (nm)	Spectral Radiance W/(m ² μm sr)
Land/Cloud/Aerosols	1	620 - 670	21.8
Boundaries	2	841 - 876	24.7
Land/Cloud/Aerosols	3	459 - 479	35.3
Properties	4	545 - 565	29.0
	5	1230 - 1250	5.4
	6	1628 - 1652	7.3
	7	2105 - 2155	1.0
Surface/Cloud	31	10780 - 11280	9.55 (300K)
Temperature	32	11770 - 12270	8.94 (300K)

4.4.2. MODIS products

The MODIS land products are produced and distributed by the Land Processes Distributed Active Archive Centre (LPDAAC), which is one of data centres within the NASA Earth Observing System Data and Information System (EOSDIS).

In this thesis MODIS Terra products were used for the retrieval of energy fluxes in the Fogera flood plain. MODIS products acquired include the land surface temperature, surface reflectance and leaf area index. All the products were acquired from collection 5, as shown in Table 4-3. Fractional vegetation cover, broad band albedo, and emissivity were retrieved using the SEBS algorithms.

Table 4-3 MODIS products acquired

Short name	Product type and name	Raster type	Resolution (m)	Temporal granularity
MOD09A1	Surface reflectance bands 1-7	tile	500	8 day
MOD11A1	Land surface temperature and emissivity	tile	1000	daily
MOD15A2	Leaf area index	tile	1000	8 day

MODIS Global products are tiled in to fixed grids of about 10° by 10°. A tile contains 1200 x 1200 grids in 1200 rows and 1200 columns. Each tile is assigned a horizontal (H) and vertical (V) coordinate from 0 to 35 horizontally and 0 to 17 vertically. The upper left corner of the tile was the starting point (0, 0) of coordinate, and the bottom right is (35,17). The Fogera flood plain lies in the tile horizontal and vertical coordinate of (21,7). The products under this tile were downloaded for further processing. These tiled products are archived with the sinusoidal projection. The global tile is shown in Fig. 4-2.

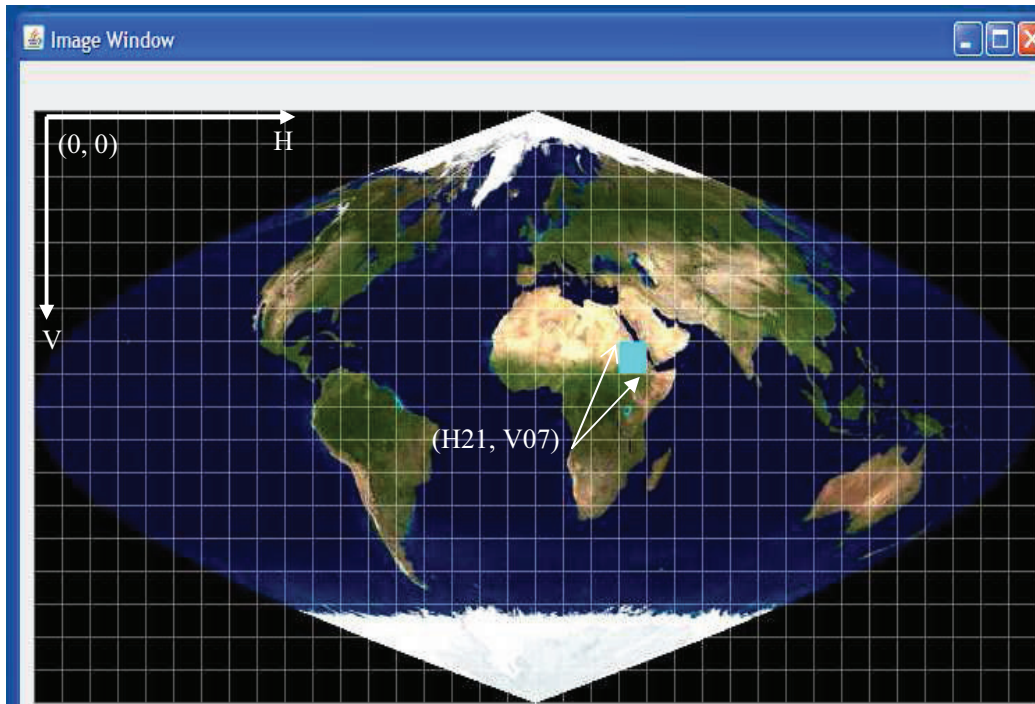


Figure 4-2 Global tiles with the respective tile of study area (35, 17)

These tiled products were re-projected, re-sampled and sub-mapped to the required study area using the open source Modis re-projection tool, downloaded from the MODIS data tools website. (<http://lpdaac.usgs.gov/datatools.asp>). The sub setting and re-projection parameters summarized in Table 4-4.

Table 4-4 Sub setting and re-projection parameters

Spatial sub setting	Latitude	Longitude
Upper left corner (X,Y)	320000	1380000
Lower right corner (X,Y)	420000	1280000
Out put file type	Geo-tiff	
Resampling type	Nearest neighbor	
Out put projection	UTM	
Out put pixel size	1000 m	
Zone	37	

4.4.3. Surface reflectance 8-day L3 global 500 m (MOD09A1)

MOD09 (MODIS Surface Reflectance) is a seven-band product computed from the MODIS Level 1B land bands of 1 (0.620-0.670 μm), 2 (0.841-0.876 μm), 3 (0.459-0.479 μm), 4 (0.545-0.565 μm), 5 (1.230-1.250 μm), 6 (1.628-1.652 μm), and 7 (2.105-2.155 μm). The product is an estimate of the surface spectral reflectance for each band as it would have been measured at ground level as if there were no atmospheric scattering or absorption. These products are corrected for the atmospheric effects.

It is an eight-day girded level-3 product in the sinusoidal projection. Each product pixel contains the best possible level 2 global product, observation during an 8-day period as selected on the basis of

high observation coverage, low view angle, absence of clouds or cloud shadow, and aerosol loading. Science data sets are included in the MOD09A1 product, these specific products with its detailed properties is shown in the Appendix B, Table B-2.

This products are validated stage 2, meaning that accuracy has been assessed over a widely distributed set of locations and time periods via several ground-truth and validation efforts. The MODIS reflectance product validation shows that there is best match between the global product, the actual observation and the result after atmospheric correction. Hence MODIS products can be used without considerable error in the final result.

The MODIS atmospheric correction algorithm was validated with Aerosol Optical Thickness (AOT), aerosol model and column water vapor derived from AERONET measurements within 30 minutes of the MODIS acquisition time, were used in 6S to perform atmospheric correction and provide a reference used in assessing the performance of the MODIS surface reflectance product (MOD09). The MODIS surface reflectance atmospheric correction is explained in detail in the Vermote and Vermeulen (1999).

Nowadays MODIS products are extensively used, which avoid time intensive atmospheric correction work. For example, Venturini et al. (2008), Shan (2007), Batra et al. (2006), and Nagler et al. (2005) have used MODIS products and reported good results. In this thesis, even though the eight day composite products were downloaded, the daily products were used. Because the study area is small, it was covered with a single day product except very few pixels for which a different day within the eight day composite were used. For this day, daily surface temperature was downloaded and used. Day of the year (DOY) product is shown in Fig. 4-3 for December 2007 and July 2008 as an example. These figures show that most pixels of the study area are covered by a single day image.

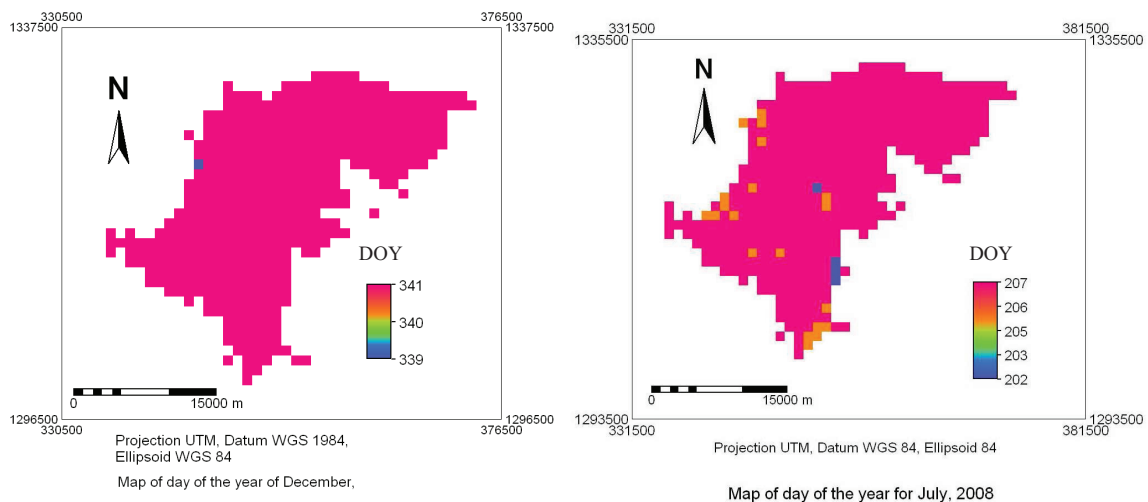


Figure 4-3 Day of the year product of (a) December 2007 and (b) July 2008

4.4.4. Land surface temperature (MOD11A1 daily LST)

MODIS is found particularly useful for the LST product, because of its global coverage, radiometric resolution and dynamic ranges for a variety of land cover types, and high calibration accuracy in multiple thermal infrared bands (<http://www.icess.ucsb.edu/modis/atbd-mod-11.pdf>).

The MODIS LST products are archived in Hierarchical Data Format - Earth Observing System (HDF-EOS) format files. These are the standard archive format. The LST product was developed by the principle of split window method (Wan, 2008). In this product temporal averaging was not effected and cloud contaminated pixels were removed. The daily level 3 LST product at 1km spatial resolution is a tile girded in the sinusoidal projection. A tile contains 1200 x 1200 grids in 1200 rows and 1200 columns. The exact grid size at 1km spatial resolution was 0.928 km by 0.928 km.

Collection 5 MOD11A1 product, LST values at all grids are from single clear-sky MODIS observations by selecting LST in MOD11_L2 files at smaller viewing zenith angles. The accuracy of daily MODIS LST product was validated within $\pm 1K$ with insitu measurement over homogeneous surfaces like lakes, grasslands and rice agricultural fields for clear sky days (Coll et al., 2005; Wan et al., 2004).

4.4.5. Leaf area index (LAI)

MODIS leaf area index products in collection 5 are validated at stage 2; i.e accuracy has been assessed over a widely distributed set of locations and time periods via several ground-truth and validation efforts. An eight-day LAI composite product is one of MODIS biophysical data products, archived in the NASA HDF-EOS data format.

The LAI (MOD15A2) products provide global LAI fields retrieved from atmospherically corrected bidirectional reflectance factors of (MOD 09 surface reflectance product) by Myneni et.al, (2002) cited in Cleugh et al.(2007), the resolution of the data is 1 km and the temporal frequencies are 1 and 8 days.

4.4.6. Images used in the analysis

In the rainy season (main growing season) two images in a month were analyzed, whereas in the rest of the period one image in a month was considered. Type of images, date and day of the year (DOY) of images analysed shown in the Table 4-5.

Table 4-5 Date and type of images used for analysis

Sr. No.	Date	Product name	DOY	Type of product
1	01 Jan.08	MOD09A1 MOD15A2 MOD11A1	1	8 day composite 8 day composite daily
2	25 Feb.08	MOD09A1 MOD15A2 MOD11A1	56	8 day composite 8 day composite daily
3	28 Mar.08	MOD09A1 MOD15A2 MOD11A1	88	8 day composite 8 day composite daily
4	26 Apr.08	MOD09A1 MOD15A2 MOD11A1	111	8 day composite 8 day composite daily
5	15 May 08	MOD09A1 MOD15A2 MOD11A1	136	8 day composite 8 day composite daily
6	25 June 08	MOD09A1 MOD15A2 MOD11A1	161	8 day composite 8 day composite daily
7	7 July 08	MOD09A1 MOD15A2 MOD11A1	189	8 day composite 8 day composite daily
8	25 July 08	MOD09A1 MOD15A2 MOD11A1	207	8 day composite 8 day composite daily
9	8 Aug. 08	MOD09A1 MOD15A2 MOD11A1	221	8 day composite 8 day composite daily
10	23 Aug. 08	MOD09A1 MOD15A2 MOD11A1	236	8 day composite 8 day composite daily
11	6 Sep. 08	MOD09A1 MOD15A2 MOD11A1	250	8 day composite 8 day composite daily
12	22 Sep 08**	MOD02 MOD03	266	Instant images
13	29 Sep 08**	MOD02 MOD03	273	Instant images
14	7 Oct. 08	MOD09A1 MOD15A2 MOD11A1	282	8 day composite 8 day composite daily
15	14 Nov. 08	MOD09A1 MOD15A2 MOD11A1	319	8 day composite 8 day composite daily
16	7 Dec. 07*	MOD09A1 MOD15A2 MOD11A1	341	8 day composite 8 day composite daily

* Because weather station data were not available yet data, the 2007 data was used.

** Days in which instantaneous images have been processed

4.4.7. Land cover classification

Land use/cover classification was prepared from Landsat decadal product, produced from combination of two ETM+ scenes with acquisition dates of 2005-2006 to avoid/minimize the loss of data due to the scan-line corrector failure. The image was dated on October 10, 2005. This image was downloaded from glovis data viewer under the decadal Landsat product. The image was geo-referenced and land cover/use classification was done using ILWIS. The spectral signature of the satellite data was assigned for the known land cover types collected during the field campaign. This was applied for different land cover types. Maximum likelihood land cover classification type was used for the land cover classification in the flood plain. The land cover classification was grouped in to seven main land cover types in the Fogera flood plain. These were bare land, cereals, grass land, maize, forest, water body and others. Rice was the main cereal crop in the flood plain. The classified map is shown in Fig.2-4.

4.4.8. Instantaneous Image processing in SEBS

Instantaneous images were used to compare the remote sensing estimations with the field observations. Here sensible heat flux, surface albedo, evaporative fraction and roughness height were compared and the result was presented.

While field data measurements were taken with the eddy flux tower, there were two TERRA satellite overpasses with appropriate view angle and less cloudy days. These two images were, the Sep. 22, 2008 and Sep.29, 2008.

The MODIS onboard Terra images of the above specified date were downloaded and processed using SEBS algorithm. The turbulent energy fluxes retrieved from the instantaneous images using the remote sensing techniques were compared with the measurement of eddy flux tower. In this case sensible heat flux was measured during the satellite overpass by the sonic anemometer with the principle of eddy covariance equation (4.5) was compared with the sensible heat flux obtained from remote sensing techniques using the Surface Energy Balance System (SEBS) algorithm (Su, 2002). In the same way the evaporative fraction computed from SEBS equation (4.42), which is assumed to be constant over the day (Bastiaanssen, 1998; Li et al., 2008; Su, 2002) was calculated during the satellite overpass from field data measurement of the net radiometer equation (4.12). Evaporative fraction is defined as the ratio of latent heat flux to the available energy. The daily latent heat flux was found as a difference of the measured net radiation from CNR1 and sensible heat flux computed from the eddy covariance method. The soil heat flux was assumed to be negligible on daily base. Instantaneous evaporative fraction was computed similarly considering soil heat flux calculated with equation (4.12). This computed evaporative fraction from CNR1 and sonic anemometer measurements was compared with the instantaneous evaporative fraction estimated from remote sensing technique. Sensible heat flux comparisons were made between both at pixel level and at averages of nearest five pixels (pixels around the eddy flux tower including the flux tower pixel) of the remote sensing technique and the eddy flux tower computations.

4.4.9. Image downloading, re projection and sub setting

The MODIS -L1B (MOD02) files with its associated geo-location (MOD03) files were obtained from <ftp://ladsweb.nascom.nasa.gov/> for Sep. 22 and Sep.29, 2008 recorded at Terra overpass time (10:55A.M and 11:00 A.M local time) over the study area. The MODIS Swathtool was used for sub setting and re-projecting the images. The parameters for sub setting and re-projection are the same as shown in Table 4.4.

These geo-tiff file format images of bands 1-7, band 31, and band 32 were imported to Integrated Land and Water Information System (ILWIS), where it was further processed. The corresponding solar and satellite zenith and azimuth angles, and the DEM files, which are obtained from geo-location file, were also imported to ILWIS. The DN values were changed to reflectance bands (1-7) and radiance (band 31 & 32) respectively using the HDF viewer tool to read calibration coefficients (scale and offset) from the header file.

4.4.10. Atmospheric correction (SMAC)

A simplified method for the atmospheric correction of satellite measurements (SMAC) was used for the atmospheric correction for the visible and near infrared bands of MODIS images (Rahman and Dedieu, 1994). MODIS desert coefficient file for the sensor was used. The atmospheric correction data were collected from different sources. The daily MODIS aerosol and water vapor products (MOD04_L2, MOD05_L2) were used for the optical thickness and water vapor content for SMAC input. The ozone content of the corresponding date of image was collected from website: http://jwocky.gsfc.nasa.gov/teacher/ozone_overhead_v8.html. Ozone content was reported with Dobson units (DU). The DU was changed to cm depth of atmosphere. (1000 DU is 1 cm of atmosphere). The local measured atmospheric surface pressure value was changed to hPa, as it was one of input for the atmospheric correction in SMAC. The corrected Geo-location files (solar zenith, solar azimuth sensor zenith, and sensor azimuth angle) maps were used as input for the atmospheric corrections. This procedure was done for all the visible and near infrared bands (band 1-7).

4.4.11. Land surface emissivity computation

Visible (Bred) and near infrared bands were used to compute surface emissivity based on Sobrino and Raissouni (2000) cited in SEBS manual Lichun (2008) algorithm which considers three different conditions depending on the NDVI value:

Bare soil, $NDVI < 0.2$, emissivity, $\varepsilon = 0.9825 - 0.051 * (r_l)$ and

- emissivity difference, $\Delta \varepsilon = -0.0001 - 0.041 * (r_l)$
- Mixed pixels, $0.2 \leq NDVI \leq 0.5$, emissivity, $\varepsilon = 0.9971 + 0.018 * (f_c)$, and emissivity difference, $\Delta \varepsilon = 0.006 * (1 - f_c)$
- Vegetation pixels $NDVI > 0.5$, emissivity, $\varepsilon = 0.99$, and emissivity difference, $\Delta \varepsilon = 0$, and
- For water pixel, where albedo < 0.035 , $\varepsilon = 0.995$

where r_f reflectance in red band (b_1) of MODIS, NDVI was calculated with equation (4.27), f_c vegetation fraction was also calculated with equation (4.26), and emissivity difference ($\Delta \varepsilon$) maps were created.

4.4.12. Land surface temperature

Land surface temperature was computed by the split window method, an algorithm developed by Sobrino and Raissouni (2000) cited in SEBS manual by Lichun (2008).

$$LST = btm32 + (1.97 + 0.2w)(btm32 - btm31) - (0.26 - 0.08w)(btm32 - btm31)^2 + (0.02 - 0.67w) + (64.5 - 7.35w)(1 - \varepsilon) - (119 - 20.4w)\Delta\varepsilon \quad (4.17)$$

where LST is the land surface temperature, $btm31$ is the brightness temperature of band 31, $btm32$ is the brightness temperature of band 32, $w = 13.73 - 13.662 * (\tau_{b31} / \tau_{b32})$ is the water vapour content, where τ_{b31} - transmittance of band 31, τ_{b32} - transmittance of band 32, ε is the surface emissivity, $\Delta\varepsilon$ is the emissivity difference.

4.4.13. Aerodynamic roughness height (z_{om})

Aerodynamic roughness height is the height above the displacement height, where the mean wind becomes zero (Brutsaert, 2005; Ramos et al., in press). It is a theoretical height that can be determined from the wind-speed profile. Aerodynamic roughness height is one of important parameters in the surface energy balance models that influences the transfer of momentum. The different approaches to estimate this height is explained as follows.

1. Aerodynamic roughness height from the eddy covariance measurements

Aerodynamic roughness height can be estimated from the friction velocity found from the eddy covariance, the measured wind speed at a reference height, as explained in section 4.3.1 equation (4.9). In this study, this method was limited for active periods of eddy flux tower measurement and limited spatial area.

2. Land use classification

Hasager and Jensen (1999) developed a look up table for the estimation of aerodynamic roughness height from the detailed land use classification map. The land use class and the respective roughness height developed is shown in Table 4-6.

This approach was recommended by Su (2002). But aerodynamic roughness height varies seasonally according to the vegetation conditions, and finding images for detailed land use classification for each analysis of ET was difficult.

Table 4-6 Land use classes with its associated z_{om} values

No	Land use classes	z_{om} (m)
1	Grass	0.0340
2	Maize	0.4966
3	Potatoes	0.0639
4	Beets	0.0639
5	Cereals	0.4966
6	Other crops	0.0639
7	Greenhouses	0.4066
8	Orchards	0.6065
9	Bulbs	0.0639
10	Deciduous forest	1.2214
11	Coniferous forest	1.2214
12	Heather	0.0408
13	Other open spaces in natural areas	0.0408
14	Bare soil in natural areas	0.0012
15	Fresh water	0.0002
16	Salt water	0.0002
17	Continuous urban area	1.1052
18	Built up area in rural area	0.5488
19	Deciduous forest in urban area	1.2214
20	Coniferous forest in urban area	1.2214
21	Built up area in dense forest	1.2214
22	Grass in built up area	0.0334
23	Bare soil in built up area	0.0012
24	Main roads and railways	0.0035
25	Buildings in rural areas	0.5488

3. Aerodynamic roughness height from vegetation height

Aerodynamic roughness height could also be estimated from the vegetation height as (Platt, 1984):

$$z_{om} = 0.136z_{veg} \quad (4.18)$$

where z_{veg} is the average vegetation height. This approach requires detailed knowledge of the vegetation height of the area under consideration. Its application will be limited in an area where there is heterogeneous land cover and for this reason difficult to apply. The measured vegetation height around the eddy flux tower, during the field campaign will be used to estimate roughness height. This estimate will be compared with the estimate from the eddy flux tower data. The weighted average vegetation height around the eddy flux tower was considered for computation of roughness height. The computation is shown in Appendix G.

4. Aerodynamic roughness height from NDVI

From field experiments empirical relationships have been developed between NDVI and aerodynamic roughness height by different researchers. Su and Jacobs (2001) cited in Wondimagegn (2006) developed a simple relationship between aerodynamic resistance and NDVI as follows.

$$z_{om} = 0.005 + 0.5 \left(\frac{NDVI}{NDVI_{max}} \right)^{2.5} \quad (4.19)$$

This equation was used for estimation of roughness height in the computation of turbulent fluxes in this study, as it gives reasonable results for higher NDVI values (Wenjing, 2006).

4.4.14. Zero-plane displacement height (d)

Zero plane displacement height is a height scale in turbulent flow over tall roughness elements associated with the average level of action of momentum transfer between the flow and the roughness elements. It is estimated as equation (4.11).

4.5. Surface Energy Balance Systems (SEBS)

4.5.1. General

Remote sensing algorithms for estimation of turbulent energy fluxes are developed to avoid the limitations of spatial scale in ground based methods. Ground based conventional ET estimations methods perform well in a limited spatial coverage around the weather station, due to heterogeneity of the land surfaces. SEBS, developed by Su (2002) is one of the remote sensing methods to estimate turbulent surface energy fluxes. SEBS uses spectral satellite observations and metrological data for the estimation of energy fluxes.

Remote sensing methods have the advantage that ET is computed directly from the energy balance equation. This avoids the complex hydrological processes in which error is propagated in the estimation of ET, as ET is estimated as a residual of mass balance and energy balance equations.

SEBS has the advantage in that it has incorporated a set of tools for the determination of land surface physical parameters like surface albedo, emissivity, fractional vegetation cover, NDVI, emissivity difference from the spectral reflectance and radiance signatures (Su, 2002). Other models included in SEBS are determination of roughness height for heat transfer (z_{oh}) and determination of evaporative fraction on the bases of the energy balance at limiting cases (Su, 2002).

For the computation of turbulent energy fluxes, SEBS requires three sets of inputs. The first set contains the radiometric satellite products: land surface albedo, surface emissivity, surface temperature, fractional vegetation cover, leaf area index (LAI) and vegetation height (roughness height). Here when there is no reliable data, Normalized Difference Vegetation Index (NDVI) can be used, from which roughness can be computed from the set tools incorporated in SEBS. The second set of inputs contains meteorological data which are: air pressure, air temperature, humidity and wind speed at the reference height. The third input data set contains incoming shortwave radiation and the long wave radiation.

4.5.2. Energy balance equation

SEBS was designed based on the concept of conservation of energy. Energy balance equation is written as:

$$R_n = G + H + \lambda E \quad (4.20)$$

The latent heat flux in the energy balance equation is calculated as a residue.

The net radiation was calculated with equation (4.14) shown above. Parameterizations of the inputs for the above the equations (4.14 and 4.20) will be explained in detail in the following sections.

4.5.3. Land surface albedo

Land surface broad band albedo was computed using the formula by Liang et al. (2003), which use the MODIS six bands (1, 2, 3, 4, 5, & 7) surface reflectance. It is expressed as:

$$\alpha = 0.16r_1 + 0.291r_2 + 0.243r_3 + 0.116r_4 + 0.112r_5 + 0.018r_7 - 0.0015 \quad (4.21)$$

Where, α is the land surface broad band albedo, $r_1, r_2, r_3, r_4, r_5, r_7$ MODIS surface reflectance products.

4.5.4. Radiation

Short wave solar radiation is measured at the Woreta weather station, which could also be calculated from the measured sun shine hours, using FAO-56 method, explained in Appendix A whereas the incoming long wave radiation calculated as:

$$R_l \downarrow = \sigma \varepsilon_a T_a^4 \quad (4.22)$$

where σ is the Stefan-Boltzmann constant = $5.67 \times 10^{-8} \text{ W}/(\text{m}^2\text{K}^4)$, T_a is the air temperature at a reference height (K), ε_a is the emissivity of the the air, defined as:

$$\varepsilon_a = 9.2 \times 10^{-6} (T_a + 273.15)^2 \quad (4.23)$$

and outgoing long wave radiation computed as:

$$R_l \uparrow = \sigma \varepsilon_s T_s^4 \quad (4.24)$$

4.5.5. Soil heat flux estimation

Soil heat flux is one component of the energy flux. It the quantity of energy which goes down to the soil during the day the amount of energy comes from the soil during the night. The soil heat flux is assumed to be zero on daily basis. It is parameterized as:

$$G = R_n (\Gamma_c + (1 - f_c)(\Gamma_s - \Gamma_c)) \quad (4.25)$$

where $\Gamma_c = 0.05$, for full vegetation cover by Monteith (1973) cited in Su (2002), and $\Gamma_s = 0.315$ for bare soil (Kustas and Daughtry, 1990). Interpolating between these limiting values, for other fractional canopy coverage (f_c), this is found from remote sensing data.

4.5.6. Fractional vegetation cover

Fractional vegetation cover is the fraction of the surface covered with vegetation. It is parameterized from the normalized difference vegetation index as Sobrino and Raissouni (2000) cited in SEBS manual by Lichun (2008).

$$f_c = \left(\frac{NDVI - NDVI_{\min}}{NDVI_{\max} - NDVI_{\min}} \right)^2 \quad (4.26)$$

where $NDVI_{max}$, $NDVI_{min}$ and $NDVI$ are the NDVI values at full vegetation, bare soil and the value of the current pixel respectively.

Here, $NDVI > 0.5$ is considered as full vegetation, $f_c = 1$, and

$NDVI < 0.2$ is considered as bare soil, $f_c = 0$

4.5.7. Normalized difference vegetation index (NDVI)

NDVI is an index to detect live green plant canopies, which is evaluated from the red and infra red bands as:

$$NDVI = \frac{r_{nir} - r_{red}}{r_{nir} + r_{red}} \quad (4.27)$$

Where, r_{red} , r_{nir} are the atmospherically corrected reflectance of red and near infrared bands.

4.5.8. Sensible heat flux

Finally to evaluate the latent heat flux as a residue, it is required to know the sensible heat flux, which is evaluated from the theory of similarity.

In the atmospheric surface layer the mean wind speed, u , and the mean temperature $\theta_o - \theta_a$ similarity can be written integral form as,

$$u = \frac{u_*}{k} \left[\ln \left(\frac{z-d}{z_{om}} \right) - \Psi_m \left(\frac{z-d}{L} \right) + \Psi_m \left(\frac{z_{om}}{L} \right) \right] \quad (4.28)$$

$$\theta_o - \theta_a = \frac{H}{ku_* \rho C_p} \left[\ln \left(\frac{z-d}{z_{oh}} \right) - \Psi_h \left(\frac{z-d}{L} \right) + \Psi_h \left(\frac{z_{oh}}{L} \right) \right] \quad (4.29)$$

where z is reference height, $u_* = (\tau_o / \rho)^{1/2}$ is the friction velocity, τ_o is the surface shear stress, θ_o is the potential temperature at the surface, θ_a is the potential air temperature at height z , Ψ_m and Ψ_h are the stability correction functions for momentum and sensible heat transfer respectively, and L is the Obukhov length defined as:

$$L = - \frac{\rho C_p u_*^3 \theta_v}{kgH} \quad (4.30)$$

where g (m^2/s) is the acceleration due to gravity, and $\theta_v(K)$ is the potential virtual temperature near the surface.

In SEBS stability Obukhov length, sensible heat flux, and friction velocity are obtained by solving (equations 4.28 - 4.30) iteratively.

The roughness height for heat transfer in SEBS is computed as formulated by Su et al. (2001):

$$z_{oh} = \frac{z_{om}}{\exp(kB^{-1})} \quad (4.31)$$

where B^{-1} is the inverse Stanton number, a dimensionless heat transfer coefficient. The value of kB^{-1} is estimated as proposed by Su et al. (2001) as follows:

$$kB^{-1} = \frac{kC_d}{4C_1 \frac{u_*}{u(h)} \left(1 - e^{-n_{ec}/2}\right)} f_c^2 + 2f_c f_s \frac{k * u / u(h) * z_{om} / h}{C_t^*} + kB_s^{-1} f_s^2 \quad (4.32)$$

where f_s is the complement of f_c , C_t is the heat transfer coefficient of the leaf, it is bounded as $0.005N \leq C_t \leq 0.075N$ (N is number of leaf sides participate in heat exchange). The heat transfer coefficient of the soil is given by:

$$C_t^* = Pr^{-2/3} R_{e*}^{-1/2} \quad (4.33)$$

Where Pr is the Prandtl number and R_{e*} the roughness Reynolds number

The wind speed extinction coefficient, n_{ec} is formulated as:

$$n_{ec} = \frac{C_d * LAI}{2u_*^2 / u(h)^2} \quad (4.34)$$

where $C_d \approx 0.2$ is the drag coefficient, $u(h)$ is the horizontal wind speed at the top of the canopy.

4.5.9. Evaporative fraction

In SEBS the main assumption made to calculate evaporative fraction is determining the limiting cases. These are: at the dry limit, where soil moisture is limited, evaporation will be zero and the sensible heat flux will have its maximum value. On the other extreme, the wet limit, where there is sufficient soil moisture for evaporation, evaporation will be limited only by the available energy and hence sensible heat flux will have its minimum value. Hence,

$$\lambda E_{dry} = R_n - G - H_{dry} = 0 \quad \text{or} \quad H_{dry} = R_n - G \quad (4.35)$$

and,

$$\lambda E_{wet} = R_n - G - H_{wet} \quad \text{or} \quad H_{wet} = R_n - G - \lambda E_{wet} \quad (4.36)$$

The relative evaporation defined as the actual evaporation divided by the potential evaporation, λE_{wet} ,

$$\Lambda_r = \frac{\lambda E}{\lambda E_{wet}} = 1 - \frac{\lambda E_{wet} - \lambda E}{\lambda E_{wet}} \quad (4.37)$$

After substituting equations, (4.20), (4.35) and (4.36) in equation (4.37), relative evaporative fraction can also be solved as,

$$\Lambda_r = 1 - \frac{H - H_{wet}}{H_{dry} - H_{wet}} \quad (4.38)$$

Considering the internal resistance to be zero from the equation similar to the Penman-Montieth combination equation given in Su (2002), is combined with equation (4.37) above, to compute the sensible heat flux at the wet limit as,

$$H_{wet} = \left((R_n - G) - \frac{\rho C_p}{r_{ew}} \cdot \frac{e_s - e_a}{\gamma} \right) / \left(1 + \frac{\Delta}{\gamma} \right) \quad (4.39)$$

where r_{ew} is the external resistance.

And the wet limit external resistance can be derived from

$$r_{ew} = \frac{1}{ku_*} \left(\ln \left(\frac{z-d}{z_{oh}} \right) - \psi_h \left(\frac{z-d}{L_w} \right) + \psi_h \left(\frac{z_{oh}}{L_w} \right) \right) \quad (4.40)$$

The wet limit stability length can be determined as:

$$L_w = \frac{\rho u_*^3}{0.61 kg (R_n - G) / \lambda} \quad (4.41)$$

Finally the evaporative fraction is given by

$$\Lambda = \frac{\lambda E}{R_n - G} = \frac{\Lambda_r \lambda E_{wet}}{R_n - G} \quad (4.42)$$

$$\text{So, } \lambda E = \Lambda (R_n - G)$$

Assuming evaporative fraction is conserved, i.e, instantaneous evaporative fraction remains constant over the day, and the daily evapotranspiration can be estimated as:

$$E_{daily} = 8.64 \times 10^7 \times \Lambda \times \frac{R_n - G}{\lambda \rho_w} \quad (4.43)$$

where, E_{daily} is the daily actual evapotranspiration (mm/day)

Λ is the daily evaporative fraction

ρ_w density of water (kg/m^3)

λ latent heat of vaporization (J/kg), which can be calculated as, $\lambda = (2.501 - 0.00237 * T_{air}) \times 10^6$.

The daily net radiation is computed as equation (4.14), and the solar radiation was computed with equation (A.9) Appendix A from the measured sunshine hours. The daily net long wave (L_{24}) is radiation given as:

$$L_{24} = \varepsilon_a \sigma T_{air}^4 - \varepsilon \sigma T_s^4 \quad (4.44)$$

where, σ is Stefan-Boltzmann constant, ε_a is emissivity of the clear sky which can be estimated with equation by Campbell and Norman (1998), cited in Su (2002) in the following form:

$$\varepsilon_a = 9.2 \times 10^{-6} (T_{a24} + 273.15)^2 \quad (4.45)$$

where T_{a24} is the daily average air temperature.

Here, equation (4.44) gives lower values of long wave radiation; as a result the daily net radiation is reduced. This in turn underestimates the daily evaporation.

Hence, in this thesis equation (4.46) will be used with locally calibrated coefficients in the computation of daily net radiation.

$$R_{n24} = (1 - \alpha_{24})\tau_{24}R_{a24} - a\tau_{24} \quad (4.46)$$

Where, R_{n24} the daily net radiation MJ/(m²day), α_{24} daily surface albedo, τ_{24} daily atmospheric transmissivity, R_{a24} daily extra terrestrial solar radiation, MJ/(m²day) determined as explained in Appendix A, equation (A-4), a is a coefficient determined from the CNR1 measurement of net radiation MJ/(m²day). Locally calibrated values for dry season $\tau_{24} = 0.7$ and about 0.6 for rainy season respectively and $a = 9.15$ MJ/(m²day).

4.5.10. Ancillary weather data for SEBS algorithm

In addition to remote sensing data, SEBS requires meteorological data for the estimation of turbulent fluxes. From July to October, the WWS station 15 minutes average at satellite overpass was used. These are solar radiation air temperature, wind speed, and computed specific humidity. The atmospheric pressure was constant. Whereas for the remaining months in the year 2008, the daily mean relative humidity and the daily wind speed at Bahir Dar station were used as it is, whereas the daily air temperature and daily solar radiation was adapted to instantaneous air temperature and solar radiation during the satellite overpass.

5. Data analysis

5.1. Introduction

In this chapter the WWS data and data from the sensors mounted on the eddy flux tower will be compared. In addition the WWS and the Bahir Dar station data sets were also compared to see the suitability of the Bahir Dar data for the estimation of ET over the Fogera flood plain. Woreta weather station has only four months record from July to October 2008. But a one year analysis of ET is intended in this study. So, the Bahir Dar station data will be adapted for the estimation of ET for the rest of the period in the year 2008. The data to be analyzed here are: air temperature, solar radiation, relative humidity, and wind speed.

5.2. Woreta weather station and the eddy flux tower

5.2.1. Temperature

The air temperature observed with the sensor at the weather station and the sensor at the flux tower was in good agreement. These were having a R^2 of 0.99 one another as shown in the Fig. 5-1.

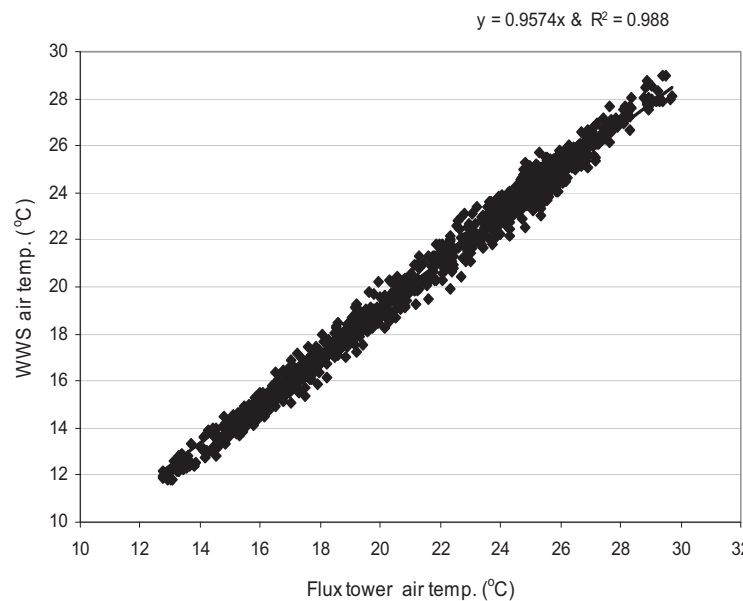


Figure 5-1 Temperature correlation between WWS and flux tower sensors

The sonic temperature was also in good agreement with the flux tower temperature, it has R^2 of 0.9. The correlation between them is shown in the Fig.5-2.

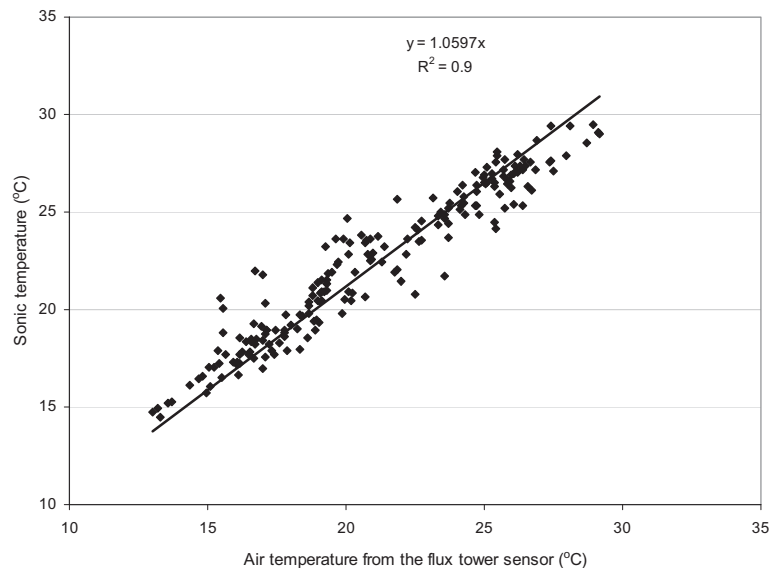


Figure 5-2 Sonic temperature and flux tower temperature sensor comparison

5.2.2. Relative humidity

The relative humidity measured at the flux tower gives relatively higher values than the measurement at the weather station. The sensors show a noticeable difference at minimum relative humidity measurements. Even though the correlation between the two sensors is R^2 of 0.99, there is relatively higher bias of about 9 %, especially at minimum relative humidity measurements. The weather station has higher range of RH measurement than the flux tower. The correlation between them is shown in Fig. 5-3.

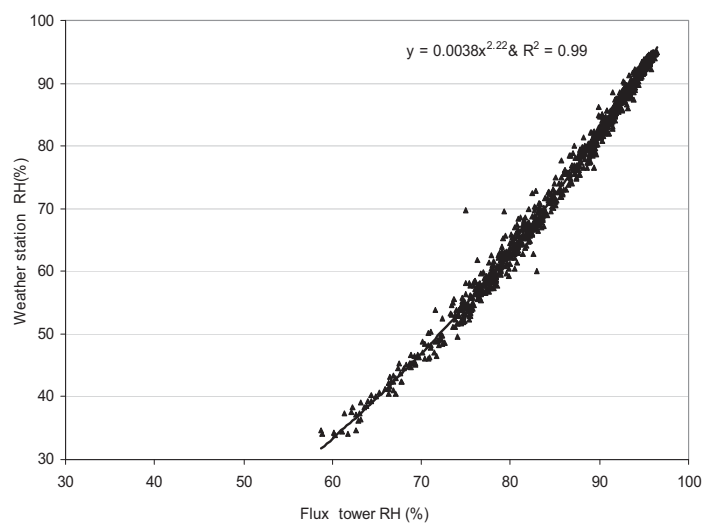
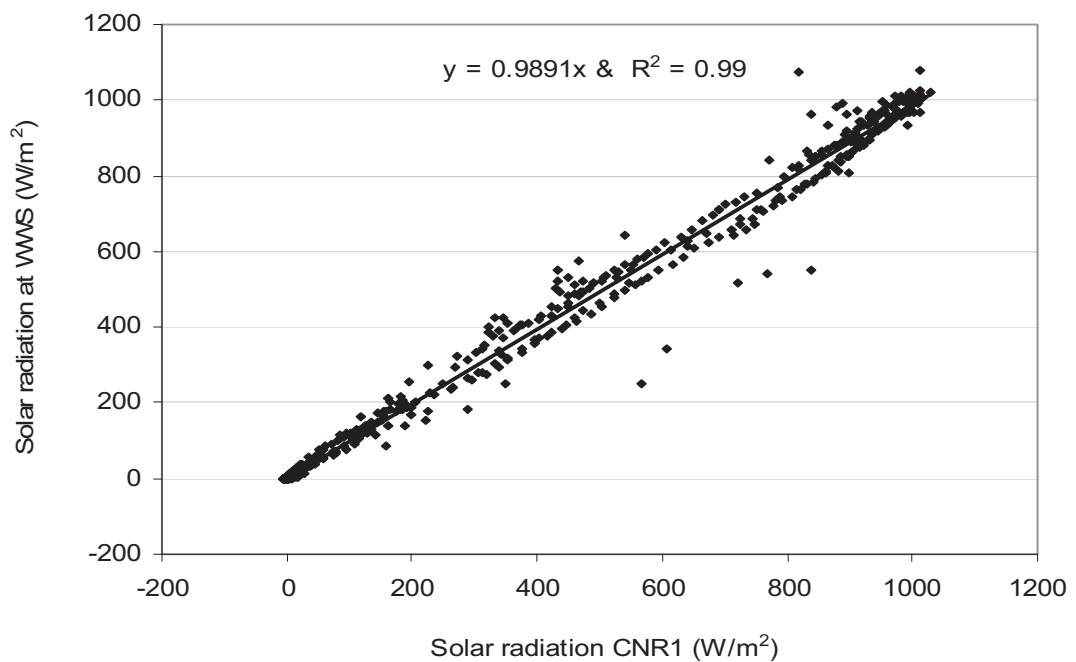


Figure 5-3 Relative humidity correlation between the flux tower and the WWS station measurements

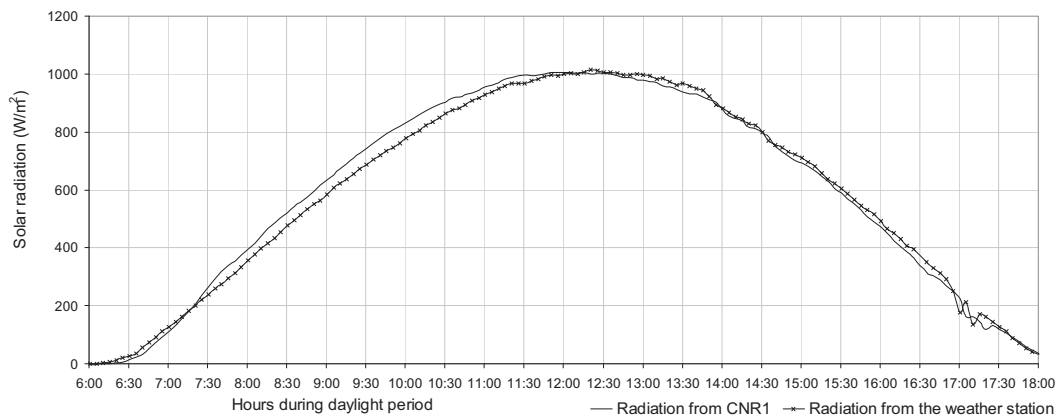
5.2.3. Radiation

The quantification of ET is highly dependant on the available radiation in an area of interest. Hence, accurate measurement or estimation of the radiation will be reflected on the accuracy of ET estimations.

The incoming solar radiation measured at the Woreta weather station and the measurement with the CNR1 was having better correlation, but there is some time shift between the two measurements. The maximum time shift was about 15 minutes in the morning. It has a correlation R^2 of 0.99 as shown in the Fig. 5-4.



(a)



(b)

Figure 5-4 Measured radiation (a) scatter plot radiation from WWS vs radiation from CNR1 (b) Solar radiation vs time during sunlight hours on 23 September 2008

The daily net radiation measured with the CNR1 was comparable with the daily net radiation computed by FAO-56 method from the measured solar radiation at WWS. But the FAO-56

computations overestimate by an average of about 0.23 MJ/m² day. This comparison was made for three days where the CNR1 was active for full day's of measurement. With in these days its correlation was R² of 0.99, RMSE of 0.25 MJ/m² day and AME of 0.23 MJ/m² day as shown in the Fig. 5-5.

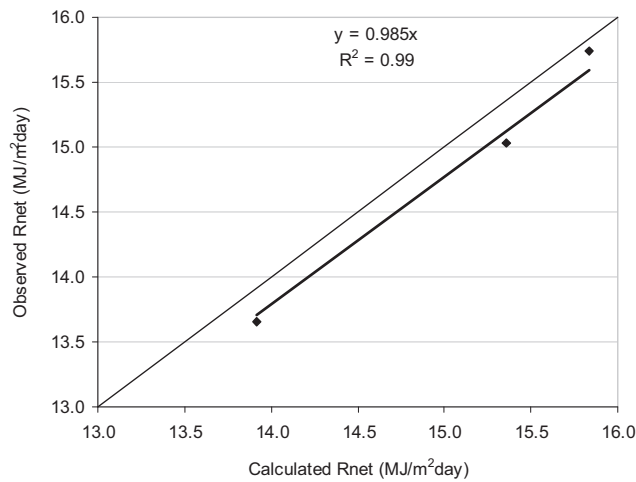


Figure 5-5 Net radiation correlation

The instantaneous solar radiation during the satellite overpass at 11:00 AM hours (local time) in the area was required for SEBS input for remote sensing inputs. This was correlated with the daily solar radiation for clear sky days. The data shows that, the instantaneous radiation at 11:00 A.M was about 3.2 times higher than daily average solar radiation. So, from the daily solar radiation computations (FAO-56 method) of clear sky days, instantaneous radiation was extracted. The relation between the daily and instantaneous solar radiation for clear sky days measured at Woreta weather station is shown in the table 5-1 and Fig. 5-6. This relation was applied on the Bahir Dar station data for the estimations of ET over the Fogera flood plain.

Table 5-1 Instantaneous and daily solar radiation relation

Clear sky days	Solar radiation (W/m ²)		Relation ratio (3) = (2)/(1)
	Daily (1)	Instantaneous at 11:00 AM (2)	
27-Jun-08	305.78	905.60	2.96
2-Oct-08	302.24	953.10	3.15
3-Oct-08	298.72	945.60	3.17
5-Oct-08	306.02	953.10	3.11
6-Oct-08	297.50	936.90	3.15
14-Oct-08	297.52	934.40	3.14
16-Oct-08	290.66	959.40	3.30
18-Oct-08	290.99	930.60	3.20
19-Oct-08	289.14	940.60	3.25
23-Sep-08	296.67	928.10	3.13
3-Nov-08	268.32	881.90	3.29
6-Nov-08	263.53	840.60	3.19
7-Nov-08	256.69	863.10	3.36
8-Nov-08	242.85	863.10	3.36
Average	4006.63	12836.1	3.20

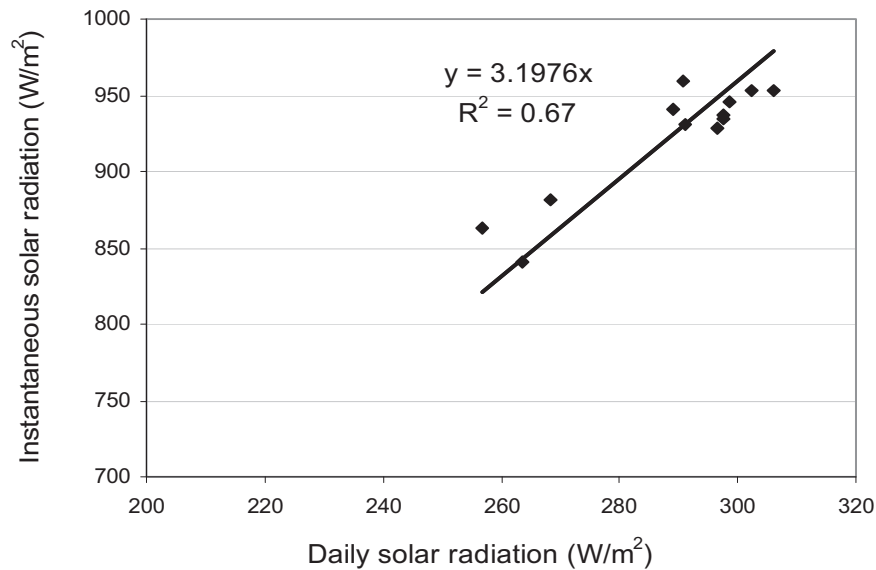


Figure 5-6 Correlation between instant solar radiation and daily solar radiation

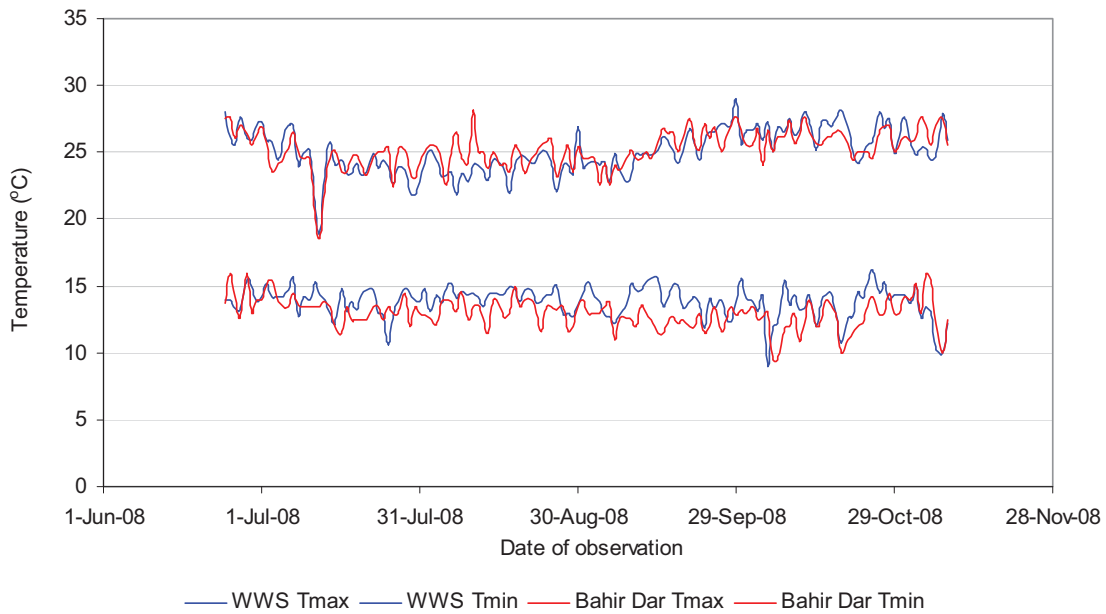
5.3. Woreta and Bahir Dar station data comparisons

As explained previously, the Bahir Dar weather station data will be adapted to the study area for the estimation of ET by both ground based conventional methods and remote sensing technique. Here, the difference between the extraterrestrial solar radiations computed at the both places was less than 1W/m². This showed that the solar radiation calculated from the sunshine hour measurement at Bahir Dar, could be used for the estimation of ET in the Flood plain.

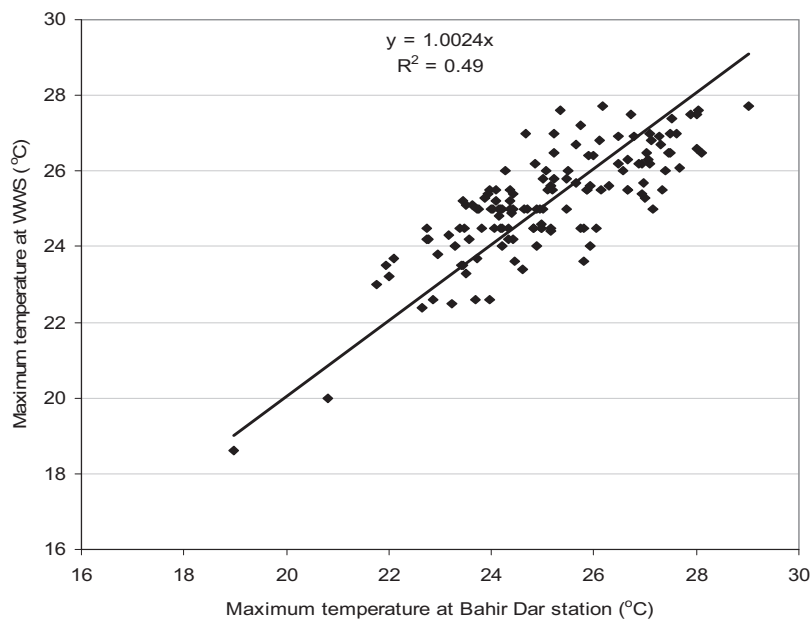
The daily air temperature and relative humidity relation between these two stations is shown in the Table 5-2 and Fig 5-7. The root mean square error (RMSE) and the absolute mean error of the mean temperature was in the range of 0.95 °C and 0.77 °C respectively. RMSE and AME of relative humidity measurements are in the range of 5.9 % and 4.4% respectively. This is shown in Table 5-2, so the Bahir Dar data could be used without considerable error in the estimation of ET in the Fogera flood plain.

Table 5-2 Maximum, minimum, mean temperature and mean relative humidity comparison between the WWS and Bahir Dar data

Weather variable	RMSE	AME
Tmean (°C)	0.95	0.77
Tmax (°C)	1.14	0.91
Tmin (°C)	1.54	1.24
RH (%)	5.9	4.4



(a)



(b)

Figure 5-7 (a) Maximum and minimum temperature graphs measured at Woreta weather station and Bahir Dar station (June 24 - Nov. 8, 2008) (b) maximum temperature correlations at WWS vs Bahir Dar stations

Remote sensing ET estimations requires instantaneous temperature data. The daily maximum temperature at Bahir Dar was correlated with the instantaneous temperature observations during satellite over pass (about 11:00 AM local time) at Woreta. It was having a coefficient of determination of R^2 of 0.61, and an equation of $T(\text{instant}) = 1.0255*(T_{\text{maxB/Dar}})-3.07$. The scatter plot is shown in the Fig-5-8.

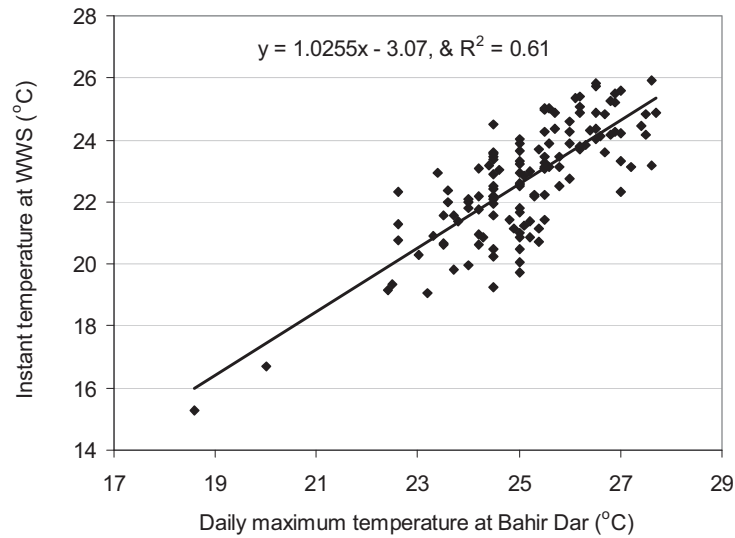


Figure 5-8 Correlation between instantaneous temperature at WWS vs daily maximum temperature at Bahir Dar station

Estimation of daily ET from remote sensing technique equation (4.44) requires computation of daily net radiation. This daily net radiation was computed with equation (4.46) which requires local calibration of the transmissibility of the atmosphere and the coefficient “*a*”. These coefficients were locally calibrated from the observation of the solar radiation obtained from the flux tower, and FAO-56 method to estimate extraterrestrial solar radiation. These locally calibrated coefficients are shown in the Table 5-3.

Table 5-3 Measured and calibrated values of transmissibility and the coefficient “*a*”

Date	CNR1 measured values			FAO-56	Calibrated values	
	Albedo (α)	R_{ns} (MJ/m ²)	R_n (MJ/m ²)	R_a (MJ/m ²)	τ	a (MJ/m ²)
23-Sep-08	0.17	21.95	15.00	36.31	0.73	9.58
24-Sep-08	0.16	19.27	13.66	36.23	0.64	8.82
28-Sep-08	0.16	22.47	15.74	35.93	0.74	9.04
Average values	16.33	21.23	14.8	36.16	0.70	9.15

6. Results and discussion

This chapter presents and discusses the results from ground based conventional methods, micrometeorology results and remote sensing ET estimation results. Comparison between different conventional methods was made. The micrometeorology observations were compared with the ground based methods and remote sensing technique. The actual ET found from SEBS was used for analyzing the spatio-temporal distribution of ET over the Fogera flood plain. The crop coefficient of the rice field was also estimated from the actual ET estimated from SEBS algorithm and the P-M reference ET.

6.1. Conventional methods

The reference P-M ET on a daily base was estimated with different methods with the data collected from the Woreta weather station for period July to October, 2008, and for the rest of the period where the Woreta weather station data was not available, the estimation was done from the Bahir Dar data. The results from both stations will be presented in the coming sections. The different conventional methods were compared with the global standard P-M reference ET.

6.1.1. Priestley Taylor vs Penman-Monteith

Priestley Taylor method was compared with the global standard P-M method. This comparison showed that P-T could give a result R^2 of 0.79, RMSE of 0.63 mm, AME of 0.57 mm and bias of 0.57 mm with the Woreta data. With the Bahir Dar data, the comparison was R^2 of 0.81, RMSE of 0.52 mm, AME of 0.45 and an average bias of 0.39 mm. Here bias is defined as the mean error when compared with P-M reference ET. The P-T method overestimates E_{To} , when compared with the Penman-Monteith E_{To} estimation. These relatively larger errors indicate that P-T coefficient may require local calibration with P-M method. After calibration has been made with a coefficient of $\alpha = 1.14$; the P-T estimation improved to R^2 of 0.79, RMSE of 0.29 mm AME of 0.25 and an average bias of 0.13 mm at WWS data and for the Bahir Dar data R^2 of 0.81, RMSE of 0.34 mm AME of 0.27 and an average bias of 0.01mm. Table 6-1 and Fig. 6-1 show the detailed result and the correlation scatter plot before calibration coefficient was applied.

Table 6-1 Comparison of P-T with P-M

P-T compared with P-M E_{To}	P-T coefficient $\alpha = 1.26$		After calibration with $\alpha=1.14$	
	WWS	Bahir Dar	WWS	Bahir Dar
R^2	0.79	0.81	0.79	0.81
RMSE	0.63	0.52	0.29	0.34
AME	0.57	0.45	0.25	0.27
Bias	0.57	0.39	0.13	0.01

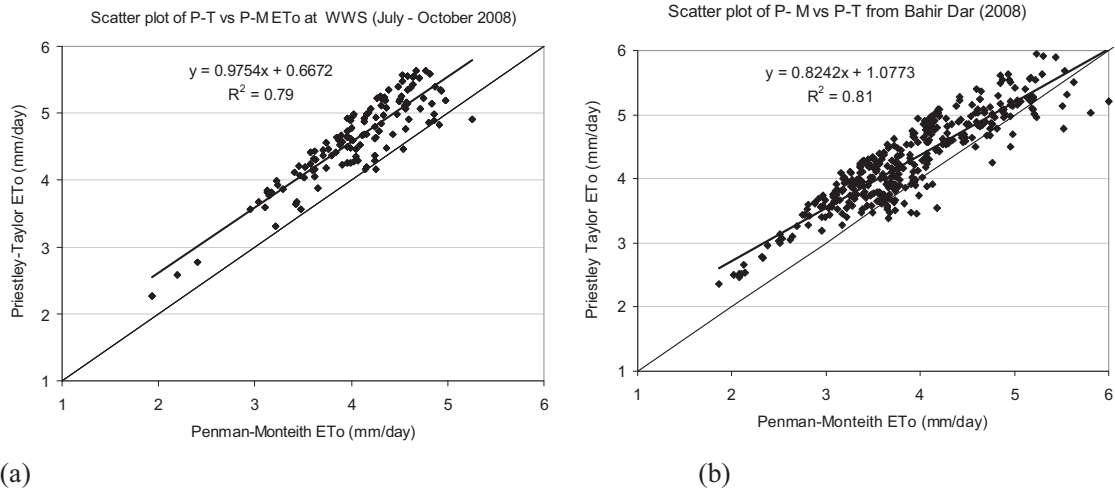


Figure 6-1 Scatter plot of P-T vs P-M ETo with (a) Woreta and (b) Bahir Dar data

6.1.2. Modified Makkink and P-M ETo comparison

The modified Makkink method was compared with the P-M ETo at both WWS and Bahir Dar data sets. With the Woreta station data set from July to October, 2008 the comparison showed R^2 of 0.93, RMSE 0.19 mm, AME of 0.16 mm and bias of 0.004 mm. The Makkink method from the Bahir Dar data set gives very similar results as of the WWS data set with R^2 of 0.88, RMSE 0.25 mm, AME of 0.19 mm and bias of 0.01 mm. This result showed that the Makkink method performs well in the study area without the need for local calibration of the coefficient. The results at both these stations are shown in Table 6-2 and Fig. 6-2.

Table 6-2 Comparison of Makkink with the P-M method

Weather variable	WWS	Bahir Dar station
R^2	0.93	0.88
RMSE	0.19	0.25
AME	0.16	0.19
Bias	0.004	0.01

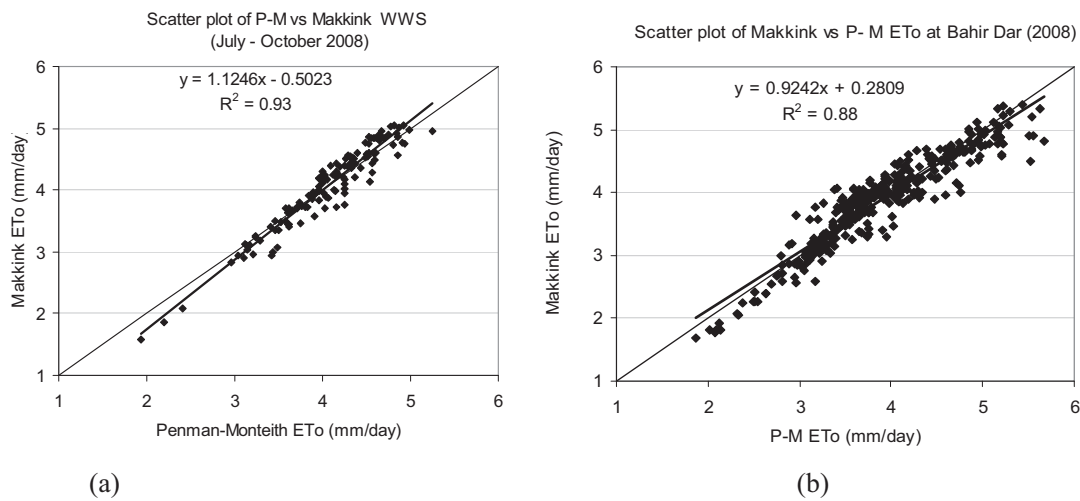


Figure 6-2 Scatter plot of Makkink vs P-M at two stations at (a) WWS and (b) Bahir Dar stations

6.1.3. Abteu simple equation vs P- M ETo

It was explained previously that Abteu simple equation gives actual ET when soil moisture is not a limiting factor for ET and potential ET when soil moisture is a limiting factor. Abteu simple equation was compared with the three days' Eddy flux observation. It was found that Abteu equation was able to estimate actual ET with an average error less than 5 %. This comparison is shown in Table 6-3.

Table 6-3 Comparison of latent heat flux from eddy flux tower and Abteu actual ET

Date	Eddy flux tower latent heat flux (mm/day)	Abteu actual ET (mm/day)	Difference	Percentage error (%)
23-Sep-08	5.3	5.5	0.3	5.0
24-Sep-08	4.8	4.9	0.1	1.3
28-Sep-08	5.3	5.7	0.4	7.7
			Average	4.7

Again Abteu's simple equation was compared with P-M ETo at both the Woreta and Bahir Dar data sets and gives a result R^2 of 0.90, RMSE of 0.6 mm and AME of 0.55 mm and bias of 0.54 mm with the WWS data, and R^2 of 0.81, RMSE of 0.63 mm and AME of 0.55 mm and a bias of 0.53 for the Bahir Dar data. These relatively larger errors indicate that Abteu simple equation requires local calibration of the coefficient. After local calibration of the coefficient with $k = 0.48$, it gives better results as shown in the Table 6-4. The scatter plot at both stations is shown the Fig. 6-3.

Table 6-4 Comparison of Abteu with the P-M method

	Original ($k=0.53$)		After calibrated ($k = 0.48$)	
	WWS	B/Dar	WWS	B/Dar
R^2	0.90	0.81	0.90	0.81
RMSE	0.6	0.63	0.25	0.34
AME	0.55	0.55	0.21	0.27
Bias	0.54	0.53	0.11	0.11

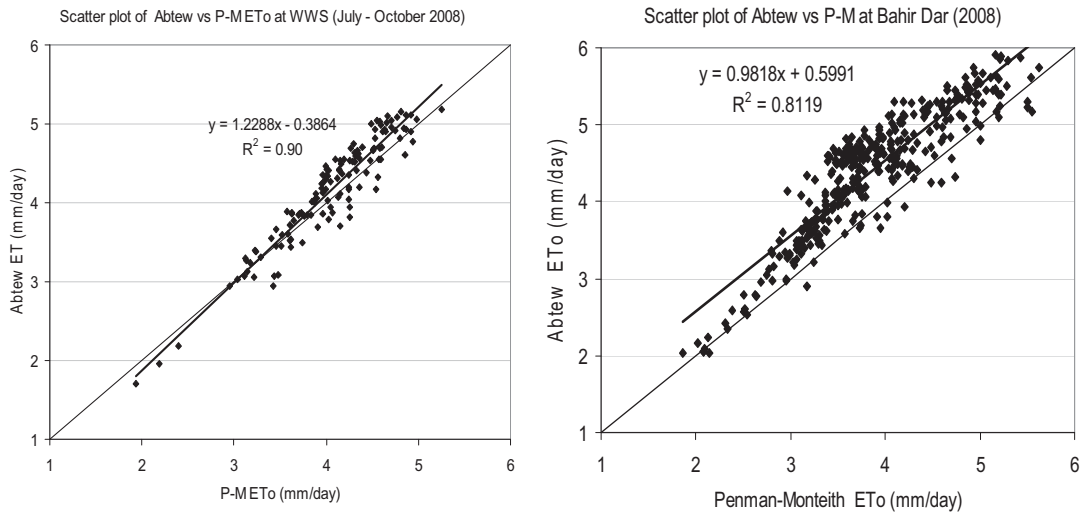


Figure 6-3 Scatter plot Abtew vs P-M equation at Bahir Dar station for drier months

6.1.4. Estimation of ETo from maximum temperature data only

The P-M reference ET sensitivity analysis for the input variables in the Fogera flood plain showed that P-M reference ETo was found equally sensitive for incoming solar radiation and temperature. In addition it was also found that simple radiation methods like Makkink and Abtew perform well in the area; and temperature and incoming solar radiation were directly related. So, temperature methods could also perform well in this area.

The measured daily maximum temperature and the estimated daily solar radiation (FAO-56) at Bahir Dar were correlated and this correlation was equated to the simple Abtew radiation equation. After doing so a simple temperature method was formulated. This equation was calibrated with the Penman-Monteith estimations from the Bahir Dar data of 2007 and 2008. This was again validated and fine tuned with the 2005 and 2006 data sets, and the following result was found. This empirical simple equation which only uses daily maximum temperature ($^{\circ}\text{C}$) to estimate ETo (mm/day), gives an average coefficient of determination R^2 of 0.73, an average RMSE of 0.47 mm and an average absolute mean error of 0.37 mm. The detailed result when compared with the standard Penman – Monteith method is shown in the Table 6-4 and the Fig. 6-4. This method estimates ETo from the maximum temperature data only as: $E_{To} = (1/965) * (T_{max})^{2.5}$, where ETo is the reference ET (mm/day), 1/965 is a coefficient in $\text{mm}/(\text{day } ^{\circ}\text{C}^{2.5})$, and T_{max} is the daily maximum temperature ($^{\circ}\text{C}$). This method could be used to estimate ETo where there is insufficient data, with a maximum error of 10 % from the P-M estimations when daily comparison was made and with in 2 % error when yearly estimations compared. Maximum temperature data is available in many weather stations even in remote areas.

Table 6-5 Comparison of new method with the P-M method on daily and yearly basis

Years	Daily comparison				Yearly comparison		
	R ²	RMSE (mm)	AME (mm)	Error %	P-M ETo (mm/year)	New method ETo (mm/year)	Error (%)
2008	0.7	0.49	0.39	10	1263*	1278*	1.16
2007	0.7	0.47	0.37	10	1424	1426	0.1
2006	0.72	0.47	0.38	9.5	1476	1418	3.9
2005	0.78	0.45	0.36	8.8	1488	1448	2.7
Average	0.73	0.47	0.37	9.6	1463	1431	1.96

* Data from January 1 to November 19, 2008 and Bahir Data only

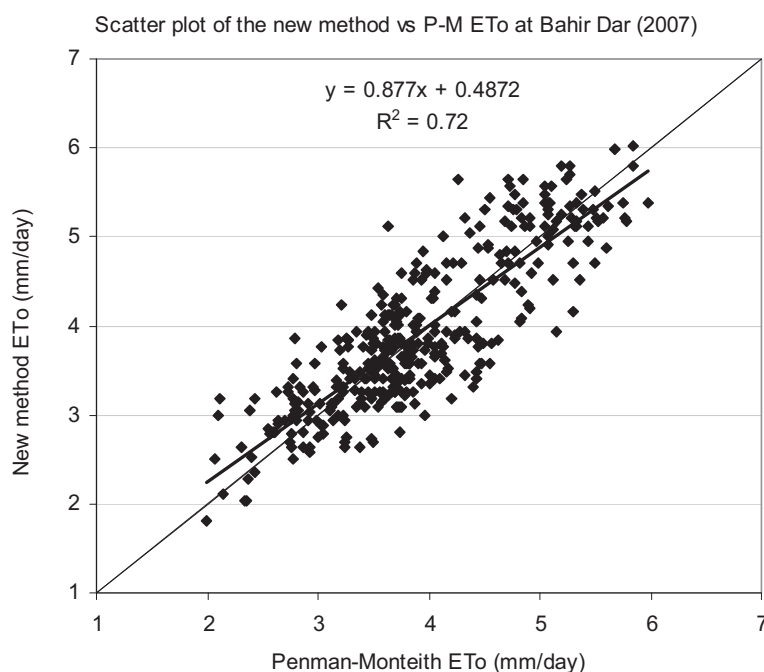


Figure 6-4 Scatter plot new method vs P-M ETo for the year 2007

6.1.5. Sensitivity analysis

The P-M reference ET sensitivity analysis for the input variables was done on monthly basis in a year, 2008 over the Fogera flood plain. The WWS data was used from July – October, 2008 and for the rest of the months in the year 2008 the Bahir Dar data set was used for the sensitivity analysis. After sensitivity analysis was done for the reference ET, in the year 2008. Incoming solar radiation was found the most sensitive weather variable independent of the seasons of the year. ETo was comparably sensitive to air temperature as the incoming solar radiation. Wind speed was less sensitive to the P-M ETo estimation next to relative humidity in the Fogera flood plain. Relative humidity influences ETo negatively, i.e. as relative humidity increases, ETo decreases and vice versa. At larger relative humidity values (during rainy season) the slope of the sensitivity analysis curve becomes steeper. This indicates that larger relative humidity influences more on ETo than smaller values. Gong et al. (2006) explained sensitivity of ETo to the input variables vary with seasons. But here sensitivity result does not change with change of seasons. This is due to the variation of weather variables in a

year is less in this area. For example the mean wind speed in the area was 1.2 m/s with standard deviation of 0.26 m/s.

During the sensitivity analysis weather station data was analysed. The daily maximum and minimum solar radiation was 27.3 MJ/(m²day) and 9.3 MJ/(m²day) in April and July respectively. The daily Maximum and minimum temperature was 32.5 °C in April and December 4.4 °C respectively. The relative humidity ranges from a minimum of 33 % to a maximum of 96 %. Minimum was in April and maximum were in July, August and September. The mean annual wind speed was as low as 1.2 m/s. The monthly average weather variables at Bahir Dar station are shown in the Table 6-6 and Fig 6-5.

Table 6-6 Monthly average weather variables at the Bahir Dar station (2008)

Date	Solar radiation MJ/(m ² day)	Temperature (°C)	RH (%)	Wind speed (m/s)
Jan-08	20.16	18.4	47.0	1.0
Feb-08	22.83	18.5	51.0	0.9
Mar-08	24.88	19.8	43.0	1.1
Apr-08	21.87	21.8	50.0	1.2
May-08	21.57	21.3	60.0	1.2
Jun-08	19.51	22.1	70.0	1.1
Jul-08	19.63	18.2	82.3	1.6
Aug-08	21.04	18.4	83.3	1.6
Sep-08	22.11	19.1	80.7	1.4
Oct-08	22.85	19.7	73.0	1.5
Nov-08	20.28	18.7	57.0	0.9
Dec-07	21.33	16.5	52.0	0.9

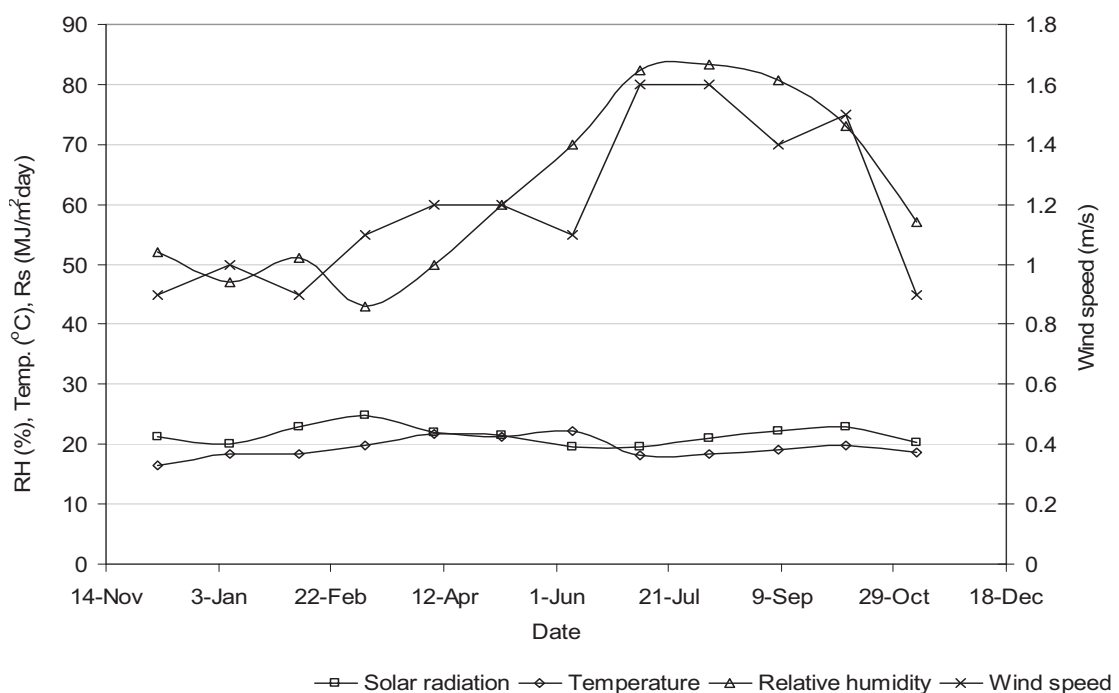


Figure 6-5 Monthly weather variables at Bahir Dar station in the year

A simple but practical way of presenting a sensitivity analysis is to plot relative changes of weather variables against changes in P-M ETo as a curve. The sensitivity analysis result for selected four months is shown in the Fig.6-6.

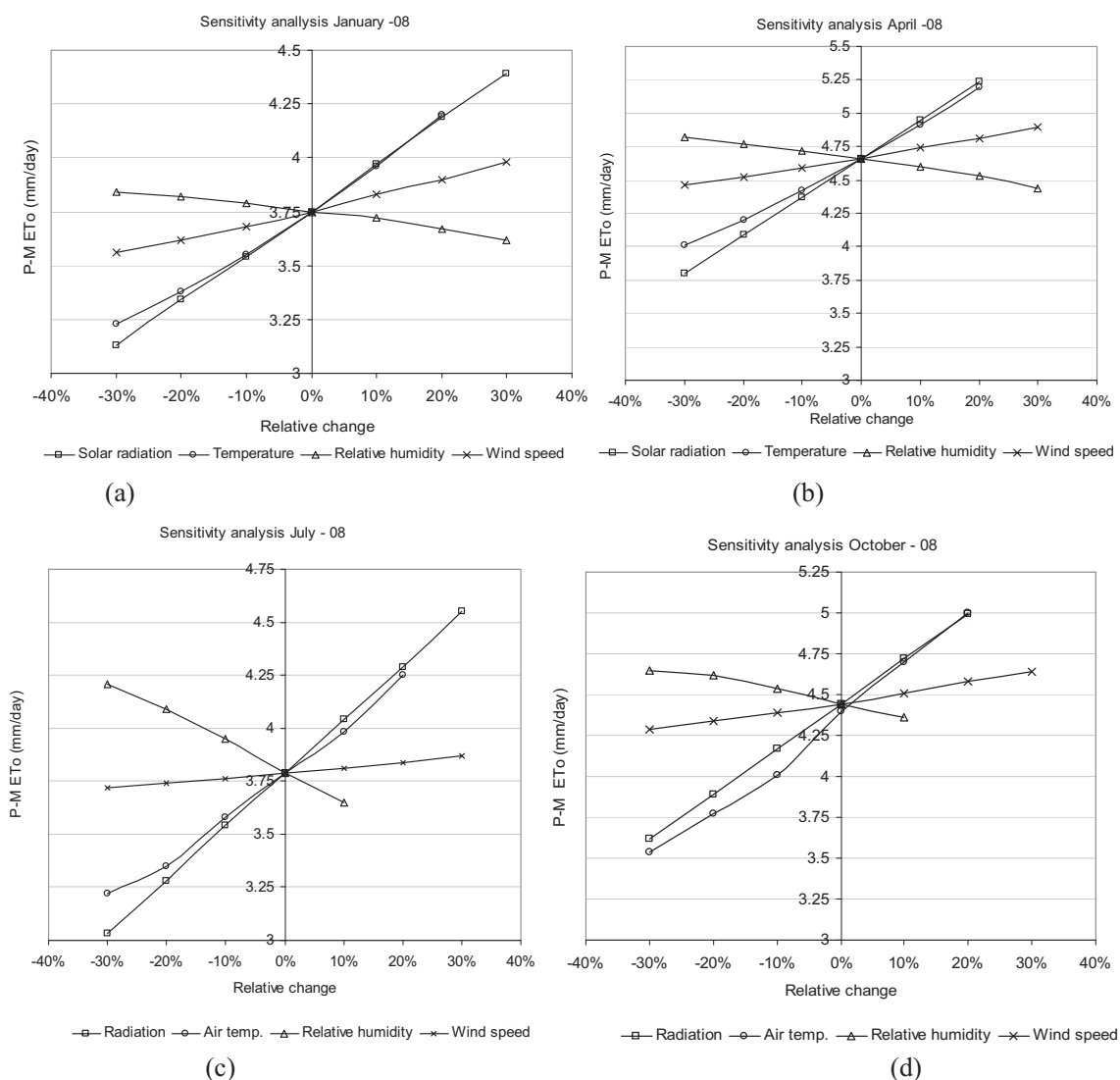


Figure 6-6 Sensitivity analysis results of ETo to input variables, (a) January - 08 (b) April - 08 (c) July - 08 and (d) October – 08

6.2. Micrometeorology

In this section sensible heat flux, latent heat flux, evaporative fraction, broad band albedo, and roughness height for momentum transfer computed from ground observations will be compared with the remote sensing and different ground based estimations.

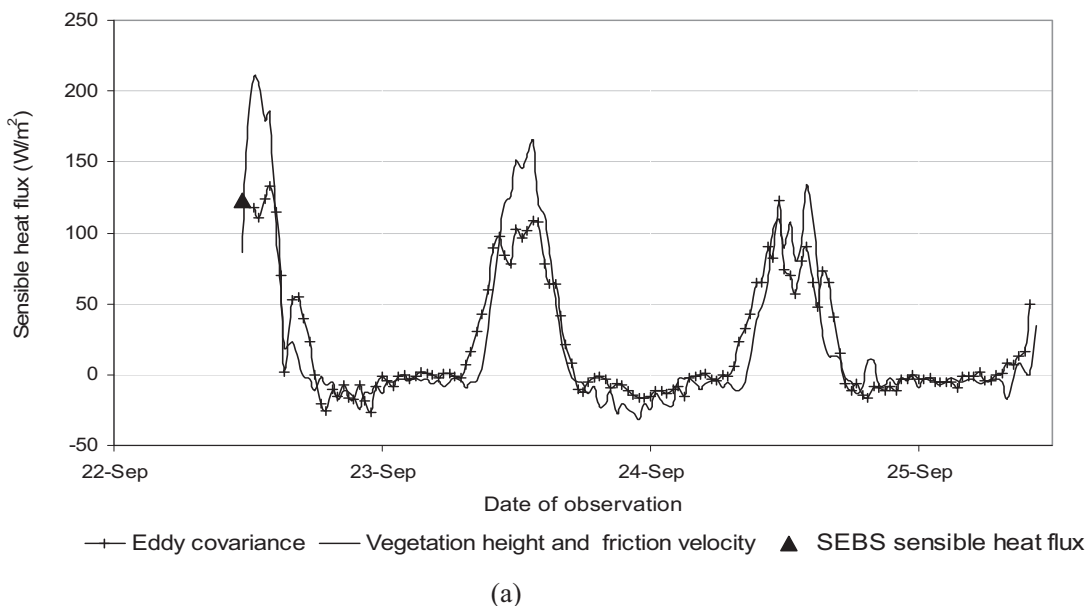
6.2.1. Sensible heat flux

Sensible heat flux computed from the sonic anemometer data was compared with the SEBS derived sensible heat flux estimations. Friction velocity is required for the computation of roughness height in equation (4.9). The slope of mean wind speed (u) vs friction velocity (u_*) was used for the computation of roughness height in equation (4.9). This is shown in Fig 6-7d.

The sensible heat flux was compared at pixel level and at an average of five nearest pixels around the eddy flux tower. Average of the nearest five pixels around the eddy flux tower including the pixel at the eddy flux tower was considered for the SEBS sensible heat flux. The comparison of the SEBS retrieved sensible heat flux and the eddy covariance method is explained as: The average of the five pixels from SEBS estimation on day 22 Sep., 2008 was 119 W/m², while the eddy covariance sensible heat was 111 W/m². At pixel level on same day SEBS overestimates by 12 W/m². The detail comparisons are shown in Table 6-7. The sensible heat flux calculated from friction velocity, measured vegetation height and the radiometric surface temperature computed from CNR1 observation during the field campaign using equations (4.7-4.9) was also compared with sensible heat flux from the eddy covariance. This sensible heat flux was having RMSE of 31 W/m² and AME of 21 W/m² when compared with sensible heat flux observed from the eddy flux tower. This comparison is shown in the Fig. 6-7a. The sensible heat flux calculated from roughness height of equation (4.9) which requires friction velocity was compared with sensible heat flux from roughness height estimated from equation (4.18). Both were almost the same as shown in Fig 6-7 c.

Table 6-7 Comparison of sensible heat flux from SEBS estimation and eddy covariance method

Date	SEBS sensible heat flux (W/m ²)			Eddy covariance sensible heat flux (W/m ²)
	Pixel	five pixels		Pixel
		Average	Standard deviation	
22-Sep-08	123	119	36	111
29-Sep-08	116	107	11	82



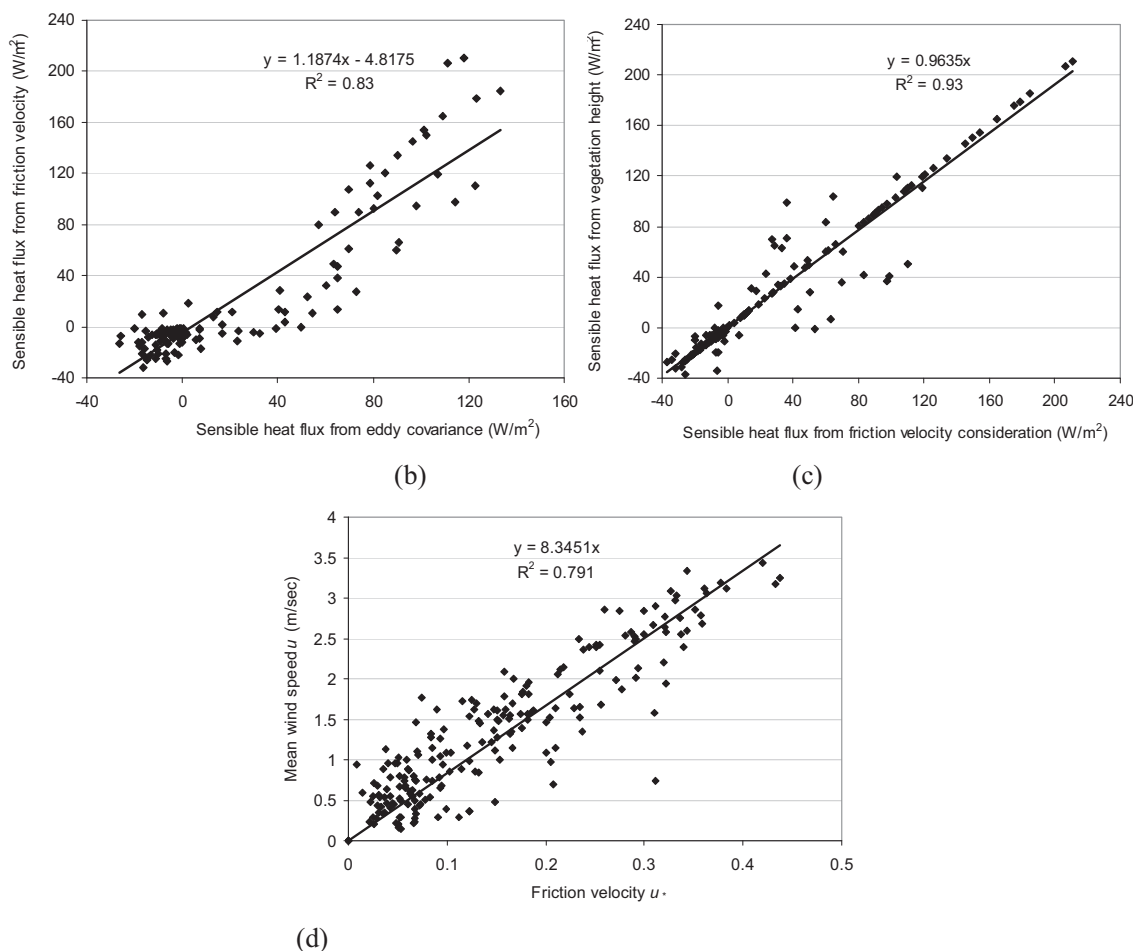


Figure 6-7 Sensible heat flux comparison between (a) eddy covariance, from friction velocity and from SEBS (b) Scatter plot sensible heat flux from friction velocity vs eddy covariance sensible heat flux, and (c) scatter plot of sensible heat flux from roughness height from vegetation vs sensible heat flux from friction velocity consideration for roughness height (d) wind speed vs friction velocity

6.2.2. Latent heat flux

The daily latent heat flux was calculated from the full three days of eddy flux tower observation using equation (4.12). This was compared with the P-M reference ET. It is shown in the Table 6-8 that the P-M ET_o was less by about 12%. This difference was comparable with the literature value of rice crop coefficient during its mid development season (Allen, 1998). Unfortunately there were no good satellite images during these three days and comparing with the SEBS actual ET estimations was not possible.

Table 6-8 Latent heat flux comparison with ET_o

Date	Sensible heat flux MJ/(m ² day)	Rnet MJ/(m ² day)	Latent heat flux (mm/day)	P-M ET _o (mm/day)	Kc
23 Sep.2008	2.045	15	5.29	4.58	1.15
24 Sep. 2008	1.813	13.66	4.84	4.33	1.12
28 Sep. 2008	2.831	15.74	5.27	4.81	1.10
average	2.23	14.8	5.13	4.57	1.12

6.2.3. Evaporative fraction

The instantaneous evaporative fraction calculated from remote sensing technique was compared with evaporative fraction computed from the eddy flux tower at the time of satellite overpass. The evaporative fraction from SEBS algorithm was comparable with the eddy flux tower computation at the time of satellite overpass. These instant values were also compared with the daily average values calculated from the eddy flux measurement equation (4.12) by the principle of energy balance. It was found that the instantaneous evaporative fraction was less by an average of about 12 %. The comparison is shown in the Table 6-9.

Table 6-9 Comparison of instantaneous and daily evaporative fraction

Date	Evaporative fraction			
	Instantaneous		Daily	Diff (%)
	From satellite data	Eddy flux data		
22-Sep-08	0.75	0.76	-	-
23-Sep-08	-	0.79	0.89	11.54
24-Sep-08	-	0.79	0.88	10.38
28-Sep-08	-	0.70	0.83	15.00
29-Sep-08	0.77	0.71	-	-

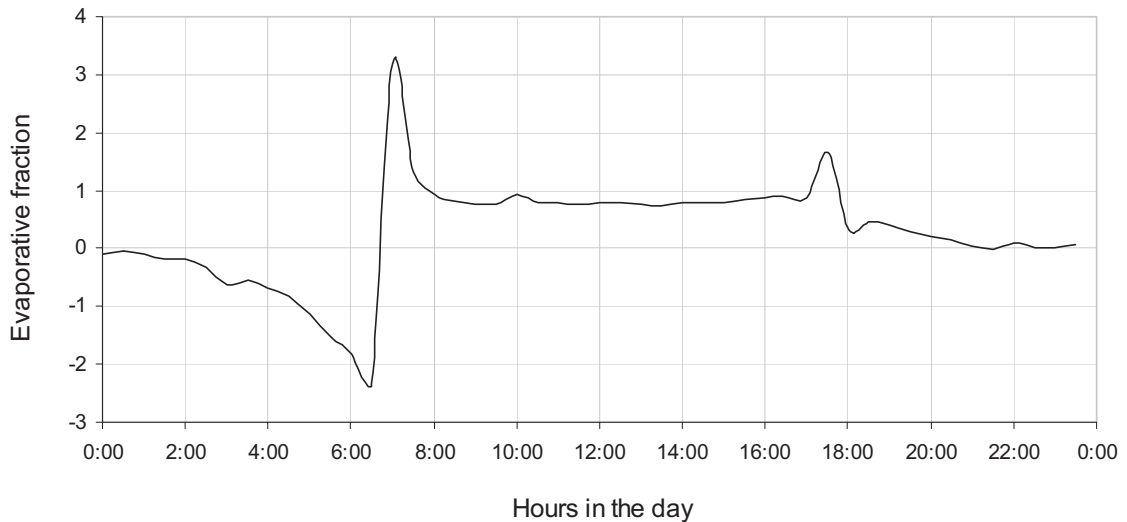


Figure 6-8 Daily variation of evaporative fraction in clear sky days

6.2.4. Surface albedo

Surface albedo was computed from the eddy flux tower observation of CNR1, for three days. The instantaneous albedo computed was compared with the calculated daily average. It was found that the instantaneous albedo was about 15% lower than the daily albedo. So the daily albedo was adjusted accordingly from the instantaneous albedo computed from the remote sensing data. This adjusted albedo was used for the estimation of daily ET in remote sensing techniques using SEBS. This ground measurement indeed improves the remote sensing estimations of daily ET over the study area. The

instant and the daily computed albedo are shown in the Table 6-10. The daily albedo variation graph is also shown in the Fig 6-9.

Table 6-10 Instant and daily albedo computed from the CNR1 observations

Date	Instant albedo at satellite overpass	Daily albedo	Percentage increase (%)
23-Sep-08	0.13	0.15	15.4
24-Sep-08	0.13	0.15	15.4
28-Sep-08	0.13	0.15	15.4
Average	0.13	0.15	15.4

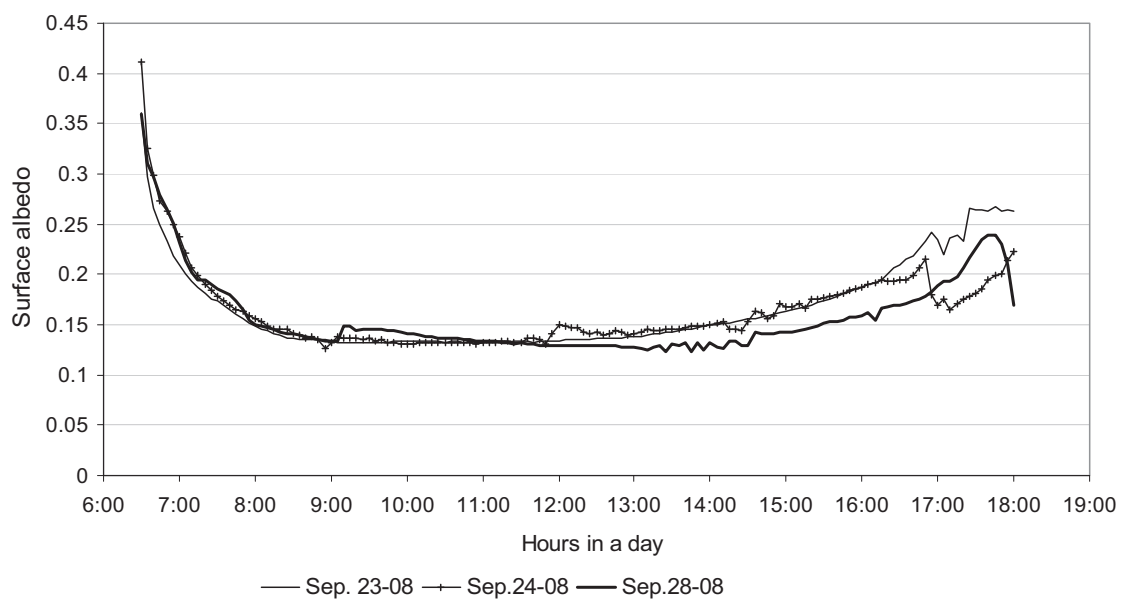


Figure 6-9 Daily surface albedo variation

6.2.5. Roughness height for momentum transfer

The roughness height for momentum transfer computed from the eddy flux measurement was compared with the SEBS estimated value from the remote sensing spectral signatures, equation (4.19). From the eddy flux measurement data roughness height was computed equation (4.9) as 0.11m and from the measured vegetation height equation (4.18), it was computed as 0.09m, whereas from the remote sensing estimations using NDVI an average value of the five pixels was found as 0.358 m. This relatively higher value of from remote sensing technique contributes to a lower value of aerodynamic resistance which in turn contributes to higher estimates of sensible heat flux. SEBS uses equations (4.19) in the estimation of roughness height for momentum transfer and equation (4.31) in the estimation of the roughness height for heat transfer and stability correction functions for heat and momentum transfer are applied in the computation of sensible heat flux.

6.3. Remote sensing Results

6.3.1. Comparison of SEBS actual evapotranspiration to P - M reference ET

In this section the remote sensing results will be explained. In general terms it is difficult to compare the results obtained from the remote sensing technique and conventional methods due to temporal and spatial scale issues. Ground based methods are limited in a smaller spatial area and computed mostly on daily basis, whereas the remote sensing technique estimates ET at larger spatial area and at instant time at satellite overpass. Taking these in to consideration, the SEBS actual ET was compared with the P-M reference ET. The average of the whole study area in remote sensing estimation was compared with the P-M estimation. This comparison is shown in Table 6-11 and Fig. 6-11.

It is well known that AET varies temporally and spatially due to soil moisture conditions, land cover heterogeneity and climatic conditions. The remote sensing estimation at specific days of computation was correlated with the P-M ETo estimations on same days. The scatter plot is shown in Fig. 6-10. This was done separately for dry and wet seasons. These correlations were applied for other days where there were no remote sensing estimations. This was used for the monthly and annual estimations of actual ET over the Fogera flood plain. The annual actual ET in the year 2008 over the Fogera flood plain from remote sensing estimation supported with P-M estimation was 1519 mm while the P-M ETo was 1498 mm. The mean annual rainfall over the last five years in the Fogera flood plain was 1296 mm. The annual actual ET was 17 % higher than the mean annual rainfall over the area. This was due to the irrigation practices in dry season over the area. Ribb and the Gumara rivers are extensively used for local irrigation scheme over the flood plain during the dry season.

Table 6-11 Daily and monthly ET in the year 2008

Date of computation	Daily ET (mm)		Months	Monthly ET (cm)	
	SEBS	P-M ETo		SEBS	P-M ETo
7-Dec-07	2.9	3.3	December	9.7	10.7
1-Jan-08	3.3	3.7	January	10.4	11.5
25-Feb-08	4.2	4.5	February	11.1	12.2
28-Mar-08	4.7	4.9	March	13.9	15.3
26-Apr-08	3.7	5	April	12.6	13.9
15-May-08	5.0	4.8	May	12.6	13.8
9-Jun-08	4.5	4.1	June	13.2	11.6
25-Jul-08	4.3	3.6	July	13.3	11.8
23-Aug-08	4.8	4.5	August	13.8	12.2
6-Sep-08	5.0	4.3	September	13.9	12.4
7-Oct-08	5.2	4.6	October	15.3	13.8
14-Nov-08	4.1	3.7	November	12.0	10.6
			Yearly ET	151.9	149.8

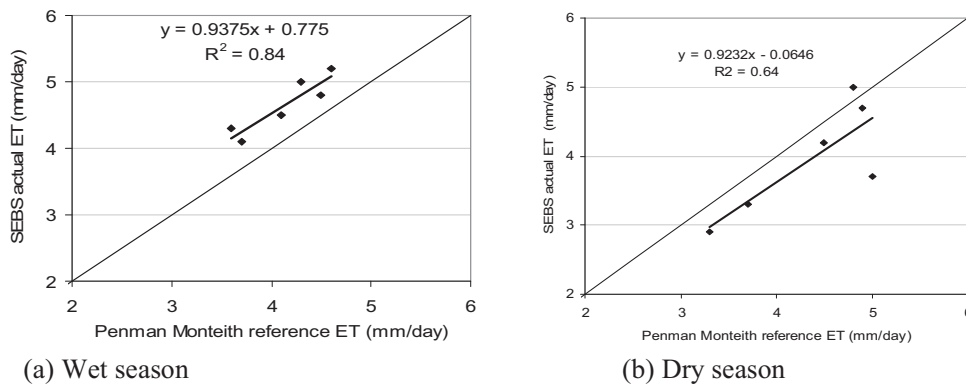


Figure 6-10 Scatter plot of SEBS actual ET vs P- M reference ET on (a) wet season and (b) dry season

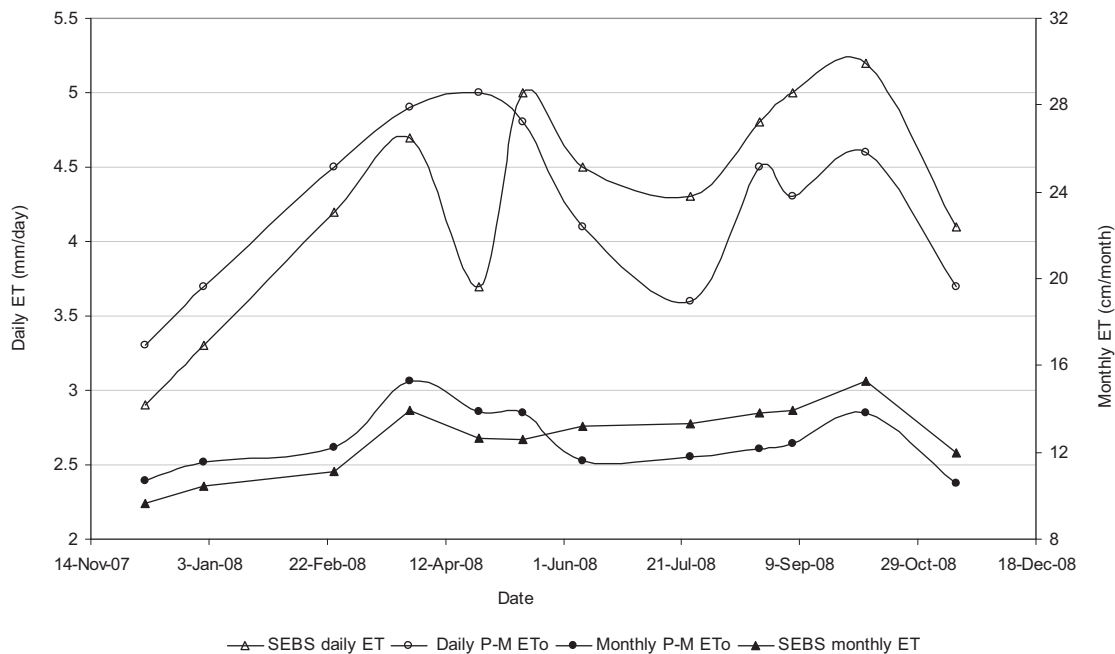


Figure 6-11 Daily actual ET, daily and monthly reference ET, and daily solar radiation and maximum temperature

In Fig. 6-11 both daily and monthly actual ET from SEBS and daily and monthly P-M ETo estimations follow similar trend. In wet months the daily estimations from SEBS was larger than the respective P-M ETo estimations, whereas in relatively dry months, the P-M ETo was larger than the remote sensing SEBS estimations. This was mainly due to the soil moisture content is the limiting factor for actual ET in dry months and the fact that the majority of the area is bare land in the dry season. April is the driest month in the Fogera flood plain. In this month soil moisture was the limiting factor for actual ET. That was why actual ET was less in this month. During rainy seasons ET was limited by the available solar energy. During this period radiation reduced due to high cloud cover in rainy season in the study area.

6.3.2. Spatio-temporal distribution of SEBS ET over the entire flood plain

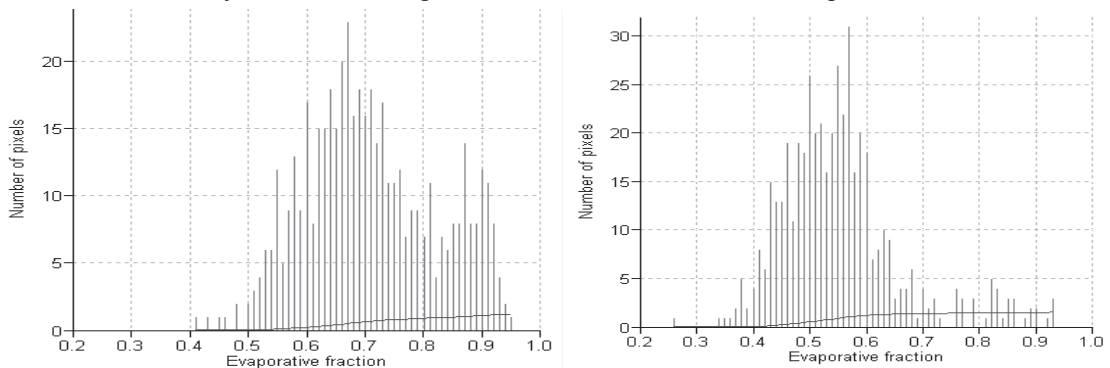
The spatial and temporal variation of ET in the entire Fogera flood plain was analysed using three selected days' images. The spatial variation over the entire area was more pronounced in the dry

months than wet months. The spatial and temporal variation of ET is shown in Fig.6-13 for selected months.

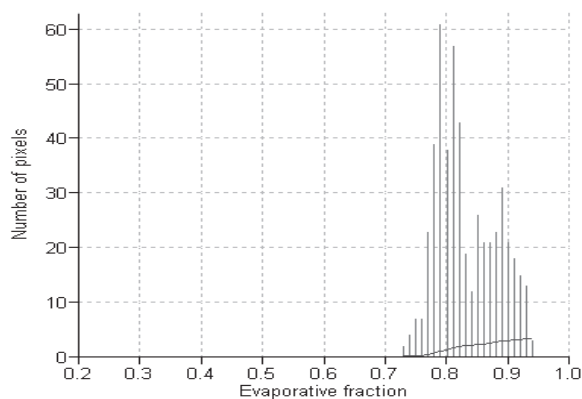
On 1 January 2008, the actual ET over the flood plain ranges from a minimum value of 2 mm in a day in bare land pixels to a maximum of about 4.6 mm a day in forest and water bodies, with mean value of 3.3 mm a day and standard deviation of 0.59 mm. The evaporative fraction shown in the Fig. 6-12a for this day ranges from 0.4 to 0.95, with the mean of 0.71 and standard deviation of 0.11.

In the same way on 26 April 2008, the spatial distribution of ET follows similar pattern as 1 January 2008, except here more pixels become drier. In this day the minimum ET was as low as 1.5 mm a day and the maximum was about 5 mm a day, with mean of 3.25 mm and standard deviation of 0.61 mm. While evaporative fraction ranges from 0.3 to 0.9 with mean of 0.55 and standard deviation of 0.11. It is shown Fig. 6-12b. Here, the mean evaporative fraction for both the 1 January and April 26 are different whereas the mean of the daily ET was very similar. This was due the difference in the available energy between these two days. The available energy in April was greater.

On 6 Sep. 2008 daily ET ranges from a minimum of about 4 mm to a maximum of 6 mm. with mean value of 4.95 mm and standard deviation of 0.37 mm. The evaporative fraction shown in the Fig.6-12c ranges from 0.74 to 0.95 with mean value of 0.83 and standard deviation of 0.05. The lower standard deviation here clearly shows that the spatial variation in wet months is not pronounced.



(a) Histogram of evaporative fraction January 1, 2008 (b) Histogram of evaporative fraction April 26, 2008



(c) Histogram of evaporative of evaporative fraction on Sep. 6, 2008

Figure 6-12 Histogram of three different days in a year over the Fogera flood plain

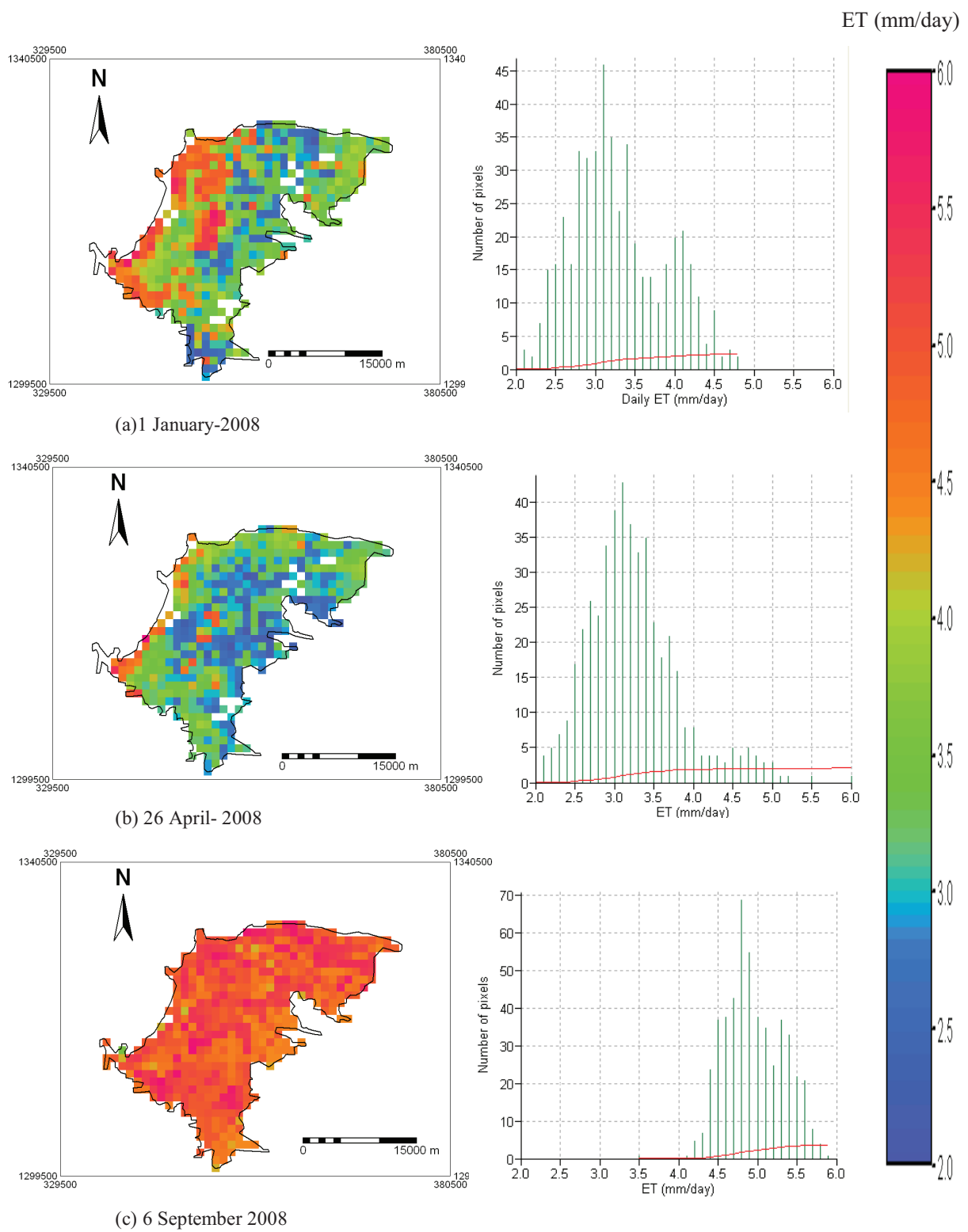


Figure 6-13 Spatio-temporal distribution of ET over the Fogera flood plain with respective histogram (a) 1 January 2008 (b) 26 April 2008 (c) 6 September 2008

6.3.3. Spatio-temporal variations of SEBS actual ET over rice fields

The spatio-temporal variation of ET over the rice field in study area was analysed using three selected images. On 7 July, 2008 the actual ET over the rice field ranges from a minimum value of 2.7 mm to a maximum of 4.7 mm a day, with mean value of 3.6 mm a day and standard deviation of 0.27 mm. Similarly, on 6 Sep., 2008 ET varies from a minimum of 3.5 mm to a maximum of 5.9 mm in a day, with mean of 4.95 mm and standard deviation of 0.37 mm. whereas, on 7 Dec., 2008 ET varies from a minimum of about 1.5 mm to a maximum of 4.7 mm in a day with a mean of 2.88 mm and standard deviation of 0.79. The lower value of standard deviation in July and September showed that the spatial variation was minimized in rice field, whereas in December the spatial variation of ET was larger as the standard deviation was also relatively larger. This is due the fact that during this period majority of the rice has been harvested.

Summarizing, the spatial variation of ET over the rice field during seedling and the fully growing seasons was not pronounced whereas the temporal variation of ET in the rice field was larger during the fully grown stage. During early and harvesting stage of rice, ET was relatively low compared to its fully growing season. The images and respective histograms of the above mentioned days are shown in the Fig. 6-14.

6.3.4. Deriving single crop coefficient (Kc) for rice field

About 56 % of the Fogera flood plain was covered by the rice production. The rice crop coefficient (Kc) was estimated as the ratio of SEBS retrieved actual evapotranspiration (AET) to P-M reference ET of the rice field in the flood plain. Crop coefficient is a traditional concept that relates the actual water needed for a crop to the reference crop. The effects of characteristics that distinguish field crops from the reference grass are integrated in to the crop coefficient (Kc). The Kc of a crop varies with the crop growing stages (Allen, 1998). Here, this has been clearly observed from the Kc images of the rice field prepared from SEBS actual ET and P-M reference ET for the rice field.

The spatial and temporal variation is shown in the Kc images in the Fig. 6-15. In this figure seasonal variation is clearly shown. In July where the rice was in seedling stage the Kc had an average value of 0.9 with standard deviation of 0.12. In September, when the rice was in its mid season, the Kc value had an average value of 1.16, with standard deviation of 0.13 and during harvesting period, Kc reduced to an average of 0.81 and standard deviation of 0.30. These values agree well with the literature values of 1.0, 1.15 and 0.7-0.45 for initial, mid and end seasons of the cropping period respectively (Allen, 1998).

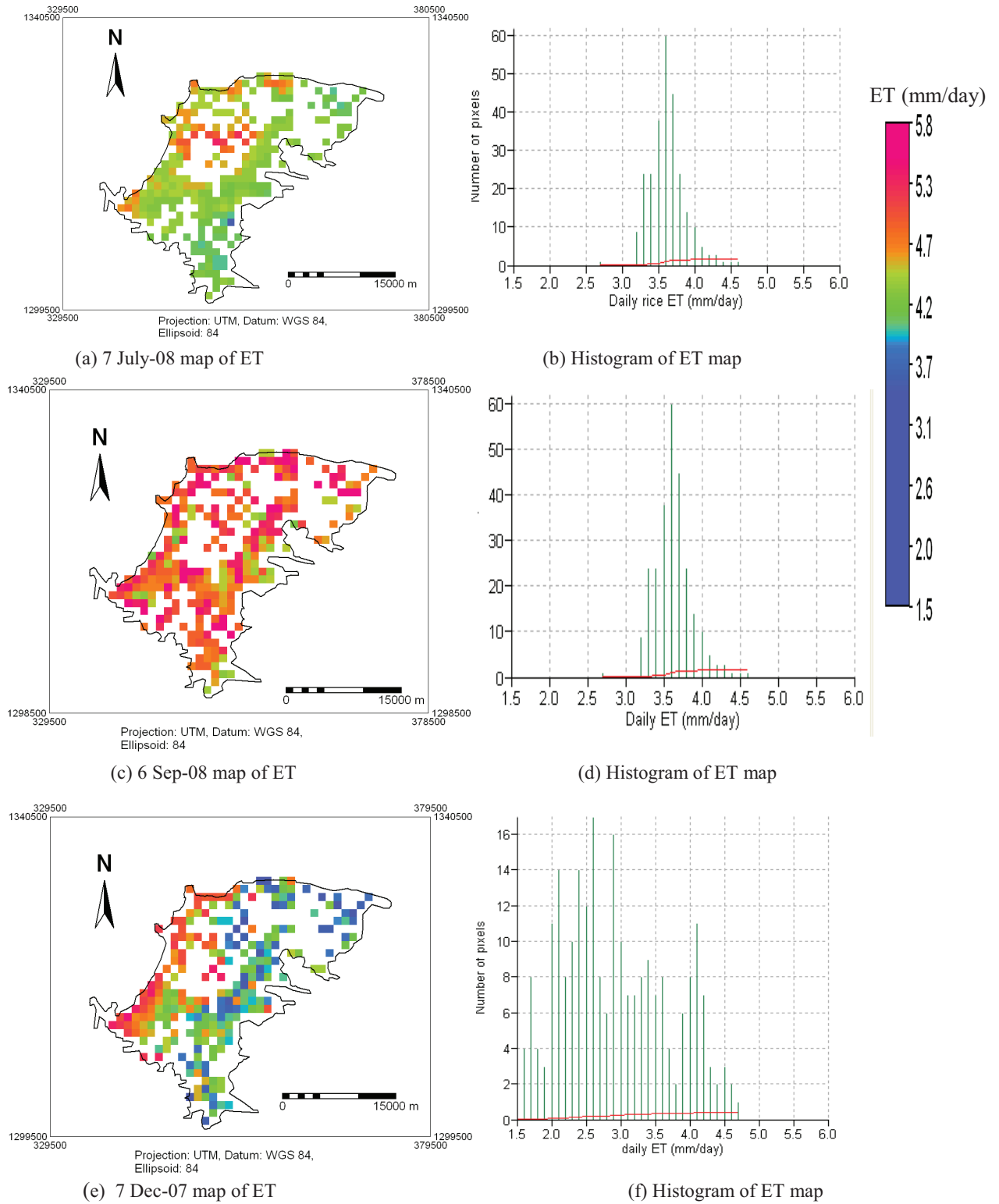
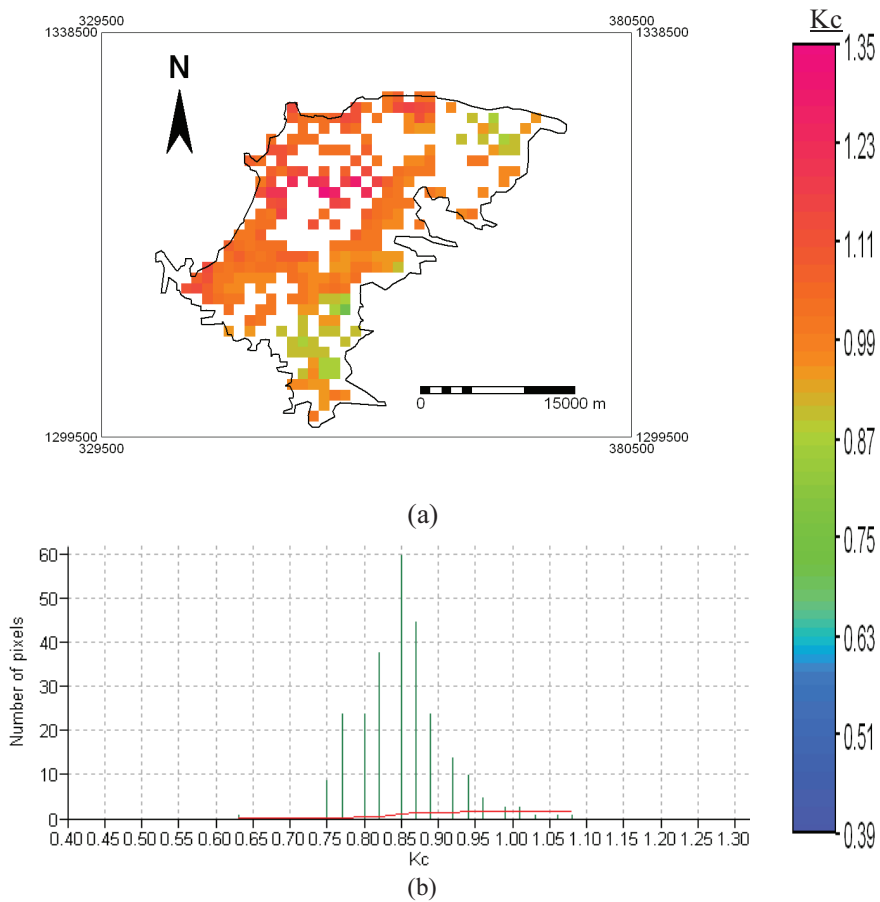


Figure 6-14 Spatio-temporal distribution map of ET over the rice field with respective histogram in the Fogera flood plain (a), (b) 7 July 2008 (c),(d) 6 September 2008 and (e),(f) 7 December 2007



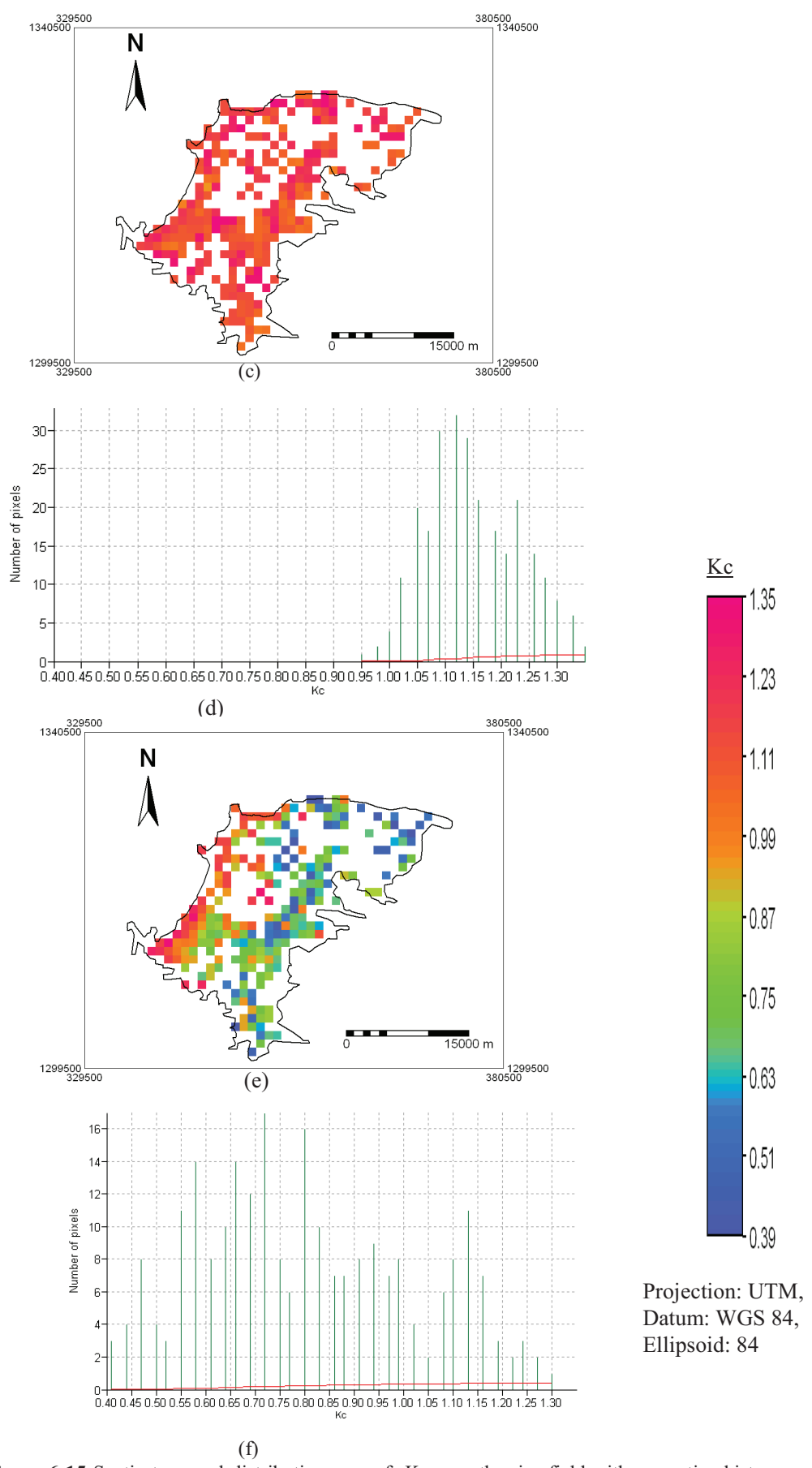


Figure 6-15 Spatio-temporal distribution map of K_c over the rice field with respective histogram (a), (b) 7 July 2008 (c),(d) 6 September 2008 and (e),(f) 7 December 2007

7. Conclusions and recommendations

7.1. Conclusions

The main objective of this study was estimation of spatial and temporal variation of ET using remote sensing data from SEBS algorithm and estimation of ET by different conventional methods that require ground based meteorological data. To do this, MODIS reflectance and land surface temperature products were used as remote sensing data. For ground based data the Woreta weather station data and the Bahir Dar weather station data was used. In addition, the eddy flux tower data installed during the field campaign were also used.

Besides remote sensing estimations of ET, ground based estimations of ET was also done using different conventional methods for the year 2008. As there was no ground based measurement of ET for validation, the different conventional methods used were compared with the Penman-Montheith reference ET. This comparison showed that, from the different conventional methods used, the modified Makkink method was the only method which does not require local calibration of the coefficient. This method performs well in this area as it gives a result with coefficient of determination R^2 of 0.93, RMSE of 0.19 mm, AME of 0.16 mm with the Woreta data set. P-T and Abteu equations require local calibration of the coefficients. The P-T method was over estimating with the coefficient, $\alpha = 1.26$. Better estimate was found when the coefficient α was reduced to 1.14. The estimations in both these methods have been improved after using the new calibrated coefficients.

The simple Abteu radiation equation which only uses incoming solar radiation was also performing well in the area after calibrating the coefficient. After calibration it gives R^2 of 0.9, RMSE of 0.25, and AME of 0.21. This concludes that, it is possible to estimate ET reasonably over the Fogera flood plain using radiation data only.

The temperature method developed based on air temperature was able to estimate reference ET in the area with less than 10 % error on daily basis comparison where as on annual based comparisons it was able to estimate with 2 % error from P-M reference ET estimates. This method will be useful in areas where there is insufficient data as it works with only maximum temperature observation.

The P-M reference ET sensitivity analysis done in the Fogera flood plain showed that, solar radiation and temperature were comparably most sensitive weather variables whereas wind speed was the least sensitive next to relative humidity

The ground based measurements were used to improve the remote sensing estimations. The daily net radiation and the daily albedo computed from the eddy flux tower observation were used to improve the remote sensing estimations. The instantaneous albedo during the satellite overpass was found about 15 % less from the daily albedo. Hence, the remote sensing albedo was increased by 15 % for estimation of daily ET. This indeed improves the remote sensing estimations of ET. Similarly, the net radiation computed from equation (4.46) was also able to improve the remote sensing estimations, as

the coefficients are calibrated from the ground based observation of eddy flux tower data and meteorological data.

The spatial average of actual ET estimated from SEBS over the area was smaller than the P-M reference ET in relatively drier periods, whereas when the soil moisture was not limiting factor for ET, the actual ET was larger than the P-M reference ET. The annual actual ET over the flood plain was found about 1519 mm whereas the annual P-M reference ET was 1498 mm. In wet seasons the spatial variation of actual ET was not well pronounced, whereas in relatively dry months the spatial variation was clearly pronounced. In dry and bare land pixels ET was smaller whereas in wet pixels like vegetated areas ET was larger.

The crop coefficient (K_c) of the rice field was estimated in the three growing seasons of the rice field. The estimations of K_c in the seedling, fully grown, and harvesting periods were: 0.9, 1.16, and 0.81 respectively. These values agree well with the literature values (Allen, 1998).

7.2. Recommendations

The recommendations with drawn from this study are:

- For more accurate estimation of ET over the Fogera flood plain, sufficient meteorological data collected in the flood plain and sufficient validation data of Eddy flux data or Lysimeter data is recommended.
- As most private agricultural fields in the area are less than 1 km, for better estimation of ET over specific fields, high resolution satellite data like ASTER and/ or Landsat is recommended.
- Until more accurate estimations of ET with more validation will be done over the area, the modified Makkink method and/or the Abteu simple equation with the calibrated coefficients could be used for future estimations of ET in the Fogera flood plain.

Appendix - A FAO-56 method for net radiation computation

The Penman-Monteith and other conventional methods for estimations of reference evapotranspiration require net radiation or solar radiation as input. The net radiation and the solar radiation were computed following the FAO-56 methodology explained here. The general Penman Monteith equation for the latent heat flux expressed as:

$$\lambda ET = \frac{\Delta(R_n - G) + \rho_a C_p \left(\frac{e_s - e_a}{r_a} \right)}{\Delta + \gamma \left(1 + \frac{r_s}{r_a} \right)} \quad (\text{A.-1})$$

Where R_n is the net radiation,

G is the soil heat flux, considered negligible on daily bases,

$e_s - e_a$ represents the vapour pressure deficit of the air,

ρ_a is the mean air density at constant pressure,

C_p is the specific heat of the air,

Δ represents the slope of the saturation vapour pressure temperature relationship,

γ is the psychrometric constant, and

r_s and r_a are the (bulk) surface and aerodynamic resistances (Allen, 1998). Parameter units defined below.

This method includes all parameters that govern energy exchange and the corresponding latent heat flux from uniform expanses of vegetation. Most of the parameters in the above equation are measured or calculated from weather data. The method used for the calculation of any crop evapotranspiration as the surface and aerodynamic resistances are crop specific. The transfer of turbulent fluxes from the evaporating surface into the air above the evaporating surface is determined by the aerodynamic resistance, assuming neutral stability conditions, (where temperature, atmospheric pressure, and wind velocity distributions follow nearly adiabatic conditions (no heat exchange)). Estimating ETo in the well-watered reference surface, heat exchanged is small, and therefore stability correction is normally not required. Hence, aerodynamic resistance can be estimated as,

$$r_a = \frac{\ln\left(\frac{z_m - d}{z_{om}}\right) \ln\left(\frac{z_h - d}{z_{oh}}\right)}{k^2 u_z} \quad (\text{A-2})$$

where r_a aerodynamic resistance (s/m), z_m height of wind speed measurements (m), z_h height of humidity measurements (m), d zero plane displacement height (m), z_{om} roughness length governing momentum transfer (m), z_{oh} roughness length governing transfer of heat and vapour (m), k von Karman's constant 0.41, u_z wind speed at height z (m/s)

For the known vegetation height (h), zero plane displacement height (d) and the roughness length for momentum can be estimated from experimental result as:

$$d = 0.67h \text{ and } z_{om} = 0.123h \quad (\text{A-3})$$

Accordingly, the roughness height for heat transfer can be estimated as, $z_{oh} = 0.1 z_{om}$, as the reference height was considered to be 0.12 m and using equation (A-3) above. The aerodynamic resistance was estimated as $r_a = 208/u_2$ and assumed a single bulk resistance for a reference grass to be $r_s = 70 \text{ s/m}$.

The extraterrestrial radiation (R_a) for the day of the year and for different locations can be calculated from the solar constant, the solar declination and the time of the year as:

$$R_a = \frac{24(60)}{\pi} G_{sc} d_r (\omega_s \sin(\varphi) \sin(\delta) + \cos(\varphi) \cos(\delta) \sin(\omega_s)) \quad (\text{A-4})$$

where R_a extraterrestrial radiation ($\text{MJ/m}^2 \text{ day}$), G_{sc} solar constant = $0.0820 \text{ (MJ/ m}^2 \text{ min)}$, d_r inverse relative distance Earth-Sun (Equation A-5), ω_s sunset hour angle (equation A-6), φ latitude (radians), δ solar declination (equation A-7)

The inverse relative distance Earth-Sun d_r , the solar declination, δ , sun hour angle ω_s , and the day light hours N , in the equation above are given in the following equations respectively as:

$$d_r = 1 + 0.003 \cos\left(\frac{2\pi}{365} J\right) \quad (\text{A-5})$$

$$\delta = 0.409 \sin\left(\frac{2\pi}{365} J - 1.39\right) \quad (\text{A-6})$$

$$\omega_s = \arccos(-\tan(\varphi) \tan(\delta)) \quad (\text{A-7})$$

$$N = \frac{24}{\pi} \omega_s \quad (\text{A-8})$$

From the measured sunshine hours (n) at Bahir Dar station, incoming solar radiation was calculated as follows.

$$R_s = \left(a_s + b_s \frac{n}{N}\right) R_a \quad (\text{A-9})$$

where R_s solar or shortwave radiation ($\text{MJ /m}^2 \text{ day}$), n actual duration of sunshine (hour), N maximum possible duration of sunshine or daylight hours (hour), n/N relative sunshine duration, a_s regression constant, expressing the fraction of extraterrestrial radiation reaching the earth on overcast days ($n = 0$), $a_s + b_s$ fraction of extraterrestrial radiation reaching the earth on clear sky days ($n = N$). The values $a_s = 0.25$ and $b_s = 0.50$ are considered.

Longwave radiation

Daily net long wave radiation was also expressed quantitatively by the Stefan-Boltzmann law. The rate of long wave energy emission is proportional to the absolute temperature of the surface raised to the fourth power. Humidity and cloud affects Stefan-Boltzmann law; so, it requires to be corrected for these two factors when estimating - the net outgoing longwave radiation where it is estimated as:(Allen, 1998)

$$R_{nl} = \sigma \left(\frac{T_{\max}^4 + T_{\min}^4}{2} \right) \left(0.34 - 0.14 \sqrt{e_a} \right) \left(1.35 \frac{R_s}{R_{so}} - 0.35 \right) \quad (\text{A-10})$$

Where R_{nl} is the net longwave radiation (MJ /m² day), σ is the Stefan-Boltzmann constant (4.903*10⁻⁹ MJ /K⁴ m² day), T_{\max} is the maximum absolute temperature during the 24-hour period (K), T_{\min} minimum absolute temperature during the 24-hour period (K), e_a actual vapour pressure (kPa), R_s/R_{so} relative shortwave radiation, R_s measured or calculated. (Equation 4.18) solar radiation (MJ/m² day), R_{so} calculated (Equation A-9) is the clear-sky radiation (MJ/m² day), it is estimated as:

$$R_{so} = (0.75 + 2(10)^{-5} z) R_a \quad (\text{A-11})$$

where z is the station elevation above sea level.

The term $(0.34 - 0.14 \sqrt{e_a})$ and $(1.35 R_s / R_{so} - 0.35)$ in the above equation are the correction for air humidity, and effect of cloudiness in the computation of net radiation using Stefan-Boltzmann law.

Psychrometric constant

The psychrometric constant, γ , is given by:

$$\gamma = \frac{C_p P}{\epsilon \lambda} = 0.665 \times 10^{-3} P \quad (\text{A-12})$$

Where, γ is the psychrometric constant (kPa /°C), P atmospheric pressure (kPa), λ is the latent heat of vaporization, 2.45(MJ/ kg), C_p specific heat at constant pressure, 1.013*10⁻³ (MJ/ kg °C), ϵ is the ratio molecular weight of water vapour/dry air = 0.622.

Mean saturation vapour pressure (e_s)

As saturation vapour pressure is related to air temperature, it can be calculated from the air temperature. The relationship is expressed by:

$$e^o(T) = 0.6108 \exp\left(\frac{17.27T}{T + 237.3}\right) \quad (\text{A-13})$$

where $e^o(T)$ saturation vapour pressure at the air temperature (kPa), T is air temperature (°C). Due to the non-linearity of the above equation, the mean saturation vapour pressure for a day, week, decade or month should be computed as the mean between the saturation vapour pressure at the mean daily maximum and minimum air temperatures for that period:

$$e_s = \frac{e^o(T_{\max}) + e^o(T_{\min})}{2} \quad (\text{A-14})$$

Slope of saturation vapour pressure curve (Δ)

For the calculation of evapotranspiration, the slope of the relationship between saturation vapour pressure and temperature, Δ is required. The slope of the curve at a given temperature is given by.

$$\Delta = \frac{4098 \left[0.6108 \exp\left(\frac{17.27T}{T + 237.3}\right) \right]}{(T + 237.3)^2} \quad (\text{A-15})$$

where Δ is slope of saturation vapour pressure curve at air temperature T (kPa/ °C)

Actual vapour pressure (e_a) derived from relative humidity data

The actual vapour pressure can also be calculated from the relative humidity. Depending on the availability of the humidity data, different equations should be used.

For RH_{\max} and RH_{\min}

$$e_a = \frac{e^\circ(T_{\min}) \frac{RH_{\max}}{100} + e^\circ(T_{\max}) \frac{RH_{\min}}{100}}{2} \quad (\text{A-16})$$

where e_a actual vapour pressure (kPa), $e^\circ(T_{\min})$ saturation vapour pressure at daily minimum temperature (kPa), $e^\circ(T_{\max})$ saturation vapour pressure at daily maximum temperature (kPa), RH_{\max} maximum relative humidity (%), RH_{\min} minimum relative humidity (%).

In the absence of RH_{\max} and RH_{\min} , the daily mean relative humidity RH_{mean} can be used to estimate e_a :

$$e_a = \frac{RH_{\text{mean}}}{100} \left[\frac{e^\circ(T_{\max}) + e^\circ(T_{\min})}{2} \right] \quad (\text{A-17})$$

where RH_{mean} is the mean relative humidity, defined as the average between RH_{\max} and RH_{\min} .

Specific humidity calculated as:

$$q = \left(\frac{\varepsilon e_a}{p - ((1 - \varepsilon)e_a)} \right) \quad (\text{A-18})$$

where q (kg/kg) is specific humidity, $\varepsilon = 0.622$, e (kPa) is actual vapour pressure, p (kPa) is the atmospheric pressure.

Actual vapour pressure was calculated from the relative humidity measurement and saturation vapour pressure, and the saturation vapour pressure was calculated as:

$$\frac{RH}{100} = \frac{e}{e_s} \quad (\text{A-19})$$

$$e_s = \frac{e}{\left(\frac{RH}{100} \right)} \quad (\text{A-20})$$

Appendix - B MODIS spectral bands

Primary Use	Band	Bandwidth ¹	Spectral Radiance ²	Required SNR ³
Land/Cloud/Aerosols Boundaries	1	620 - 670	21.8	128
	2	841 - 876	24.7	201
Land/Cloud/Aerosols Properties	3	459 - 479	35.3	243
	4	545 - 565	29.0	228
	5	1230 - 1250	5.4	74
	6	1628 - 1652	7.3	275
	7	2105 - 2155	1.0	110
Ocean Color/ Phytoplankton/ Biogeochemistry	8	405 - 420	44.9	880
	9	438 - 448	41.9	838
	10	483 - 493	32.1	802
	11	526 - 536	27.9	754
	12	546 - 556	21.0	750
	13	662 - 672	9.5	910
	14	673 - 683	8.7	1087
	15	743 - 753	10.2	586
Atmospheric Water Vapor	16	862 - 877	6.2	516
	17	890 - 920	10.0	167
	18	931 - 941	3.6	57
Surface/Cloud Temperature	19	915 - 965	15.0	250
	20	3.660 - 3.840	0.45(300K)	0.05
	21	3.929 - 3.989	2.38(335K)	2.00
	22	3.929 - 3.989	0.67(300K)	0.07
Atmospheric Temperature	23	4.020 - 4.080	0.79(300K)	0.07
	24	4.433 - 4.498	0.17(250K)	0.25
Cirrus Clouds Water Vapor	25	4.482 - 4.549	0.59(275K)	0.25
	26	1.360 - 1.390	6.00	150(SNR)
	27	6.535 - 6.895	1.16(240K)	0.25
Cloud Properties	28	7.175 - 7.475	2.18(250K)	0.25
	29	8.400 - 8.700	9.58(300K)	0.05
Ozone	30	9.580 - 9.880	3.69(250K)	0.25
	31	10.780 - 11.280	9.55(300K)	0.05
Surface/Cloud Temperature	32	11.770 - 12.270	8.94(300K)	0.05

Cloud Top	33	13.185 - 13.485	4.52(260K)	0.25
Altitude	34	13.485 - 13.785	3.76(250K)	0.25
	35	13.785 - 14.085	3.11(240K)	0.25
	36	14.085 - 14.385	2.08(220K)	0.35
¹ Bands 1 to 19 are in nm; Bands 20 to 36 are in μm ² Spectral Radiance values are ³ SNR = Signal-to-noise ratio ⁴ NE(Δ)T = Noise-equivalent temperature difference				

Table B-1 Science data sets for 8-day composite reflectance products (MOD09A1), with respective specific products under MOD09A1

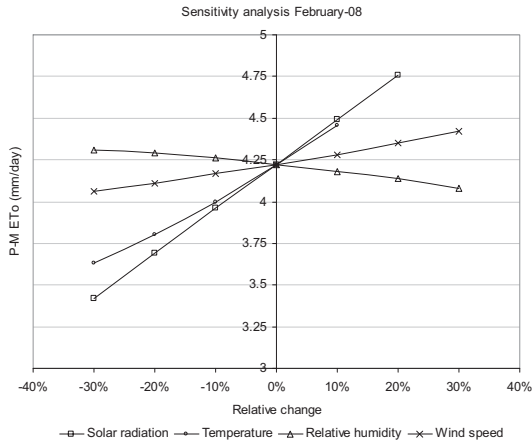
Science data sets	Units	Scale Factor
250m surface reflectance band 1 (620-670 nm)	Reflectance	0.0001
250m surface reflectance band 2 (841-876 nm)	Reflectance	0.0001
500m surface reflectance band 3 (459-479 nm)	Reflectance	0.0001
500m surface reflectance band 4 (545-565 nm)	Reflectance	0.0001
500m surface reflectance band 5 (1230-1250 nm)	Reflectance	0.0001
500m surface reflectance band 6 (1628-1652 nm)	Reflectance	0.0001
500m surface reflectance band 7 (2105-2155 nm)	Reflectance	0.0001
500m reflectance band quality	Bit Field	NA
Solar zenith angle	Degree	0.01
Solar zenith angle 16-bit	Degree	0.01
View zenith angle	Degree	0.01
Relative azimuth angle	Degree	0.01
500m state flags	Bit field	NA
Day of year	Julian day	NA

Table B - 2 The Science data sets for daily LST (MOD11A1) products

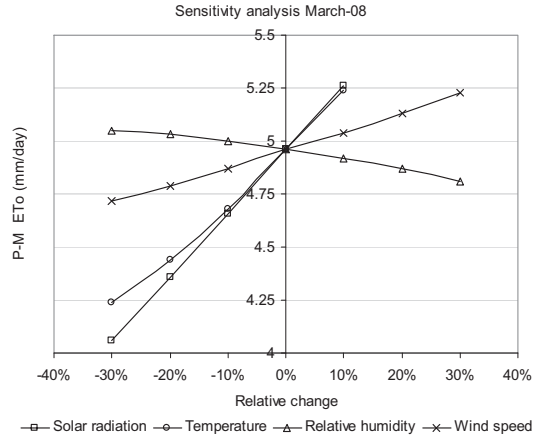
Product SDS Name	Long Name	Unit	scale factor	add offset
LST_Day_1km	Daily daytime 1km grid Land-surface Temperature	K	0.02	0.0
QC_Day	Quality control for daytime LST and emissivity	none	NA	NA
Day_view_time	(local solar) Time of daytime Land-surfaceTemperature observation	hrs	0.1	0
Day_view_time	(local solar) Time of daytime Land-surfaceTemperature observation	hrs	0.1	0
Day_view_time	(local solar) Time of daytime Land-surfaceTemperature observation	hrs	0.1	0
Day_view_angle	View zenith angle of daytime Land-surface Temperature	deg	1.0	-65.0
Emis_31	Band 31 emissivity	none	0.002	0.49
Emis_32	Band 32 emissivity	none	0.002	0.49
Clear_day_cov	day clear-sky coverage	none	0.0005	0.0

Appendix - C Sensitivity analysis result

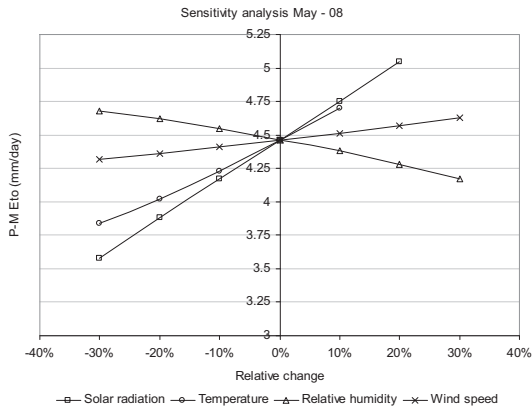
The sensitivity analysis result is shown in the figures below



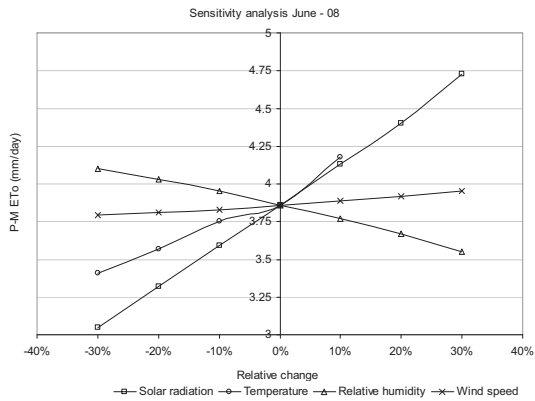
(a) February



(b) March



(c) May



(d) June

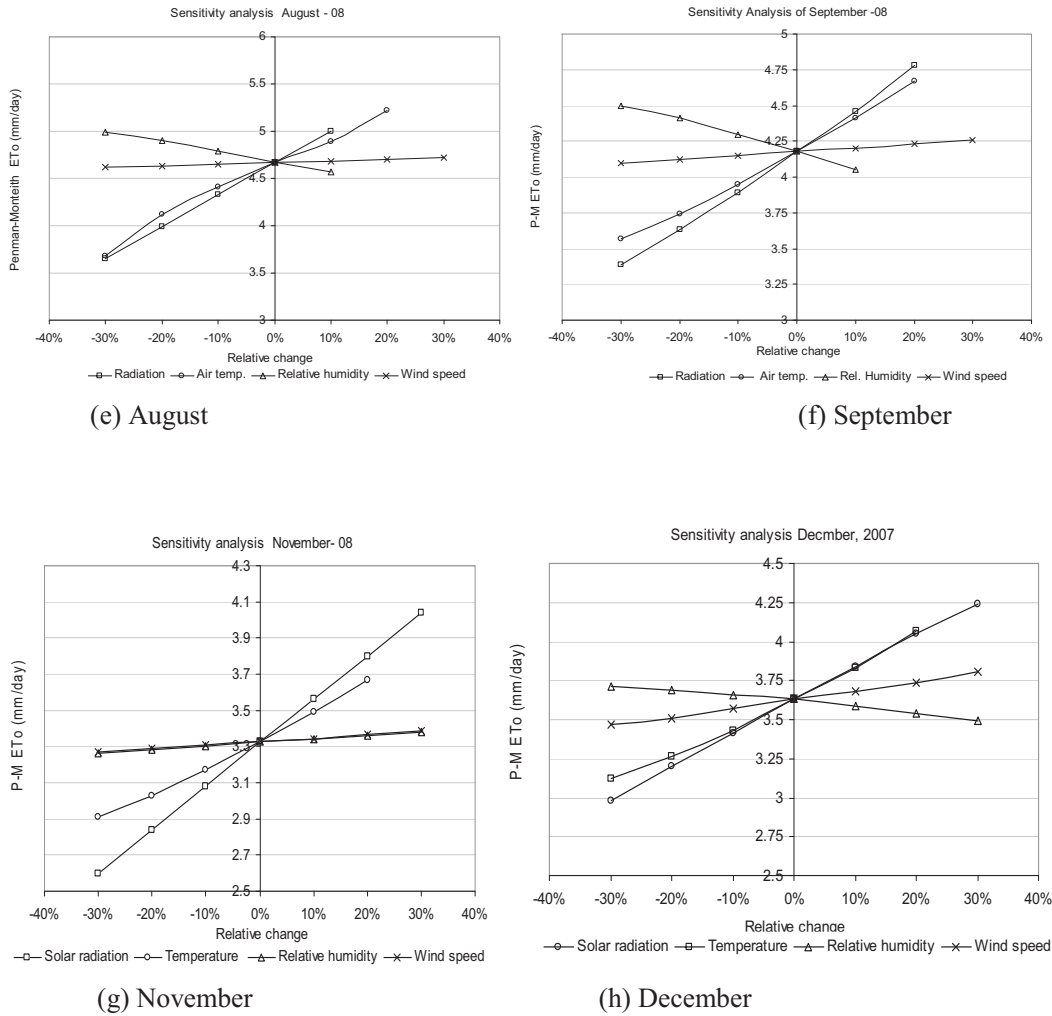
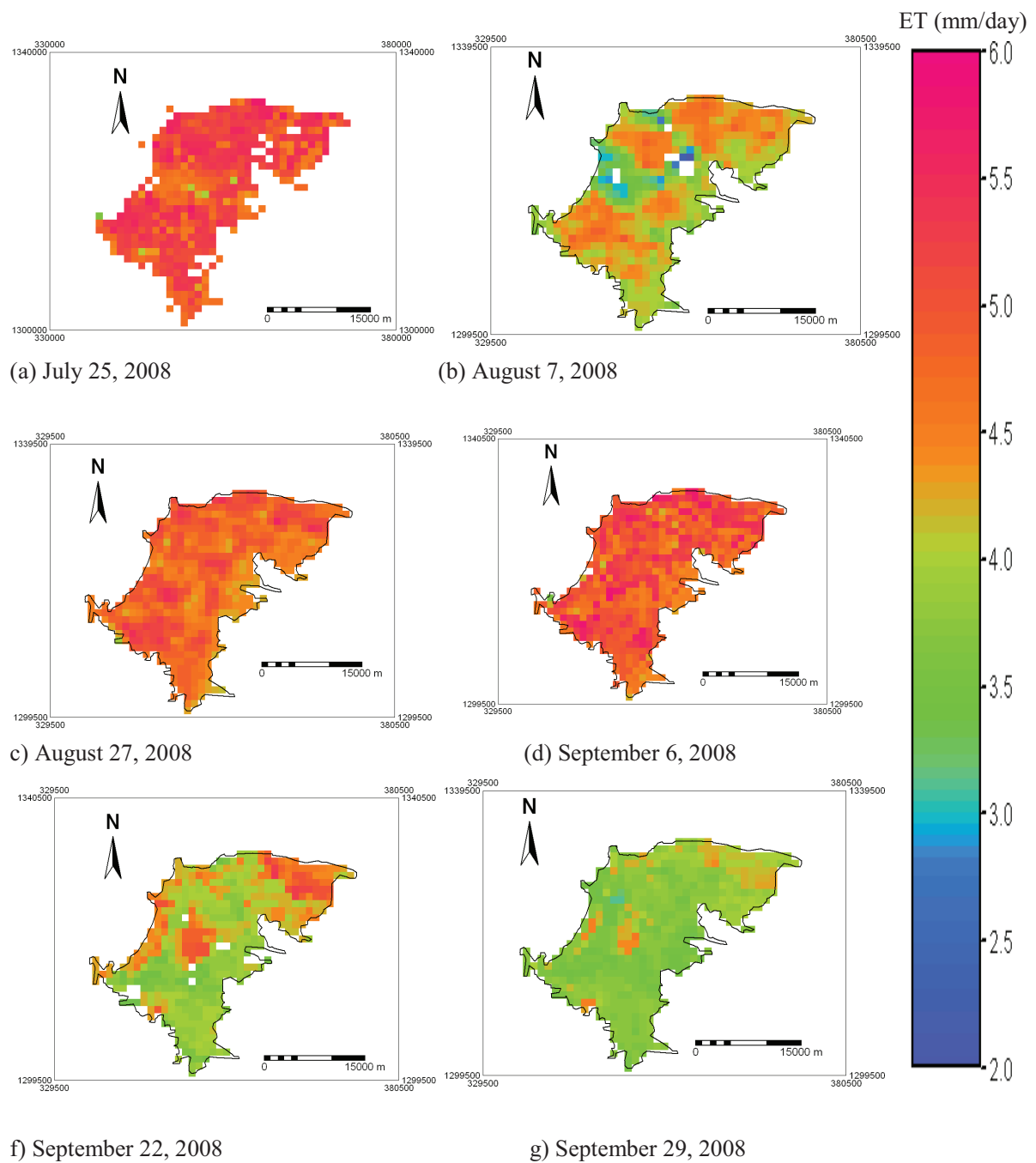
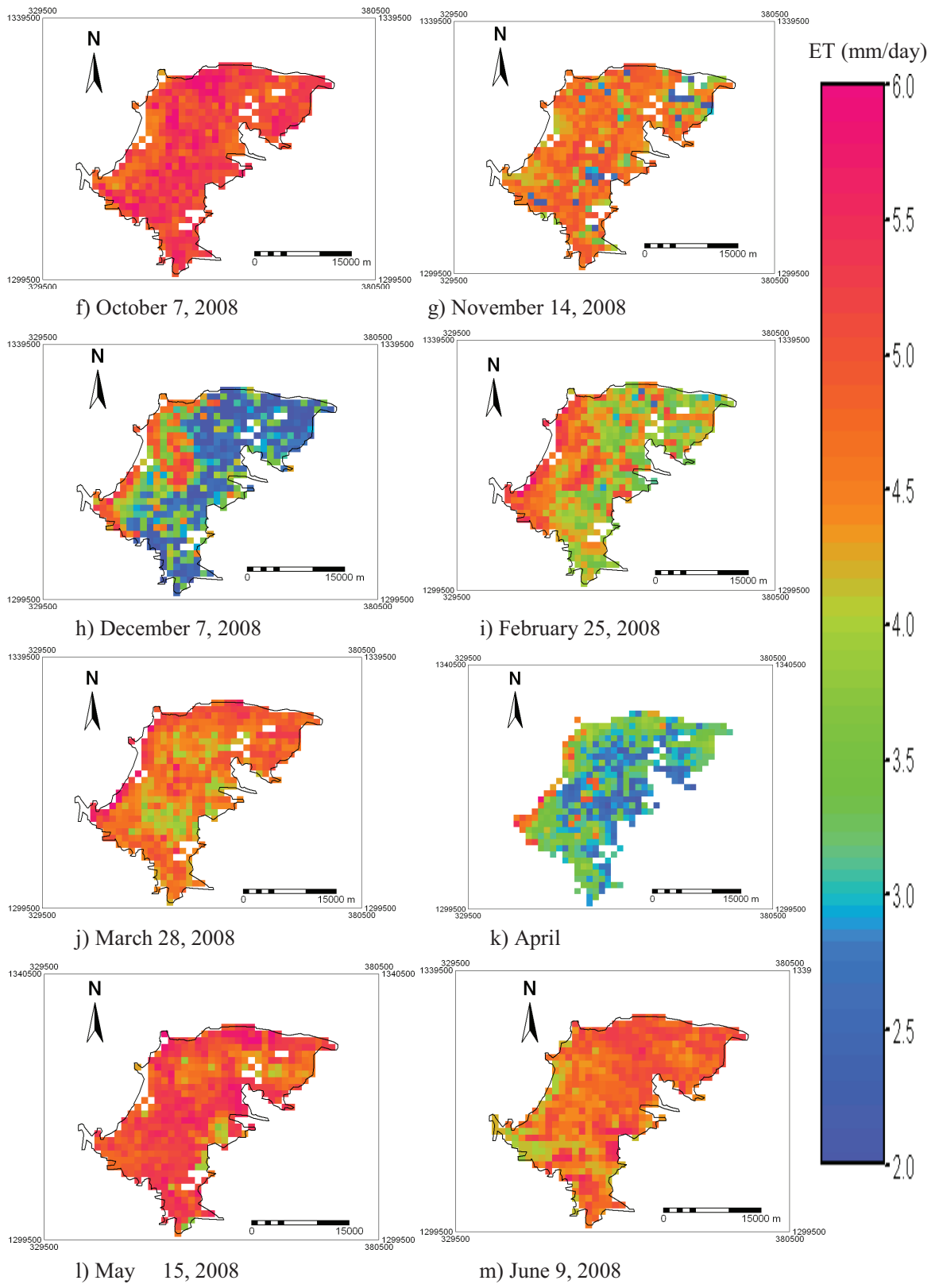


Figure C-1 Monthly sensitivity analysis result (a) February, (b) March, (c) May, (d) June, (e) August, (f) September, (g) October, and (h) December

Appendix - D Daily evapotranspiration maps

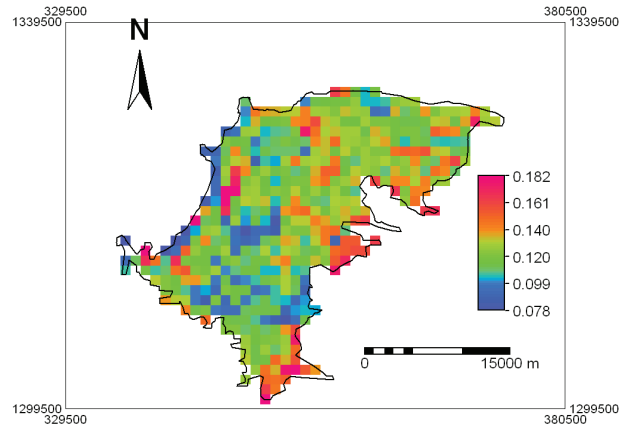


ESTIMATION OF EVAPOTRANSPIRATION FROM SATELLITE REMOTE SENSING AND METEOROLOGICAL DATA OVER THE FOGERA FLOOD PLAIN - ETHIOPIA

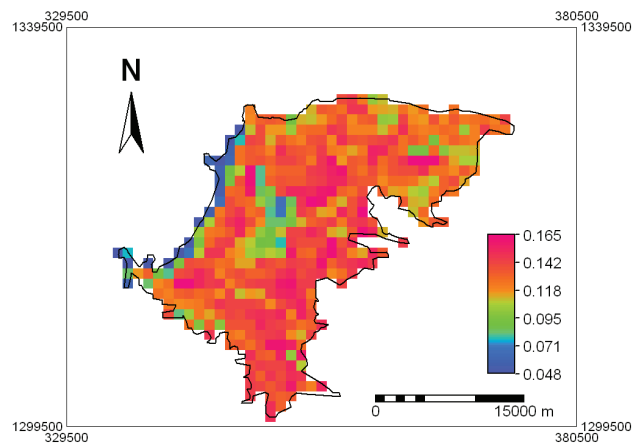


Projection: UTM, Datum: WGS 84, Ellipsoid: 84

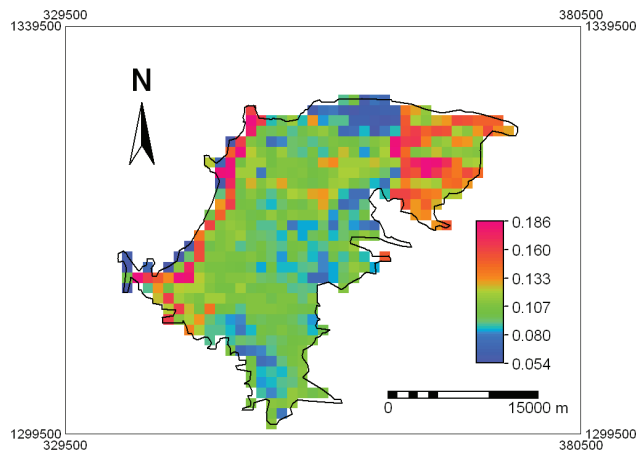
Appendix - F Some of the daily albedo maps



(a) September 6, 2008



(b) January 1, 2008



(c) April 26, 2008

Projection: UTM, Datum: WGS 84, Ellipsoid: 84

Appendix - G Weighted average vegetation height computation around the eddy flux tower

Vegetation type	Size of plot	Approximate area	Average height	Weighted average height
Rice	40*40	1600	0.75	0.033
Teff	60*40	2400	0.5	0.033
Millet	45*46	2070	0.95	0.054
Teff	35*60	2160	0.75	0.044
Onien	26*60	1560	0.55	0.024
grass+some trees	40*110	4400	0.5	0.060
Teff	150*90	13500	0.52	0.192
Rice	40*40	1600	0.75	0.033
Rice	120*60	7200	0.9	0.178
	sum	36490	sum	0.651

List of symbols

a	Coefficient
n_{ec}	Wind speed extinction coefficient
w	Water vapor content
Δe	Change in vapor pressure
ΔS	Change in storage
ΔT	Change in temperature
B	Bowen ratio
B^{-1}	Inverse Stanton number
C_t^*	Heat transfer coefficient of the soil
C_l	Thermal conductivity of soil
c_1, c_2	Constants
C_d	Drag coefficient
C_p	Specific heat capacity of the air
d	Zero plane displacement height
e_a	Actual vapor pressure
e_s	Saturation vapor pressure
ET_o	Reference evapotranspiration
f_c	Vegetation fraction
G	Soil heat flux
G_{in}	Incoming ground water flow
G_{out}	Out going ground water flow
H	Sensible heat flux
H_{dry}	Sensible heat flux at dry condition
H_{wet}	Sensible heat flux at wet condition
k	von Kermann constant
K_c	Crop coefficient
L	Obukhov length
L_w	Wet limit stability length
P	Precipitation
Pr	Prandtl number
q'	Specific humidity fluctuations
Q_{in}	Incoming surface water flow
Q_{out}	Out going surface water flow
r	Reflectance
R_{a24}	Daily extra terrestrial solar radiation
r_{ah}	Aerodynamic resistance for heat transfer
Re^*	Roughness Reynolds number
r_{ew}	External resistance
R_l	Long wave radiation
R_n	Net radiation
R_{n24}	Daily net radiation
r_{nir}	Reflectance in near infrared band

List of symbols cont.

R_{nl}	Net long wave radiation
r_{red}	Reflectance in red band
R_s	Incoming solar radiation
T	Temperature
T'	Temperature fluctuations
T_a	Air temperature
T_s	Radiometric surface temperature
u	Horizontal wind speed
u^*	Friction velocity
u_2	Wind speed at 2 m
w'	Vertical wind speed fluctuations
z	Reference height
z_1	Depth at level 1
z_{oh}	Roughness height for heat transfer.
z_{om}	Roughness height for momentum
z_{veg}	Vegetation height
α	Broad band surface albedo
α_{24}	Daily surface albedo
γ	Psychometric constant
Γ_c	Canopy fractional vegetation cover
Γ_s	Bare soil fractional vegetation cover
Δ	Slope of vapor pressure curve
ε	Emissivity of the surface
θ_v	Potential virtual temperature
λ	Latent heat of vaporization
A	Evaporative fraction
λE	Latent heat flux
λE_{dry}	Latent heat flux at dry condition
λE_{wet}	Latent heat flux at wet condition
Λr	Relative evaporative fraction
ρ_a	Density of air
ρ_w	Density of water
σ	Stefan-Boltzmann constant
τ_{24}	Daily transmissivity
ψ_h	Stability correction functions for heat
ψ_m	Stability correction functions for momentum

List of Acronyms

AET	Actual EvapoTranspiration
AME	Absolute Mean Error
DEM	Digital Elevation Model
DN	Digital Number
DOY	Day Of the Year
DU	Dobson Units
EOS	Earth Observing System
EOSDIS	Earth Observing System Data and Information System
ET	EvapoTranspiration
ETM+	Enhanced Thematic Mapper
FAO	Food and Agriculture Organization of United Nations
GPS	Global Positioning System
HDF-EOS	Hierarchical Data Format - Earth Observing System
ILWIS	Integrated Land and Water Information System
IR	Infra Red
LAADS	Level 1 and Atmosphere Archive and Distribution System
LAI	Leaf Area Index
LANDSAT	LAND remote sensing SATellite
LP DAAC	Land Processes Distributed Active Archive Center
LST	Land Surface Temperature
MODIS	Moderate Resolution Imaging Spectroradiometer
NASA	National Aeronautics and Space Administration
NDVI	Normalized Difference Vegetation Index
RH	Relative Humidity
RMSE	Root Mean Square Error
SDS	Scientific Data Sets
SEBAL	Surface Energy Balance Algorithm for Land
SEBS	Surface Energy Balance Systems
SMAC	Simplified Atmospheric Correction
SRTM	Shuttle Radar Topography Mission
TSEB	Two Source Energy Balance
USA	United States of America
USGS	United States Geological Survey
UTM	Universal Transverse Mercator
WGS	World Geodetic System
WWS	Woreta Weather Station

References

- Abeyou, W., 2008. Hydrological balance of Lake Tana upper Blue Nile basin, Ethiopia, ITC, Enschede, 94 pp.
- Abteu, W., 1996. Evapotranspiration measurements and modeling for three wetland systems in South Florida. In: *Water Resources Bulletin*, 32(1996)3, pp. 465-473.
- Abteu, W. and Obeysekera, J., 1995. Lysimeter study of evapotranspiration of cattails and comparison of three estimation methods. In: *Transactions of the American society of Agricultural Engineers ASAE*, 38(1995)1, pp. 121-129.
- Allen, R.G., 1998. *Crop evapotranspiration : guidelines for computing crop water requirements*. FAO irrigation and drainage paper;56. FAO, Rome, 300 pp.
- Assefa, M. and Nangia, V., 2005. Estimation of spatially distributed surface energy fluxes using remotely-sensed data for agricultural fields. *Hydrological Processes*, 19(14): 2653-2670.
- Assefa, M.M., Wossenu, A. and Tibebe, D., 2008. Simple model and Remote sensing of Evaporation Estimation for Rift Vally Lakes in Ethioia. In: A.M. Wossenu Abteu (Editor), *Hydrology and Ecology of the Nile Basin under Extreme Conditons*, Addis Ababa, Ethiopia.
- Bastiaanssen, W.G.M., 1998. *Remote sensing in water resources management: the state of the art*. International Water Management Institute (IWMI), Colombo, 118 pp.
- Batra, N., Islam, S., Venturini, V., Bisht, G. and Jiang, L., 2006. Estimation and comparison of evapotranspiration from MODIS and AVHRR sensors for clear sky days over the Southern Great Plains. *Remote Sensing of Environment*, 103(1): 1-15.
- Bois, B., Pieri, P., Van Leeuwen, C., Wald, L., Huard, F., Gaudillere, J.P. and Saur, E., 2008. Using remotely sensed solar radiation data for reference evapotranspiration estimation at a daily time step. *Agricultural and Forest Meteorology*, 148(4): 619-630.
- Bowen, I., 1926. The ratio of heat losses by conduction and evaporation from any water surface. *Physical review*, 27: 779-787.
- Brutsaert, W., 2005. *Hydrology : an introduction*. Cambridge University Press, Cambridge, 605 pp.
- Cleugh, H.A., Leuning, R., Mu, Q. and Running, S.W., 2007. Regional evaporation estimates from flux tower and MODIS satellite data. *Remote Sensing of Environment*, 106(3): 285-304.
- Coll, C., Caselles, V., Galve, J.M., Valor, E., Niclòs, R., Sánchez, J.M. and Rivas, R., 2005. Ground measurements for the validation of land surface temperatures derived from AATSR and MODIS data. *Remote Sensing of Environment*, 97(3): 288-300.
- Dagnachew, L. and Woubet, G., 2008. Flood Hazard and Risk Assesment in Fogera Woreda using GIS & Remote sensing. In: W.A.a.A.M. Melesse (Editor), *Hydrology and Ecology of the Nile Basin under Extreme Conditions*, Addis Ababa, Ethiopia.
- De Bruin, H.A.R., 1981. The determination of (reference crop) evapotranspiration from routine weather data. *Proc. and Inform.Comm. Hydr. Research TNO, The Hague*, 28: 25-37.
- Dingman, S.L., 2002. *Physical hydrology*. Prentice Hall, Upper Saddle River, 646 pp.
- Eddy Moors, 2008. Evaporation. In: M.F.P Bierkens, A.J.Dolman and P.A.Troch. (Editors), *Climate and the Hydrological cycle*. IAHS Pess.
- Gieske, A.M.S., 2003. Operational solutions of actual of evapotranspiration. In: I. Simmers (Editor), *Understanding Water in a Dry Envoronment Hydrological Processes in Arid and Semi-arid Zones*. A.Abalakama Pubilishers.

- Gong, L., Xu, C.-y., Chen, D., Halldin, S. and Chen, Y.D., 2006. Sensitivity of the Penman-Monteith reference evapotranspiration to key climatic variables in the Changjiang (Yangtze River) basin. *Journal of Hydrology*, 329(3-4): 620-629.
- Hasager, C. and Jensen, N.O., 1999. Surface - flux aggregation in heterogeneous terrain. *Q.J.R.meteorological society*, 125: 1-28.
- Hiwot, G.G., 2008. Groundwater recharge modelling a case study in the central Veluwe, The Netherlands, ITC, Enschede, 91 pp.
- Hoedjes, J.C.B., Chehbouni, A., Jacob, F., Ezzahar, J. and Boulet, G., 2008. Deriving daily evapotranspiration from remotely sensed instantaneous evaporative fraction over olive orchard in semi-arid Morocco. *Journal of Hydrology*, 354(1-4): 53-64.
- Jia, L., Su Zhongbo, van den Hurk Bart, Menenti Massimo, Moene Arnold, De Bruin Henk A. R., Yrisarry J. Javier Baselga, Ibanez Manuel and Cuesta Antonio, 2003. Estimation of sensible heat flux using the Surface Energy Balance System (SEBS) and ATSR measurements. *Physics and Chemistry of the Earth, Parts A/B/C*, 28(1-3): 75-88.
- Kebede, S., Travi, Y., Alemayehu, T. and Marc, V., 2006. Water balance of Lake Tana and its sensitivity to fluctuations in rainfall, Blue Nile basin, Ethiopia. *Journal of Hydrology*, 316(1-4): 233-247.
- Kersten, M.S., 1949. Thermal properties of soils. University of Minnesota Engineering Experiment. Station Bulletin 28, 227
- Kustas, W.P. and Daughtry, C.S.T., 1990. Estimation of the soil heat flux/net radiation ratio from spectral data. *Agricultural and Forest Meteorology*, 49(3): 205-223.
- Li, S., Kang, S., Li, F., Zhang, L. and Zhang, B., 2008. Vineyard evaporative fraction based on eddy covariance in an arid desert region of Northwest China. *Agricultural Water Management*, 95(8): 937-948.
- Liang, S., Shuey, C.J., Russ, A.L., Fang, H., Chen, M., Walthall, C.L., Daughtry, C.S.T. and Hunt, R., 2003. Narrowband to broadband conversions of land surface albedo: II. Validation. *Remote Sensing of Environment*, 84(1): 25-41.
- Lichun, W., 2008. Processing MODIS level_1B data for SEBS in ILWIS Instructions.
- McCabe, M.F. and Wood, E.F., 2006. Scale influences on the remote estimation of evapotranspiration using multiple satellite sensors. *Remote Sensing of Environment*, 105(4): 271-285.
- Monteith, J.L., 1965. Evaporation and surface temperature. *Quart. J. Roy. Met. Soc.*, 107: 1-27.
- Nagler, P.L., Scott, R.L., Westenburg, C., Cleverly, J.R., Glenn, E.P. and Huete, A.R., 2005. Evapotranspiration on western U.S. rivers estimated using the Enhanced Vegetation Index from MODIS and data from eddy covariance and Bowen ratio flux towers. *Remote Sensing of Environment*, 97(3): 337-351.
- Norman, J.M., Divakarla, M. and Goel, N.S., 1995. Algorithms for extracting information from remote thermal-IR observations of the earth's surface. *Remote Sensing of Environment*, 51(1): 157-168.
- Penman, H.L., 1948. Natural evaporation from open water, bare soil, and grass. *Proc. R. Soc., London*, vol A193: 120-145.
- Platt, C.M.R., 1984. *Evaporation into the atmosphere, theory, history and applications*: By Wilfried H. Brutsaert. Reidel, Dordrecht, 1982, x + 299 pp., Dfl. 80.00/ US\$ 34.95 cloth. *Agricultural and Forest Meteorology*, 33(2-3): 267-268.
- Priestley, C.H.B. and Taylor, R.J., 1972. On the assessment of surface heat flux and evaporation using large scale parameters. In: *Monthly Weather Review*, 100(1972)2, pp. 81-92.

- Rahman, H. and Dedieu, G., 1994. SMAC: a simplified method for the atmospheric correction of satellite measurements in the solar spectrum. *International Journal of Remote Sensing*, 15(1): 123 - 143.
- Ramos, J.G., Cratchley, C.R., Kay, J.A., Casterad, M.A., Martínez-Cob, A. and Domínguez, R., in press. Evaluation of satellite evapotranspiration estimates using ground-meteorological data available for the Flumen District into the Ebro Valley of N.E. Spain. *Agricultural Water Management*, In Press, Corrected Proof.
- Rana, G. and Katerji, N., 2000. Measurement and estimation of actual evapotranspiration in the field under Mediterranean climate: a review. *European Journal of Agronomy*, 13(2-3): 125-153.
- Shan, X., 2007. Regional evapotranspiration over the arid inland Heihe river basin in Northwest China, ITC, Enschede, 98 pp.
- SMEC, 2007. Hydrological Study of the Tana-Beles sub-basins, SMEC International Pty. Ltd.
- Su, Z., 2002. The Surface Energy Balance System (SEBS) for estimation of turbulent heat fluxes. *Hydrology and Earth System Sciences*, 6(1): 85-99.
- Su, Z., Schmugge, T., Kustas, W.P. and Massman, W.J., 2001. evaluation of two models for estimation of the roughness height for heat transfer between the land surface and the atmosphere. In: *Journal of applied meteorology*, 40(2001)11, pp. 1933-1951.
- Sumner, D.M. and Jacobs, J.M., 2005. Utility of Penman-Monteith, Priestley-Taylor, reference evapotranspiration, and pan evaporation methods to estimate pasture evapotranspiration. *Journal of Hydrology*, 308(1-4): 81-104.
- Teixeira, A.H.d.C., Bastiaanssen, W.G.M.p. and Bos, M.G.p., 2008. Measurements and modelling of evapotranspiration to assess agricultural water productivity in basins with changing land use patterns : a case study in the Sao Francisco river basin, Brazil, Wageningen University, Wageningen, 239 pp.
- Venturini, V., Islam, S. and Rodriguez, L., 2008. Estimation of evaporative fraction and evapotranspiration from MODIS products using a complementary based model. *Remote Sensing of Environment*, 112(1): 132-141.
- Vermote and Vermeulen, A., 1999. Atmospheric correction algorithm: Spectral Reflectances (MOD09).
- Wan, Z., 2008. New refinements and validation of the MODIS Land-Surface Temperature/Emissivity products. *Remote Sensing of Environment*, 112(1): 59-74.
- Wan, Z., Zhang, Y., Zhang, Q. and Li, Z.L., 2004. Quality assessment and validation of the MODIS global land surface temperature. *International Journal of Remote Sensing*, 25(1): 261 - 274.
- WaterWatch, 2005. Remote Sensing Studies of Tana-Beles Sub Basins, A Nile Basin Initiative project.
- Wenjing, L., 2006. Satellite based regional scale evapotranspiration in the Hebei plain, Northern China, ITC, Enschede, 101 pp.
- Widmoser, P., A discussion on and alternative to the Penman-Monteith equation. *Agricultural Water Management*, In Press, Corrected Proof.
- Wondimagegn, S.H., 2006. Remote sensing analysis of summer time evapotranspiration using SEBS algorithm : a case study in Regge and Dinkel, The Netherlands, ITC, Enschede, 130 pp.